PREDICTING INDUCED SEDIMENT OXYGEN FLUX IN OXYGENATED LAKES AND RESERVOIRS

Kevin A. Bierlein

Dissertation submitted to the Faculty of
Virginia Polytechnic Institute and State University
in partial fulfillment of the requirements for the degree of

Doctor of Philosophy
in
Civil Engineering

John C. Little, Chair
Daniel L. Gallagher
Adil F. Godrej
Francisco J. Rueda

May 6, 2015
Blacksburg, Virginia

Keywords: bubble plume, hypolimnetic oxygenation, oxygen flux, sediment kinetics, hydrodynamic modeling, water quality modeling, Si3D

PREDICTING INDUCED SEDIMENT OXYGEN DEMAND IN OXYGENATED LAKES AND RESERVOIRS

Kevin A. Bierlein

Abstract

Bubble plume oxygenation systems are commonly used to mitigate anoxia and its deleterious effects on water quality in thermally stratified lakes and reservoirs. Following installation, increases in sediment oxygen flux (J_{O2}) are typically observed during oxygenation and are positively correlated with the bubble plume gas flow rate. Studies show that J_{O2} is controlled by the thickness of the diffusive boundary layer (DBL) at the sediment-water interface (SWI), which is in turn controlled by turbulence. As a result, J_{O2} can be quite spatially and temporally variable.

Accurately predicting oxygenation-induced J_{O2} is vitally important for ensuring successful oxygenation system design and operation. Yet despite the current understanding of physical and chemical controls on J_{O2}, methods for predicting oxygenation-induced J_{O2} are still based on empirical correlations and factors of safety. As hypolimnetic oxygenation becomes more widely used as a lake management tool for improving and maintaining water quality, there is a need to move from the current empirically based approach to a mechanistic approach and improve the ability to predict induced J_{O2}. This work details field campaigns to investigate and identify appropriate models of oxygen supply to the SWI and oxygen demand exerted from the sediment, with the intent to use these models to predict oxygenation-induced J_{O2}.

Oxygen microprofiles across the SWI and near-sediment velocity measurements were collected *in situ* during three field campaigns on two oxygenated lakes, providing simultaneous measurements of J_{O2} and turbulence. Field observations show that oxygenation can increase J_{O2} by increasing bulk hypolimnetic oxygen concentrations, which increases the concentration gradient across the SWI. Oxygenation can also enhance turbulence, which decreases the DBL thickness and increases J_{O2}. Existing models of interfacial flux were compared to field measurements to determine which model best predicted the observed J_{O2}. Models based on the

Batchelor scale, friction velocity, and film-renewal theory all agree reasonably well with field observations in both lakes. Additionally, the oxygen microprofiles were used to fit a transient model of oxygen kinetics in lake sediment and determine the appropriate kinetic model. Oxygen microprofiles in both lakes can be described using zero-order kinetics, rather than first-order kinetics.

The interfacial flux and sediment kinetic models are incorporated into a coupled bubble plume and 3-D hydrodynamic lake model, allowing for spatial and temporal variation in simulated J_{O2}. This comprehensive model was calibrated and validated to field data from two separate field campaigns on Carvin's Cove Reservoir, Virginia. Simulated temperature profiles agreed quite well with field observations, while simulated oxygen profiles differed from observed profiles, particularly in the bottom 1 m of the water column. The model overestimates oxygen concentrations near the sediment, which results in higher simulated J_{O2} than was observed during the field campaigns. These discrepancies are attributed to oxygen-consuming chemical processes, such as oxidation of soluble metals, which are not accounted for in the hydrodynamic model. Despite this, the model is still able to capture the impact of bubble plume operation on J_{O2}, as simulated J_{O2} is higher when the diffusers are operating. With some additional improvements to the water quality modeling aspects of the model, as well as further calibration and validation, the model should be able to reproduce observed J_{O2} provided oxygen concentrations near the SWI are accurately reproduced as well. The current work is an attempt to push toward a comprehensive lake oxygenation model. A comprehensive model such as this should improve the ability to predict oxygenation-induced J_{O2} and lead to improvements in the design and operation of hypolimnetic oxygenation systems.

Acknowledgements

There are many people I would like to thank for their guidance, assistance, and support during the course of this research and my graduate studies at Virginia Tech. First, I would like to thank my advisor, Dr. John Little, for his continual guidance, advice, and encouragement through all stages of my Ph.D. research. It has been a pleasure working with him and I am thankful for and sincerely appreciate the opportunity to have him as an advisor and mentor. Thank you, John, for everything you've done along the way.

Second, I would like to thank my committee members for their advice, encouragement, time, and attention. Thank you, Dr. Daniel Gallagher, Dr. Adil Godrej, and Dr. Francisco Rueda. I would also like to extend additional thanks to Francisco for his support and contributions to the hydrodynamic modeling portion of this work.

Next, I would like to extend my thanks and gratitude to Dr. Scott Socolofsky and Maryam Rezvani. It has been a pleasure to collaborate with you both throughout this work, and I sincerely appreciate all of your contributions. Special thanks to Maryam for being a great friend and colleague.

I would also like to thank the people and organizations that contributed to the field portions of this research. Thank you, Bob Benninger, Jamie Morris, Jeff Booth, Cheryl Brewer, Elizabeth Hetz, and the rest of the Western Virginia Water Authority Staff for granting access to their resources and reservoirs, and providing assistance in field sampling and sample analysis. I would also like to thank the Western Virginia Water Authority for their financial support in funding this work. I would also like to thank EAWAG and Kanton Aargau for access to their resources and Lake Hallwil, as well as their assistance in coordinating and conducting the field campaigns in Switzerland, especially Dr. Johny Wüest, Dr. Arno Stöckli, and Michi Schurter – thank you all. It was a great opportunity and pleasure to collaborate with you at such a world-class research institution.

I would like to thank those who helped with various portions of fieldwork along the way: Melissa Stewart, Rick Browne, Mallory Barkdull, and Lee Bryant. A special thanks to Lee for

her help during the Lake Hallwil campaigns and with the microprofiler data analysis. You are a wonderful colleague.

I would also like to thank the organizations that provided funding for this research and my graduate studies: the National Science Foundation, the Western Virginia Water Authority, the Edna Bailey Sussman Fund, and the G.V. Loganathan Fellowship Award.

Finally, but certainly not least, I would like to thank my family and friends for their unwavering love, support, and encouragement, and I am thankful to have each and every one of you in my life.

Attributions

Many colleagues aided in developing the research described in this dissertation, collecting data in the field, processing and analyzing the data, and other activities vital to this work. A description of their background and contributions to each section is included here.

Dr. John Little (Professor, Civil & Environmental Engineering Dept., Virginia Tech) is the primary advisor and committee chair. Dr. Little provided guidance and feedback during all phases of this work, including data collection, data analysis, computer simulations, and manuscript development and editing.

Chapter 2: Increased sediment oxygen flux in oxygenated lakes: the impact of bubble plumes

Maryam Rezvani (doctoral candidate, Department of Civil Engineering, Texas A&M University) provided vital assistance in collecting data during the field campaigns. She also led the analysis of the velocity and turbulence data and provided input on the interpretation of the results.

Dr. Scott Socolofsky (Professor, Department of Civil Engineering, Texas A&M University) provided assistance in collecting data during the field campaigns and interpretation of the results. Several instruments from his research group were also provided for use during the field campaigns.

Dr. Lee Bryant (Assistant Professor, Department of Architecture and Civil Engineering, University of Bath) provided valuable assistance in collecting data, particularly during the Lake Hallwil field campaign. She also provided guidance and instruction on using the microprofiler and analyzing oxygen microprofiles.

Dr. John Little provided guidance and input on the data analysis and interpretation, as well as the manuscript development and editing. He also provided support during the field data collection.

Chapter 3. A transient model of dissolved oxygen kinetics in lake sediment

Dr. Lee Bryant provided valuable assistance in collecting field data with the microprofiler during the Lake Hallwil field campaign. She also provided guidance and instruction on using the microprofiler and analyzing the oxygen microprofiles.

Dr. John Little provided valuable guidance and input on the data analysis, interpretation, and model development, as well as manuscript development and editing. He also provided support during the field sampling campaigns.

Chapter 4. Toward a comprehensive lake model for predicting mixing-induced sediment oxygen uptake

Dr. Francisco Rueda (Professor, Instituto del Agua y Departamento Ingenieria Civil, Universidad de Granada) provided extensive support and guidance in all phases of work with the coupled 3D hydrodynamic model. He also provided input on analyzing the model output and interpreting the results.

Dr. John Little provided valuable guidance and input on the field data analysis and interpretation. He also provided input on interpreting the model results, provided support during the field sampling campaigns, and assisted in manuscript development and editing.

Table of Contents

Chapter 3. A transient model of dissolved oxygen kinetics in lake sediment

Chapter 4. Toward a comprehensive lake model for predicting mixing-induced sediment oxygen uptake

List of Tables

List of Figures

Chapter 1. Literature Review

Hypoxia and Anoxia in Freshwater Lakes

Water may prove to be the most critical natural resource affecting human and ecosystem health. There is mounting evidence that the condition of water supplies in many regions of the world, including the United States, is worsening both in terms of water quality and water quantity (Natural Resource Council 2012). For example, the growing demand for water in the Colorado River Basin, which supplies water to forty million people in seven states, is projected to exceed the available supply by almost 4000 gigaliters by 2060 due to decreased precipitation and increased temperatures stemming from climate change (Bureau of Reclamation 2012).

Depletion of oxygen in eutrophic, stratified water bodies is a frequent and challenging water-quality problem (Bryant et al. 2010; Stachowitsch et al. 2007; Wetzel 2001). Low dissolved oxygen (DO) in the hypolimnion of lakes and reservoirs is undesirable due to its negative impacts on water treatment processes, cold-water fisheries, and water quality downstream of hydropower dams (Singleton and Little 2006). In the United States, discharge from hydropower reservoirs typically must comply with state water-quality criteria for minimum oxygen concentration (Peterson et al. 2003). Oxygen depletion can lead to increases in ammonia, phosphorus, methane, methyl-mercury, and hydrogen sulfide, and can cause reduced iron and manganese in the sediments to solubilize (Funkey et al. 2014; Gao et al. 2014; Kleeberg et al. 2013; Testa and Kemp 2012; Gantzer et al. 2009a; Beutel et al. 2008; Huttunen et al. 2006, Davison 1993). Ammonia can be toxic to aquatic life. If entrained into the productive surface zone, phosphorus may stimulate algal and cyanobacteria growth, ultimately fueling additional oxygen demand once the algae die and settle through the water column. Methane is a well-known greenhouse gas, with much recent research occurring in an attempt to quantify the contribution of methane fluxes from freshwater lakes to the global carbon emissions budget. Methyl-mercury is extremely toxic to aquatic life, capable of accumulating in higher trophic levels. Hydrogen sulfide and reduced iron and manganese cause aesthetic problems associated with taste, odor, and color if hypolimnetic water is treated for potable use (Cooke and Carlson 1989). The presence of reduced compounds results in increased oxygen demand in water treatment plants, leading to higher drinking water treatment costs. The increased use of oxidants

such as chlorine in the presence of dissolved organic matter contributes to the formation of disinfection by-products such as haloacetic acids or trihalomethanes (Hua and Reckhow 2007). Hypolimnetic anoxia also has the potential to cause winter fish kills in ice-covered lakes (Mackenthun and Stefan 1998) and can impair natural fish reproduction by disrupting the endocrine system (Wu et al. 2003).

Hypolimnetic Oxygenation

Hypolimnetic oxygenation, which preserves thermal stratification, is increasingly used to replenish dissolved oxygen (Singleton and Little 2006; Beutel and Horne 1999). There are several devices used to accomplish this: the Speece Cone (McGinnis and Little 1998), the airlift aerator (Burris et al. 2002; Little 1995; Ashley 1985), the side-stream super-saturation system (Gerling et al. 2014; Toffolon et al. 2013), and the bubble plume (Wüest et al. 1992), which is becoming one of the more common hypolimnetic oxygenation devices. Bubble-plume diffusers are generally circular or linear and inject either air or oxygen gas into the hypolimnion at a relatively low gas flow rate. These systems are most suited to deeper lakes, where most of the bubbles are able to dissolve in the hypolimnion and the upward momentum generated by the plume is low enough to prevent significant erosion of the thermocline (Singleton and Little 2006). While effective at adding oxygen, bubble plumes also add energy, which may induce large-scale hypolimnetic mixing, depending on design and operation (Singleton et al. 2010). Plume-induced mixing can alter the thermal structure of the reservoir, and plume performance depends strongly on the vertical density gradient, establishing a feedback loop that continually alters plume behavior. Partial erosion of the thermocline and hypolimnetic warming may result in premature destratification of the reservoir or lake (Beutel and Horne 1999), increasing the potential for a late fall algal bloom. Hypolimnetic warming and plume-induced mixing can also be responsible for increased hypolimnetic oxygen demand, with sediment oxygen flux (J_{O2}), increasing by over a factor of 5 – 7 in many cases (Gantzer et al. 2009b; Prepas and Burke 1997). In large reservoirs, with plume-induced mixing intensity localized near the diffusers, J_{O2} may change as a function of distance from the diffuser, altering the horizontal migration rate of DO added by the bubble plume. The enhanced mixing may increase turbulence, generate or alter basin-scale circulation patterns, and affect other biogeochemical fluxes across the sediment-water interface (SWI).

Although hypolimnetic oxygenation systems are becoming more common, current oxygenation system design is still in a relatively nascent state when it comes to predicting the effects of oxygenation on lake hydrodynamics, thermal structure, and oxygen budget. Accurately predicting the induced J_{O2} is vitally important to ensuring successful design and operation, yet there remains no method to reliably predict the magnitude of oxygenation-induced J_{O2}. Current best practice is to use the measured oxygen demand before diffuser installation and a factor of safety. Studies by Moore et al. (1996), Beutel (2003), and others provide guidelines for estimating an appropriate factor of safety, but these approaches are not ideal, as they are based on empirical equations derived from laboratory experiments. Ideally, predictions of induced J_{O2} should be derived from chemically- and physically-based models. As hypolimnetic oxygenation becomes more widely used, there is a need to move from an empirical approach to a mechanistic approach and improve the ability to estimate induced sediment oxygen flux.

Interfacial Flux at the Sediment–Water Interface

Oxygen flux across the SWI is typically considered to be the dominant sink of DO in the hypolimnion. It often comprises the majority of the total hypolimnetic oxygen demand, which also includes various chemical and biological processes in the water column that consume oxygen.

Processes on both sides of the SWI influence J_{O2}. Below the SWI, oxygen may be transported deeper into the sediment pore water via diffusion or interstitial flow. It can be consumed within the sediments by microbial respiration and chemical oxidation of reduced species, such as Fe^{2+} or Mn^{2+}. The myriad processes that consume oxygen are often lumped together into an overall reaction rate when describing oxygen consumption in lake sediments, as this is often a reasonable simplification, especially when the oxygen budget in the lake is of greater concern than the specific oxygen chemistry within the sediment. Depending on the individual study, the consumption of DO below the SWI has been described using zero-order, first-order, and Monod kinetics (equations 1.1 – 1.3; House 2003):

$$\frac{\partial C}{\partial t} = D_s \frac{\partial^2 C}{\partial z^2} - k_0 \tag{1.1}$$

$$\frac{\partial C}{\partial t} = D_s \frac{\partial^2 C}{\partial z^2} - k_1 C \tag{1.2}$$

$$\frac{\partial C}{\partial t} = D_s \frac{\partial^2 C}{\partial z^2} - \mu \frac{C}{K_{O2} + C} \tag{1.3}$$

where C is the oxygen concentration, t is time, D_s is the effective diffusion coefficient of oxygen in the sediment ($D_s = \varphi D$), φ is the sediment porosity, D is the molecular diffusion coefficient of oxygen in water, z is depth below the SWI, k_0 is a zero-order rate constant, k_1 is a first-order rate constant, μ is the maximum oxidation rate, and K_{O2} is the half-saturation constant. On the water side of the SWI, oxygen transport to the SWI is slowed by the presence of the diffusive boundary layer (DBL). Molecular diffusion is the primary oxygen transport mechanism across this thin, milimeter-scale film, thus the supply of oxygen to the SWI is diffusion-limited. The observed J_{O2}, then, is a balance between the demand for oxygen exerted from the sediment side of the SWI and the supply of oxygen that is transported to the SWI from the bulk hypolimnetic water.

Many studies have investigated the role of the DBL, confirming its importance for limiting J_{O2} under typical conditions found in lakes and reservoirs. Laboratory experiments using sediment core incubations linked changes in the DBL thickness (δ_{DBL}) and J_{O2} to water velocity near the SWI (Beutel 2003; Moore et al. 1996). More recent field studies linked changes in J_{O2} to turbulence in the bottom boundary layer as a result of natural seiche activity, finding the turbulence dissipation rate to be the primary driver to changes in δ_{DBL}, rather than current velocity (Bryant et al. 2010; Lorke et al. 2003). As highlighted by Bryant et al. (2010), when turbulence in the bottom boundary layer increases, δ_{DBL} decreases, reducing the diffusive resistance to oxygen transport and increasing J_{O2}. Conversely, during relatively quiescent periods δ_{DBL} increases, thus decreasing J_{O2}. Using oxygen microprofiles measured *in situ*, Bryant et al. (2010) observed changes in J_{O2} on an hourly timescale by a factor of approximately six in direct response to changes in the turbulence dissipation rate and δ_{DBL}.

The generic form of interfacial flux is given in equation 1.4, where k_t is the transfer velocity (also called the mass transfer coefficient), C is the bulk solute concentration, and C_0 is the solute concentration at the interface. Applied to oxygen flux across the SWI this becomes equation 1.5, where C_B is the DO concentration in the bulk water above the SWI and C_{SWI} is the DO concentration at the SWI.

$$J = k_t\left(C - C_0\right) \tag{1.4}$$

$$J_{O2} = k_t\left(C_B - C_{SWI}\right) \tag{1.5}$$

Many models are proposed in the literature for calculating k_t from the characteristics of turbulent flow at the interface. Thin-film theory, also called the Lewis-Whitman model, is one of the simplest, calculating k_t simply as D/δ_{DBL} (O'Connor et al. 2009; Lewis and Whitman 1924). The film renewal model calculates an average transfer velocity which depends on the renewal frequency, r, which is the time between turbulent events that replenish the DO supply from the bulk water to the interface (equation 1.6) (King 1966; Danckwerts 1951; Toor and Marchello 1958; Higbie 1935). The renewal frequency can be calculated using a timescale that is characteristic of the turbulence, such as the Kolmogorov time scale or integral time scale, which represent the smallest and largest eddies in the turbulent flow, respectively. There are also models for calculating k_t based on mathematical scaling arguments (equations 1.7 and 1.8), where α and β are empirical parameters, u_* is the shear velocity, Sc is the Schmidt number, ε is the turbulence dissipation rate, and v is viscosity (O'Connor et al. 2009; O'Connor and Hondzo 2008; Lorke and Peeters 2006). Equation 1.7 is derived from law-of-the-wall scaling arguments, and equation 1.8 is based on the Batchelor scale (Batchelor 1959), which describes the smallest fluctuations in tracer concentrations before diffusion dominantes. Typical values for α and β reported in the literature range from 0.052 – 0.164 and -7/10 – -2/3, respectively (O'Connor et al. 2009).

$$k_t = \sqrt{\frac{4Dr}{\pi}} \tag{1.6}$$

$$k_t = \alpha u_* Sc^{\beta} \tag{1.7}$$

$$k_t = \frac{1}{2\pi} Sc^{-1/2} (\varepsilon \nu)^{1/4} \quad (1.8)$$

Despite the abundance of work in the literature studying interfacial flux, much of it has focused on air-water exchange, rather than flux across the SWI. Relatively few have investigated oxygen flux across the SWI, even though J_{O2} has profound implications for the lake oxygen budget, redox conditions, chemical cycling, and overall water quality. Further, the studies that have focused on exchange across the SWI typically use *ex situ* measurements on incubated sediment cores or dredged sediments (e.g., Beutel et al. 2007; House 2003; Rasmussen and Jørgensen 1992) which may not be representative of ambient conditions in the hypolimnion. O'Connor et al. (2009) represents the only study investigating the best models for estimating k_t for predicting J_{O2}, arguing that an expression for k_t in the form of equation 1.7 and based on prior work from their group (O'Connor and Hondzo 2008) provided the best estimate for J_{O2}. This, too, was a laboratory study, not an *in situ* measurement. Under idealized flow conditions in the laboratory, with constant flow conditions, it is unsurprising that a model for k_t based on law-of-the-wall scaling would provide an excellent fit to experimental measurements. Law-of-the-wall scaling may not always be representative of *in situ* conditions, however, since periodic forcing of internal waves and currents can cause an oscillatory boundary layer to form, which may not conform to the law-of-the-wall scaling (Lorke et al. 2002).

Lorke et al. (2003) and Bryant et al. (2010) investigated the influence of hydrodynamics on J_{O2} using *in situ* field experiments in a sub-basin of Lake Lucerne, Switzerland, directly measuring J_{O2} and turbulence. Both studies found that ε controls J_{O2}, and Lorke also showed that the Batchelor length scales well with δ_{DBL}. Bryant et al. (2011) performed a similar study, this time in an oxygenated reservoir, finding that the oxygenation system increased ε and J_{O2}. It is worth noting, however, that turbulence dissipation rates were directly calculated from J_{O2} and δ_{DBL} measurements assuming law-of-the-wall scaling, therefore J_{O2} and ε measurements were not independent. There remains a need to perform *in situ* experiments in oxygenated lakes and reservoirs to determine the appropriate k_t model for predicting J_{O2} based on hydrodynamics.

Bubble Plume and Hydrodynamic Models

Though many models for predicting plume dynamics and/or oxygen transfer from bubble-plumes have been developed, very little research has focused on modeling the complex interaction between bubble plumes and ambient water bodies. Most of the bubble plume/reservoir models in the literature do not account for oxygen transfer from bubbles to the ambient water, since they simulate artificial circulation or destratification systems, in which gas transfer to the surrounding water is not of primary concern (Johnson et al. 2000; Schladow 1993; Zic et al. 1992). Lindenschmidt and Hamblin (1997) coupled DYRESM, a 1-D hydrodynamic model, to stirring and bubbler modules to simulate vertical mixing in the lake induced by aeration. Imteaz and Asaeda (2000) coupled the DYRESM model to a bubble-plume model as well as an ecological model to track phytoplankton growth, investigating the potential effectiveness of destratification via bubble-plumes for reducing or controlling algal blooms. None of these coupled models, however, included mass transfer between the bubbles and water, which is crucial for accurate predictions of the performance of hypolimnetic oxygenation systems. Furthermore, 1-D models such as DYRESM assume homogeneous conditions in both horizontal directions, ignoring the fact that there are substantial differences between the near- and far-field conditions and that it is the near-field conditions that determine the operational behavior of bubble plumes (McGinnis et al. 2004).

Singleton et al. (2010) successfully coupled a validated linear bubble plume model (Singleton et al. 2007) used for hypolimnetic oxygenation with a 3-D hydrodynamic model (Si3D) to simulate the complex interaction between bubble plumes and the large-scale processes of transport and mixing. Si3D is based on the continuity equation for incompressible fluids, the Reynolds-averaged form of the Navier-Stokes equations for momentum, the transport equation for temperature, and an equation of state for density as a function of temperature. It uses a 2.5 order Mellor – Yamada model (Mellor and Yamada 1982) with improvements and modifications proposed by Galperin et al. (1988) and Kantha and Clayson (1994) to calculate eddy diffusivity and eddy viscosity for simulating sub-grid size turbulent transport (Rueda and Schladow 2002, 2003). Si3D uses a semi-implicit finite-difference method on a structured Cartesian grid, solving the layer-averaged form of the governing equations. Though perhaps not as well known as some other lake models such as DYRESM, CE-QUAL-W2, or ELCOM, Si3D has been extensively

described in the literature and used with much success (Acosta et al. 2015; Singleton et al. 2010; Smith 2006; Rueda et al. 2005; Smith et al. 2005; Rueda and Schladow 2002, 2003).

Singleton et al. (2010) found that the coupled model accurately simulated the evolution of oxygen and temperature fields that occurred during two full-scale tests in Spring Hollow Reservoir, Virginia. The model correctly predicted the overall rate of oxygen addition by the plume, but used an empirical correlation for J_{O2} as a function of diffuser gas flow rate to predict oxygen flux at the SWI. While this approach may have provided reasonable end results, a comprehensive bubble-plume and 3-D hydrodynamic lake model should ideally include expressions for J_{O2} based on the physical and chemical processes occurring within the lake, rather than an empirical expression. Additionally, the scenario modeled by Singleton et al. (2010) represents a relatively simple scenario, in which there is a relatively small sediment surface area in the hypolimnion, minimal natural currents, and weak bubble plume-induced currents due to the low applied gas flow rate, thus the empirical correlation for J_{O2} proved acceptable. Larger and more energetic systems, such as those studied by Bryant et al. (2011), are subject to increased spatial variability in turbulence, and thus J_{O2}, which reduces the likelihood of a simple correlation between J_{O2} and diffuser gas flow rate providing acceptable results for the overall oxygen budget. By incorporating a model for J_{O2} based on hydrodynamics and chemistry, J_{O2} will be allowed to vary throughout the simulated reservoir with changes in the local hydrodynamics, diffuser operation and oxygen distribution, thus improving the simulation of the overall oxygen budget in the entire hypolimnion. Such a comprehensive model should vastly improve the ability to predict diffuser-induced J_{O2}, leading to improvements in the design and operation of hypolimnetic oxygenation systems.

Research Objectives

The overall goal of this research is to improve our capacity to model and predict the flux of oxygen across the SWI in oxygenated lakes and reservoirs. These advances will move oxygenation system design away from the current empirical approach and toward an improved, mechanistic approach.

To meet the overall research goal, three specific research objectives will be pursued:

1. Determine an appropriate model for interfacial flux at the SWI, linking J_{O2} to lake hydrodynamics using data collected *in situ* from two oxygenated lakes;
2. Determine the appropriate kinetic model and associated rate constants for oxygen consumption in the lake sediment of two oxygenated lakes; and
3. Incorporate the interfacial flux and kinetic models into an existing coupled bubble-plume 3-D hydrodynamic lake model, thus linking predicted J_{O2} to the simulated hydrodynamics, allowing for spatial and temporal variability in J_{O2} in response to changes in bubble-plume diffuser operation.

A chapter is dedicated to discussing each of the three specific research objectives outlined above, with chapters presented in manuscript format: Chapter 2 is in the style of Water Resources Research, Chapter 3 is in the style of Water Research, and Chapter 4 is also in the style of Water Resources Research.

Chapter 2 describes the field sampling campaigns performed on Carvin's Cove Reservoir and Lake Hallwil in detail, investigating the effects of bubble-plume operation on J_{O2}. Simultaneous measurements of J_{O2} and velocity in the bottom boundary layer are used in concert and compared to several proposed models of interfacial flux from the literature. By comparing the *in situ* field data to the predicted J_{O2} from the interfacial flux models, the most appropriate models for predicting J_{O2} in oxygenated lakes are identified.

Chapter 3 details the development of a transient model of oxygen transport in lake sediment. The transient model is fit to field data from Carvin's Cove Reservoir and Lake Hallwil to determine: 1) whether zero-order or first-order reaction kinetics is more appropriate for describing oxygen consumption in the sediments, and 2) what is the best-fit value of the zero-order and first-order rate constants describing oxygen consumption in the sediments.

Chapter 4 integrates the previous two chapters, incorporating the most appropriate interfacial flux and sediment kinetic models into an existing coupled bubble-plume 3-D hydrodynamic model, Si3D. This coupled model is applied to Carvin's Cove Reservoir and modified to link J_{O2} in a given grid cell to the local turbulence dissipation rate in the bottom boundary layer. Data

from the 2011 and 2013 Carvin's Cove Reservoir field campaigns are used to calibrate and validate the model, respectively.

References

Acosta, M., Anguita, M., Fernández-Baldomero, F. J., Ramón, C. L., Schladow, S. G., and Rueda, F. J., 2015. "Evaluation of a nested-grid implementation for 3D finite-difference semi-implicit hydrodynamic models." *Environmental Modelling & Software,* 64 (2), 241-262.

Ashley, K. I., 1985. "Hypolimnetic aeration: Practical design and application." *Water Research,* 19 (6), 735-740.

Batchelor, G. K., 1959. "Small-scale variation of convected quantities like temperature in turbulent fluid." *Journal of Fluid Mechanics,* 5 (1), 113-133.

Beutel, M. W., and Horne, A. J., 1999. "A review of the effects of hypolimnetic oxygenation on lake and reservoir water quality." *Lake and Reservoir Management,* 15 (4), 285-297.

Beutel, M., 2003. "Hypolimnetic anoxia and sediment oxygen demand in California drinking water reservoirs." *Lake and Reservoir Management,* 19 (3), 208-221.

Beutel, M., Hannoun, I., Pasek, J., and Kavanagh, K. B., 2007. "Evaluation of hypolimnetic oxygen demand in a large eutrophic raw water reservoir, San Vicente Reservoir Calif." *Journal of Environmental Engineering,* 133 (2), 130-138.

Beutel, M. W., Leonard, T. M., Dent, S. R., and Moore, B. C., 2008. "Effects of aerobic and anaerobic conditions on P, N, Fe, Mn, and Hg accumulation in waters overlaying profundal sediments of an oligo-mesotrophic lake." *Water Research,* 42 (8-9), 1953-1962.

Bryant, L. D., Lorrai, C., McGinnis, D. F., Brand, A., Wuest, A., and Little J. C., 2010. "Variable sediment oxygen uptake in response to dynamic forcing." *Limnology and Oceanography*, 55 (2), 950-964.

Bryant, L. D., Gantzer, P. A., and Little, J. C., 2011. "Increased sediment oxygen uptake caused by oxygenation-induced hypolimnetic mixing." *Water Research,* 45 (12), 3692-3703.

Bureau of Reclamation, 2012. "Colorado River Basin Water Supply and Demand Study." Retrieved from http://www.usbr.gov/lc/region/programs/crbstudy/finalreport/index.html

Burris, V. L., McGinnis, D. F., and Little, J. C., 2002. "Predicting oxygen transfer and water flow rate in airlift aerators." *Water Research,* 36 (18), 4605-4615.

Cooke, G. D., and Carlson, R. E, 1989. "Reservoir management for water quality and THM precursor control." American Water Works Association Research Foundation, Denver, CO.

Danckwerts, P. V., 1951. "Significance of liquid-film coefficients in gas absorption." *Industrial and Engineering Chemistry,* 43 (6), 1460-1467.

Davison, W., 1993. "Iron and manganese in lakes." *Earth-Science Reviews,* 34, 119-163.

Funkey, C. P., Conley, D. J., Reuss, N. S., Humborg, C., Jilbert, T., and Slomp, C. P., 2014. "Hypoxia sustains cyanobacteria blooms in the Baltic Sea." *Environmental Science and Technology*, 48 (5), 2598-2602.

Galperin, B., Kantha, L. H., Hassid, S., and Rosati, A., 1988. "A quasi-equilibrium turbulent energy model for geophysical flows." *Journal of the Atmospheric Sciences,* 45 (1), 55-62.

Gantzer P. A., Bryant, L. D., and Little, J. C., 2009a. "Controlling soluble iron and manganese in a water-supply reservoir using hypolimnetic oxygenation." *Water Research,* 43 (5), 1285-1294.

Gantzer, P. A., Bryant, L. D., and Little, J. C., 2009b. "Effect of hypolimnetic oxygenation on oxygen depletion rates in two water-supply reservoirs." *Water Research,* 43 (6), 1700-1710.

Gao, Y., Cornwell, J. C., Stoecker, D. K., and Owens, M. S., 2014. "Influence of cyanobacteria blooms on sediment biogeochemistry and nutrient fluxes." *Limnology and Oceanography,* 59 (3), 959-971.

Gerling, A. B., Browne, R. G., Gantzer, P. A., Mobley, M. H., Little, J. C., and Carey, C. C., 2014. "First report of the successful operation of a side stream supersaturation hypolimnetic oxygenation system in a eutrophic, shallow reservoir." *Water Research,* 67, 129-143.

Higbie, R., 1935. "The rate of absorption of a pure gas into a still liquid during short periods of exposure." *Transactions of the American Institute of Chemical Engineers,* 31, 365-389.

House, W., 2003. "Factors influencing the extent and development of the oxic zone in sediments." *Biogeochemistry,* 63 (3), 317-334.

Hua, G., and Reckhow, D. A., 2007. "Comparison of disinfection byproduct formation from chlorine and alternative disinfectants." *Water Research,* 41 (8), 1667-1678.

Huttunen, J. T., Väisänen, T. S., Hellsten, S. K., and Martikainen, P. J., 2006. "Methane fluxes at the sediment-water interface in some boreal lakes and reservoirs." *Boreal Environment Research,* 11 (1), 27-34.

Imteaz, M. A., and Asaeda, T., 2000. "Artificial mixing of lake water by bubble plumes: effects of bubbling operations on algal blooms." *Water Research,* 34 (6), 1919-1929.

Johnson G. P., Hornewer, N. J., Robertson, D. M., Olson, D. T., and Gioja, J., 2000. "Methodology, data collection and data analysis for determination of water-mixing patterns induced by aerators and mixers." Water-Resources Investigations Report 00-4101, U. S. Geological Survey.

Kantha, L. H., and Clayson, C. A., 1994. "An improved mixed layer model for geophysical applications." *Journal of Geophysical Research,* 99 (C12), 25235-25266.

King, C. J., 1966. "Turbulent liquid phase mass transfer at free gas-liquid interface." *Industrial and Engineering Chemistry Fundamentals*, 5 (1), 1-8.

Kleeberg, A., Herzog, C., and Hupfer, M., 2013. "Redox sensitivity of iron in phosphorus binding does not impede lake restoration." *Water Research,* 47 (3), 1491-1502.

Lewis, W. K., and Whitman, W. G., 1924. "Principles of gas absorption." *Industrial and Engineering Chemistry,* 16 (12), 1215-1220.

Lindenschmidt, K. E., and Hamblin, P. F., 1997. "Hypolimnetic aeration in Lake Tegel, Berlin." *Water Research,* 31 (7), 1619-1628.

Little, J. C., 1995. "Hypolimnetic aerators – predicting oxygen-transfer and hydrodynamics." *Water Research,* 29 (11), 2475-2482.

Lorke, A. Umlauf, L, Tobias, J., and Wüest, A., 2002. "Dynamics of turbulence in low-speed oscillating bottom-boundary layers of stratified basins." *Environmental Fluid Mechanics,* 2, 291-313.

Lorke, A., Müeller, B., Maerki, M., and Wüest, A., 2003. "Breathing sediments: The control of diffusive transport across the sediment-water interface by periodic boundary-layer turbulence." *Limnology and Oceanography,* 48 (6), 2077-2085.

Lorke, A., and Peeters, F., 2006. "Toward a unified scaling relation for interfacial fluxes." *Journal of Physical Oceanography*, 36 (5), 955-961.

Mackenthun, A. A., and Stefan, H. G., 1998. "Effect of flow velocity on sediment oxygen demand: Experiments." *Journal of Environmental Engineering,* 124 (3), 222-230.

McGinnis, D. F., and Little, J. C., 1998. "Bubble dynamics and oxygen transfer in a Speece Cone." *Water Science and Technology,* 37 (2), 285-292.

McGinnis, D. F., Lorke, A., Wüest, A., Stockli, A., and Little, J. C., 2004. "Interaction between a bubble plume and the near field in a stratified lake." *Water Resources Research,* 40 (10), W10206.

Mellor, G. L., and Yamada, T., 1982. "Development of a turbulence closure model for geophysical fluid problems." *Reviews of Geophysics and Space Physics,* 20 (4), 851-875.

Moore, B. C., Chen, P., Funk, W. H., and Yonge, D., 1996. "A model for predicting lake sediment oxygen demand following hypolimnetic aeration." *Water Resources Bulletin,* 32 (4), 723-731.

National Research Council, 2012. "Challenges and Opportunities in the Hydrologic Sciences." Washington, D. C., National Academic Press.

O'Connor, B. L., Hondzo, M., and Harvey, J. W., 2009. "Incorporating both physical and kinetic limitations in quantifying dissolved oxygen flux to aquatic sediment." *Journal of Environmental Engineering,* 135 (12), 1304-1314.

O'Connor, B. L, and Hondzo, M., 2008. "Dissolved oxygen transfer to sediments by sweep and eject motions in aquatic environments." *Limnology and Oceanography,* 53 (2), 566-578.

Peterson, M. J., Cada, G. F., Sale, M. J., and Eddlemon, G. K., 2003. "Regulatory approaches for addressing dissolved oxygen concerns at hydropower facilities." U.S. Department of Energy, Energy Efficiency and Renewable Energy, Wind and Hydropower Technologies.

Prepas, E. E., and Burke, J. M., 1997. "Effects of hypolimnetic oxygenation on water quality in Amisk Lake, Alberta, a deep, eutrophic lake with high internal phosphorus loading rates." *Canadian Journal of Fisheries and Aquatic Sciences,* 54 (9), 2111-2120.

Rasmussen, H., and Jørgensen, B. B., 1992. "Microelectrode studies of seasonal oxygen uptake in a coastal sediment: role of molecular diffusion." *Marine Ecology Progress Series,* 81 (3), 289-303.

Rueda, F. J., and Schladow, S. G., 2002. "Quantitative comparison of models for barotropic response of homogeneous basins." *Journal of Hydraulic Engineering,* 128 (2), 201-213.

Rueda, F. J., and Schladow, S. G., 2003. "Dynamics of a large polymictic lake. II: Numerical simulations." *Journal of Hydraulic Engineering,* 129 (2), 92-101.

Rueda, F. J., Schladow, S. G., Monismith, S. G., and Stacey, M. T., 2005. "On the effects of topography on wind and the generation of currents in a large multi-basin lake." *Hydrobiologia,* 532, 139-151.

Schladow, S. G., 1993. "Lake destratification by bubble-plume systems – Design methodology." *Journal of Hydraulic Engineering – ASCE,* 119 (3), 350-368.

Singleton, V. L., and Little, J. C., 2006. "Designing hypolimnetic aeration and oxygenation systems – A review." *Environmental Science and Technology,* 40 (24), 7512-7520.

Singleton, V. L., Rueda, F. J., and Little, J. C., 2010. "A coupled bubble plume-reservoir model for hypolimnetic oxygenation." *Water Resources Research*, 46 (12), W12538.

Smith, P. E., 2006. "A semi-implicit, three-dimensional model for estuarine circulation." U.S. Geological Survey Open-file Report 2006-1004, 176 p.

Smith, P., Donovan, J., and Wong, H., 2005. "Applications of 3D hydrodynamic and particle tracking models in the San Franciso Bay-Delta estuary." Impacts of Global Climate Change, p 1-8. doi: 10.1061/40792(173)393

Stachowitsch, M., Riedel, B., Zuschin, M., and Machan, R., 2007. "Oxygen depletion and benthic mortalities: the first in situ experimental approach to documenting an elusive phenomenon." *Limnology and Oceanography: Methods*, 5, 344-352.

Testa, J. M., and Kemp, W. M., 2012. "Hypoxia-induced shifts in nitrogen and phosphorus cycling in Chesapeake Bay." *Limnology and Oceanography,* 57 (3), 835-850.

Toffolon, M., Ragazzi, M., Righetti, M., Teodoru, C. R., Tubino, M., Defrancesco, C., and Pozzi, S., 2013. "Effects of artificial hypolimnetic oxygenation in a shallow lake. Part 1: Phenomenological description and management." *Journal of Environmental Management,* 114, 520-529.

Toor, H. L., and Marchell, J. M., 1958. "Film-penetration model for mass and heat transfer." *A.I.Ch.E. Journal,* 4 (1), 97-101.

Wu, R. S. S., Zhou, B. S., Randall, D. J., Woo, N. Y. S., and Lam, P. K. S., 2003. "Aquatic hypoxia is an endocrine disruptor and impairs fish reproduction." *Environmental Science and Technology,* 37 (6), 1137-1141.

Wüest, A., Brooks, N. H., and Imboden, D. M., 1992. "Bubble plume modeling for lake restoration." *Water Resources Research,* 28 (12), 3235-3250.

Zic, K., Stefan, H. G., and Ellis, C., 1992. “Laboratory study of water destratification by a bubble plume.” *Journal of Hydraulic Research,* 30 (1), 7-27.

Chapter 2. Increased Sediment Oxygen Flux in Oxygenated Lakes: The Impact of Bubble Plumes

Kevin A. Bierlein[1], Maryam Rezvani[2], Scott A. Socolofsky[2], Lee D. Bryant[3], and John C. Little[1].

[1]Via Department of Civil and Environmental Engineering, Virginia Tech, Blacksburg, Virginia, USA

[2]Zachry Department of Civil Engineering, Texas A&M University, College Station, Texas, USA

[3]Department of Architecture and Civil Engineering, University of Bath, Bath, United Kingdom

Abstract

Hypolimnetic oxygenation is an increasingly common lake management strategy for mitigating hypoxia/anoxia and its associated deleterious effects on water quality. A common side effect of oxygenation is increased oxygen consumption in the hypolimnion, and predicting the magnitude of the increase is the crux of effective oxygenation system design. Simultaneous measurements of sediment oxygen flux (J_{O2}) and turbulence in the bottom boundary layer of two oxygenated lakes were used to investigate the impact of oxygenation on J_{O2}. Oxygenation, particularly at high flow rates, increased J_{O2} in both lakes via two mechanisms: suppressing the thickness of the diffusive boundary layer (DBL), and increasing the bulk oxygen concentration, which steepens the diffusive gradient across the DBL. A transect along one of the lakes also showed J_{O2} to quite spatially variable, with near-field and far-field J_{O2} differing by a factor of 4. Using these *in situ* measurements, physical models of interfacial flux were compared to the observed J_{O2} to determine which models adequately predict J_{O2} in oxygenated lakes. Models based on friction velocity, turbulence dissipation rate, and the integral scale of turbulence agreed well with observed J_{O2} in both lakes. These models could potentially be used to predict induced oxygen consumption and improve oxygenation system design methods.

Keywords: diffusive boundary layer, hypolimnetic oxygenation, interfacial flux, mass transfer, sediment oxygen demand, turbulence

Introduction

Seasonal oxygen depletion is a common water-quality issue affecting many thermally stratified lakes. Oxygen (O_2) is depleted in the water column and the lake sediment by many processes, including oxidation of both organic detritus and reduced chemical species. Low dissolved oxygen (DO) in the hypolimnion can lead to increases in phosphorus, methyl-mercury, and hydrogen sulfide, and can cause reduced iron and manganese in the sediments to solubilize [*Funkey et al.* 2014; *Testa and Kemp* 2012; *Gantzer et al.* 2009a; *Beutel et al.* 2008; *Davison* 1993.]. Phosphorus can stimulate algal growth, fueling additional oxygen demand once the algae die and settle through the water column. Methyl-mercury is extremely toxic to aquatic life, capable of bioaccumulating in higher trophic levels. Hydrogen sulfide and reduced iron and manganese increase oxidant costs during drinking water treatment processes and can cause problems associated with taste, odor, and color if not adequately removed during treatment.

Sediment oxygen flux (J_{O2}) is often considered the dominant sink for DO in the hypolimnion. This flux is partly controlled by the presence of a diffusive boundary layer (DBL) immediately above the sediment, which restricts the transport of DO from the bulk hypolimnion to the sediment to diffusion only. J_{O2} is also a function of the DO gradient between the bulk hypolimnetic water and the DO concentration at the sediment-water interface (SWI); an increased concentration gradient drives increases in diffusive transport across the DBL.

Several studies have confirmed the importance of the DBL in controlling J_{O2}. Laboratory experiments using sediment core incubations linked changes in DBL and J_{O2} to water velocity [*Moore et al.* 1996; *Beutel* 2003]. Recent field studies showed J_{O2} responding to changes in near-sediment turbulence as a result of natural seiche activity [*Lorke et al.* 2003; *Bryant et al.* 2010], finding the turbulence dissipation rate to be primary driver to DBL changes, rather than current velocity. As observed by *Bryant et al.* [2010], when turbulence increases, the diffusive boundary layer (DBL) above the sediment erodes, thus decreasing the resistance to diffusive transport of DO across the SWI and increasing J_{O2}. Conversely, during relatively quiescent periods the DBL thickens, decreasing J_{O2}. Using in-situ oxygen microprofiles, *Bryant et al.* [2010] observed changes in J_{O2} on an hourly timescale by a factor of approximately six in response to changes in near-sediment turbulence and DBL thickness (δ_{DBL}).

Hypolimnetic oxygenation, which preserves thermal stratification, is increasingly used to replenish hypolimnetic DO, using a Speece Cone, airlift aerator, side-stream super-saturation system, or bubble plume diffuser to introduce oxygen into the hypolimnion [*Beutel and Horne* 1999; *Singleton and Little* 2006]. Bubble plumes, one of the more common types, are generally linear or circular and can be designed to inject either air or oxygen gas into the hypolimnion at a relatively low gas flow rate. In deeper lakes, the bulk of the bubbles dissolve within the hypolimnion and the upward momentum generated by the plume is low enough to prevent significant disruption of the thermocline. When correctly designed and operated these systems are often successful at mitigating hypoxia and its associated effects [*Müller et al.* 2014; *Debroux et al.* 2012; *Liboriussen et al.* 2009; *Gantzer et al.* 2009a; *Beutel* 2006].

Interestingly, a common side effect of bubble-plume oxygenation is increased hypolimnetic oxygen demand (HOD) [*Gantzer et al.* 2009b; *Beutel* 2003; *Moore et al.* 1996]. Elevated hypolimnetic DO concentrations resulting from oxygenation increase the DO gradient across the DBL, thus enhancing the rate of diffusive transport through the DBL and increasing J_{O2}, and can also increase oxidation in the water column due to the increased DO availability. A study by *Gantzer et al.* [2009b] which studied oxygen depletion rates in two water-supply reservoirs showed that hypolimnetic oxygen demand increases as a function of the gas flow rate applied to the oxygen diffusers.

While effective at adding O_2, bubble plumes also add energy in the hypolimnion, enhancing mixing in the near field and generating large scale circulation patterns in the hypolimnion, observed both in field experiments and computer simulations. Field observations and computer simulations from *McGinnis et al.* [2004] highlight the enhanced mixing in the bubble plume near field as a result of diffuser operation. Computer simulations by *Singleton et al.* [2010] demonstrated the ability of bubble-plume oxygenation systems to drive circulation of hypolimnetic water throughout the hypolimnion, even at low gas flow rates. Field observations by *Bryant et al.* [2010] demonstrated the importance of these large-scale currents in supplying oxygenated water to the SWI in the far field, as J_{O2} rapidly decreased after turning off the

bubble-plume diffuser, yet required approximately five days for currents to reestablish and replenish the SWI with oxygenated water.

Enhanced mixing, caused by bubble plume operation, can also enhance turbulence in the hypolimnion. This additional turbulence could drive decreases in δ_{DBL}, and thus increase J_{O2}, in a manner similar to that observed in naturally forced lakes, such as Lake Alpnach [*Lorke et al.* 2003; *Bryant et al.* 2010]. Therefore, the underlying mechanisms for the observed increases in HOD resulting from hypolimnetic oxygenation may stem from both increased hypolimnetic DO concentrations, as well as enhanced turbulence. Further, since bubble plumes affect hypolimnetic mixing and DO concentrations in the near field and far field, their influence on J_{O2} may be spatially variable as well.

Despite the current level of understanding of how bubble plumes impact lake hydrodynamics and DO distribution, it remains difficult to accurately predict bubble plume-induced HOD when designing a bubble-plume oxygen diffuser. Current best practice is to use an induced HOD multiplier as a factor of safety, as suggested by *Moore et al.* [1996], *Beutel* [2003], or others. This approach is not ideal, given that it is based on empirical equations derived from laboratory experiments, rather than being based on *in situ* data or chemically- and physically-based models. As hypolimnetic oxygenation becomes more widely used, there is a need to improve the ability to estimate induced HOD.

This study aims to investigate the effect of diffuser flow rate on both δ_{DBL} and J_{O2}, as well as the spatial variability of J_{O2}. Further, it compares in situ measurements of J_{O2} to existing physical models of interfacial flux to determine which, if any, may be appropriate for predicting J_{O2} in oxygenated lakes. An appropriate model of J_{O2} could improve our ability to predict induced HOD, improving oxygenation system design methods, operation, and management.

Methods

Study Sites

Carvin's Cove Reservoir

Carvin's Cove Reservoir (CCR) is a eutrophic water-supply reservoir in southwestern Virginia, USA, that serves as one of the primary sources of drinking water for the City of Roanoke (Table 2.1). A hypolimnetic oxygenation system consisting of two linear bubble-plume diffusers, which bubble oxygen gas into the hypolimnion, was installed near the water-treatment plant intake in 2005 to mitigate episodic increases in iron and manganese stemming from seasonal hypoxia. The oxygenation system has been quite successful at maintaining adequate hypolimnetic DO and preventing hypoxic release of reduced iron and manganese [*Gantzer et al.* 2009a].

From 26 May to 2 June 2013, a microprofiler (Unisense MP4) was deployed approximately 30 m from the midpoint of the oxygenation system to collect *in situ* microprofiles of DO in the bottom boundary layer (Figure 2.1). The field campaign was designed to capture the effect of bubble-plume diffuser flow rate on δ_{DBL} and J_{O2}. During this campaign, the diffuser flow rate was adjusted once daily, with flow rates ranging from zero to 68 NCMH, the maximum design flow rate of the oxygenation system, allowing measurement of J_{O2} across the entire range of possible diffuser flow rates. An acoustic Doppler velocimeter (ADV, Nortek Vector) was deployed on a separate mooring alongside the microprofiler and measured three-dimensional water velocity (longitudinal, transversal, and vertical) 15 cm above the SWI at 16 Hz.

Lake Hallwil

Lake Hallwil (LH) is a medium-sized lake located on the Swiss Plateau, north of Lucerne, Switzerland (Table 2.1). Early in the 20th century, phosphorous loading from the watershed increased and led to excessive algal production and seasonal anoxia in the hypolimnion of LH [*Holtzner et al.* 2012]. In 1985, six circular diffusers, 6.5 m in diameter each and arranged in a 300 m diameter circular configuration, were installed in the deep, central region of the lake to mitigate seasonal anoxia in the hypolimnion, with a target DO concentration of 4 mg L^{-1} [*Müller et al.* 2014; *Holtzner et al.* 2012]. During the summer months, oxygen-enriched air is released through the diffusers at low flow rates, supplying oxygen to the hypolimnion without disrupting thermal stratification. During winter, air is released through the diffusers at high flow rates to

enhance circulation and stimulate O_2 transfer from the atmosphere. Along with a concurrent reduction in external phosphorous loading, the diffusor system has significantly improved water quality in LH [*Müller et al.* 2014].

The microprofiler was deployed at four sites in LH from 14 May to 1 June 2012 to collect *in situ* DO microprofiles in the DBL and investigate the spatial variation of δ_{DBL} and J_{O2}. The four sites lie roughly along the main axis of the lake and are located 30, 300, and 3700 m outside the circle of diffusers, and 30 m inside the circle of diffusers (Figure 2.1). While sampling at the two locations 30 m to either side of the diffuser, the oxygenation system was turned off for 2-3 days to assess the impact of diffuser operation on J_{O2} in this near-field region. During the field campaign, the diffusers were operated in summer oxygenation mode. An acoustic Doppler velocimeter was deployed on a separate mooring alongside the microprofiler and measured three-dimensional water velocity 15 cm above the SWI at 8 Hz.

Oxygen Flux Measurements

During both field campaigns, J_{O2} was calculated from *in situ* oxygen microprofiles measured with a microprofiler equipped with a Clark-type oxygen microsensor (Unisense OX-100) and a thermocouple temperature sensor (Unisense TP-200). Triplicate measurements were made at 1 Hz at the following vertical resolutions: 10 mm resolution from 100 mm to 10 mm above the SWI, 1 mm resolution from 10 mm to 5 mm above the SWI, and 0.1 mm resolution from 5 mm above the SWI to 5 mm below the SWI. With this profiling scheme, oxygen microprofiles were obtained approximately every 50 – 55 minutes. For each profile, J_{O2} was calculated from the water-side portion using the direct method [*Bryant et al.* 2010]:

$$J_{O_2,water} = D_w \left.\frac{\partial C}{\partial z}\right|_w = D_w \frac{C_B - C_{SWI}}{\delta_{DBL}} \tag{2.1}$$

where D_w is the molecular diffusion coefficient of O_2 in water ($m^2\ d^{-1}$), $\partial C/\partial z|_w$ is the oxygen gradient in the DBL immediately above the SWI (mmol m^{-4}), C_B is the DO concentration in the bulk water in the BBL, immediately above the DBL (mmol m^{-3}), C_{SWI} is the DO concentration at

the SWI (mmol m^{-3}), and δ_{DBL} is the thickness of the DBL (m). Additionally, J_{O2} was estimated using the sediment-side of the DO microprofile using an analogous equation:

$$J_{O_2,sed} = \phi D_s \left.\frac{\partial C}{\partial z}\right|_s \tag{2.2}$$

where ϕ is the sediment porosity (m^3 voids m^{-3} volume), D_s is the molecular diffusion coefficient of O_2 in the sediment pore-water (m^2 d^{-1}; estimated as $D_s = \phi D_w$), and $\partial C/\partial z|_s$ is the oxygen gradient immediately below the SWI (mmol m^{-4}). Measurements of ϕ (0.96 for CCR; 0.94 for LH) were made from sediment cores collected from both lakes during field sampling campaigns conducted prior to those described in this study.

The location of the SWI was determined by visually examining each profile to identify the linear region in the DBL and the change in slope associated with the difference in porosity between the water column and the sediment. Standard deviations of the measurements at each point in the microprofiles were also used to aid and verify the correct positioning of the SWI, since the standard deviation in the measurements should decrease as the microsensors approach the SWI. Because the exact location of the boundary between the upper DBL and the BBL can be somewhat ambiguous when analyzing oxygen microprofiles, the "effective DBL" proposed by *Jørgensen and Revsbech* [1985] was used. This approach extrapolates the oxygen gradient at the SWI until the DO concentration is equal to C_{Bulk}, using this distance as δ_{DBL}.

Turbulence Calculations

Turbulence, quantified by the turbulent kinetic energy dissipation rate (ε), was calculated from the high-frequency velocity measurements collected with the ADV using the widely accepted inertial dissipation method [*Bryant et al.* 2010; *Grant et al.* 1962]. Dissipation rates were calculated using 50-minute segments of velocity measurements in both the CCR campaign and LH campaigns, which corresponds to the measurement period of the oxygen microprofiles. The velocity measurements were rotated such that the longitudinal velocity is maximized and the transversal velocities are minimized. The longitudinal velocity fluctuations were transformed to the wave number (k) domain, given as

$$E(k) = \alpha \varepsilon^{2/3} k^{-5/3} \tag{2.3}$$

using a value of α = (18/55). This power spectrum is then multiplied by $k^{5/3}$, providing a spectrum that is dependent only on ε when $E(k) \times k^{5/3}$ is constant. The dissipation rate is the average of this inertial subrange.

Physical Models for Interfacial Flux

The generic form of the equation for interfacial flux is given by equation 2.4, where J is the flux (M L^{-2} T^{-1}), C is the bulk concentration (M L^{-3}), C_0 is the concentration at the interface (M L^{-3}), and k_t is the transfer velocity (L T^{-1}).

$$J = k_t (C - C_0) \tag{2.4}$$

There are several proposed models for determining k_t. The Lewis-Whitman model [*O'Connor et al.* 2009; *Lewis and Whitman* 1924], also known as "thin-film theory" is one of the simplest, calculating k_t as D/δ, where D is the molecular diffusion coefficient and δ is the thickness of the mixing layer. This model is of the same form as the equations used for calculating J_{O2} from DO microprofiles (equations 2.1 and 2.2). The film renewal model [*King* 1966; *Danckwerts* 1951; *Toor and Marchello* 1958; *Higbie* 1935] calculates k_t as:

$$k_t = \sqrt{\frac{4Dr}{\pi}} \tag{2.5}$$

where r is the renewal frequency, which is a characteristic of the turbulence, and can be calculated using the small-eddy or large-eddy estimates. The small-eddy estimate of r is based on the Kolmogorov time scale, and is calculated as:

$$r = \sqrt{\frac{u_*^3}{h\nu}} \tag{2.6}$$

where u_* is the shear velocity, h is the shear layer depth, and v is viscosity. The large-eddy estimate is based on the integral time scale of the turbulence (t_I), and is simply calculated as:

$$r = \frac{1}{t_I} \tag{2.7}$$

Many studies in the literature use a scaling relationship to estimate k_t using an equation of the form:

$$k_t = \alpha u_* Sc^{\beta} \tag{2.8}$$

where α and β are empirical parameters and Sc is the Schmidt number. Typical values for α range from 0.052 – 0.164, and values for β range from -7/10 – -2/3, with -2/3 most commonly used. This equation is derived from theory and scaling arguments, arguing that k_t is a function of u_*. For the current study, we use α = 0.164 and β = -2/3 to calculate k_t, following *O'Connor et al.* [2009] and *O'Connor and Hondzo* [2008a], which found these values to be the best fit for calculating J_{O2} in a laboratory flume.

Yet another model for determining k_t was suggested by *Lorke and Peters* [2006] and is based on the Batchelor scale [*Batchelor* 1959]. This model calculates the transfer velocity as:

$$k_t = \frac{1}{2\pi} Sc^{-1/2} \left(\varepsilon \nu\right)^{1/4} \tag{2.9}$$

Lorke and Peeters proposed this model as a potential universal scaling relationship for interfacial flux. Law-of-the-wall scaling is often assumed to be valid in the bottom boundary layer in lakes. This assumption may not always be valid, however, as wind-driven lakes may have an oscillatory boundary layer, under which law-of-the-wall conditions fail to reliably predict bottom boundary layer dynamics [*Lorke and Peeters* 2006; *Lorke et al.* 2002]. Since this model is based on the turbulence dissipation rate, rather than friction velocity, it allows for estimates of k_t under conditions where the law-of-the-wall is not a valid assumption.

Using the turbulence data calculated from the ADV data, the film renewal model (with both large-eddy and small-eddy estimates) as well as the u_* scaling relationship (hereafter referred to as the u_* model) and *Lorke and Peters* model were used to calculate the average transfer velocity for every 24-hour period of field data. This transfer velocity was then multiplied by the average difference between the bulk water DO concentration and the DO concentration at the SWI (C_B - C_{SWI}) as measured with the microprofiler over the same 24-hour period, to obtain daily estimates of J_{O2} based on these interfacial flux models. The predicted J_{O2} from these models are compared to the observed J_{O2} calculated from the water side of the oxygen microprofiles for each microprofiler deployment, using the root mean square error (RMSE; equation 2.10).

$$RMSE = \sqrt{\frac{1}{n}\sum_{i=1}^{n}\left(J_{O_2,sim_i} - J_{O_2,obs_i}\right)^2} \tag{2.10}$$

Results and Discussion

Carvin's Cove Reservoir

DO concentrations measured in the bottom 10 cm of the water column with the microprofiler are displayed in Figure 2.2 as time series plots with the calculated J_{O2} values overlaid, along with measured δ_{DBL} and the bubble-plume diffuser gas flow rate, showing the stepped flow rate adjustment scheme. This data is also shown in Figure 2.3 as boxplots to more clearly show the effect of diffuser flow rate on J_{O2}, DO concentrations, and δ_{DBL}. DO concentrations in this portion of the water column typically ranged from about 3.5 – 7 mg L^{-1}. J_{O2} typically ranged from approximately 2 – 12 mmol m^{-2} d^{-1} and δ_{DBL} generally varied from 0.5 – 6 mm. Observed water velocities were low, typically less than 2.5 cm s^{-1}, with infrequent spikes up to ~ 5 cm s^{-1}. Turbulence dissipation rates calculated from this data ranged from 1.57×10^{-12} – 1.17×10^{-8} W kg^{-1}, with a mean of 5.43×10^{-10} W kg^{-1}. A time series of the dissipation rates is shown in Figure 2.4. A detailed analysis of velocity measurements and the effects of diffuser operation on CCR hydrodynamics can be found in *Rezvani et al.* [2015].

When the diffuser is operated at relatively high flow rates (above ~35 NCMH), the DO overlaying the SWI is relatively high, around 6 – 7 mg L^{-1}, but decreases to almost 4 mg L^{-1}

when the diffuser is operated at low flow rates (less than ~35 NCMH) or turned off. J_{O2} and δ_{DBL} are also influenced by the diffuser flow rate. While the diffuser is operated at relatively high flow rates, δ_{DBL} generally decreases to ~ 2mm or less and J_{O2} concurrently increases to generally 6 – 12 mmol m^{-2} d^{-1}. At lower flow rates (less than ~35 NCMH) no clear relationship between diffuser flow rate and either δ_{DBL} or J_{O2} can be deciphered. This suggests that the impact of the flow rate on δ_{DBL} and J_{O2} is minimized at low flow rates and naturally forced hypolimnetic circulation patterns exert an equal or greater control on δ_{DBL} and J_{O2}, somewhat masking the influence of the bubble plume.

These findings show the capability of bubble-plume diffusers to enhance J_{O2} via two distinct pathways: decreasing the resistance to diffusion by decreasing δ_{DBL} and increasing the diffusive gradient by increasing bulk water DO concentrations. When the oxygen diffuser is operated at high flow rates, bubble-plume induced currents suppress δ_{DBL}, thus reducing resistance to diffusive transport and enhancing J_{O2}. Second, the elevated DO concentrations overlaying the SWI increase the concentration gradient at the SWI, thus driving additional O_2 into the sediment and increasing the observed J_{O2}. At lower gas flow rates, when the bubble-plume induced turbulence is weak enough to be on par with or overshadowed by naturally forced turbulence, this increase in bulk water DO may be the primary mechanism for the increased J_{O2} and HOD that is typically observed in oxygenated water bodies. Even at relatively high diffuser flow rates, when the effect of plume-enhanced turbulence can be observed, elevated DO in the bulk water is still an important mechanism for increasing HOD in oxygenated lakes, since fluctuations in J_{O2} respond to fluctuations in DO at the SWI at all flow rates (Figure 2.2).

A previous study on CCR [*Bryant et al*. 2011] focused on the effects of diffuser operation in the far field, finding that diffuser operation was necessary to maintain a continuous supply of DO to the SWI. When the diffuser was turned off, the water near the SWI rapidly became anoxic, and oxic conditions did not reestablish until approximately five days after the diffuser had been turned on. The CCR 2013 field study, along with the *Bryant et al.* study, shows the impact and importance of diffuser-induced currents on enhancing J_{O2} in both the plume near-field and far-field.

Bryant et al. [2011] also observed a much clearer relationship between J_{O2} and ε than was observed in the CCR 2013 campaign. This can likely be attributed to the differences in methods for estimating ε in the two studies: the current study calculated ε from direct measurements of velocity in the bottom boundary layer, while *Bryant et al.* calculated ε based on δ_{DBL} as measured from oxygen microprofiles and assuming law-of-the-wall conditions. Velocity profiles in the bottom boundary layer, measured with an ADCP (Nortek Aquadopp) during the CCR 2013 field study showed that the bottom boundary layer in CCR is oscillatory and therefore often deviates from law-of-the-wall scaling [*Rezvani et al.* 2015].

Lake Hallwil

Similar interactions between the oxygenation system and DO concentrations, J_{O2}, and δ_{DBL} were observed in Lake Hallwil. Figure 2.5 displays the DO concentrations in the bottom 10 cm of the water column as measured with the microprofiler from 28 May to 1 June, when the microprofiler was deployed 30 m outside the diffuser ring, with calculated J_{O2} values overlaid. The six circular diffusers were operating at a combined flow rate of 130 NCMH (air and oxygen mixture) before being turned off on 30 May. As observed in CCR, the DO in the water near the sediment was higher during diffuser operation (~4.5 – 5.5 mg L^{-1}) than when the diffusers were not in operation (~3.5 – 4 mg L^{-1}). J_{O2} was also significantly higher when the diffusers were operating (range: 4.5 – 17.5 mmol m^{-2} d^{-1}; mean = 10.7 mmol m^{-2} d^{-1}) than when the diffusers were turned off (range: 3.4 – 11.0 mmol m^{-2} d^{-1}; mean = 7.2 mmol m^{-2} d^{-1}), an increase of nearly 50% in average J_{O2}. δ_{DBL} was slightly smaller while the diffusers were operating (range: 0.125 – 2.54 mm; mean = 0.61 mm) than when the diffusers were turned off (range: 0.180 – 2.84 mm; mean = 0.64 mm). Water velocities were typically less than 2 cm s^{-1}, but increased up to 4 cm s^{-1} for brief periods. Dissipation rates calculated from the ADV data ranged from 4.60×10^{-12} – 1.19×10^{-8} W kg^{-1}, with a mean of 1.09×10^{-9} W kg^{-1}. A time series of the dissipation rates is shown in Figure 2.6. As with CCR, a detailed analysis and discussion of the velocity measurements and the interaction between the bubble plume diffuser and the lake hydrodynamics in LH can be found in *Rezvani et al.* [2015].

Similar to the observations made in CCR, operation of the oxygen diffusers in LH enhances J_{O2} through both physical and chemical pathways. When the diffuser is operating, it generates

additional turbulence, which decreases δ_{DBL} and enhances J_{O2}. The diffuser also supplies DO to the surrounding water, increasing the DO concentration gradient across the SWI, and subsequently increasing J_{O2}. We can infer that the increased availability of DO is the primary driver of the observed increases in J_{O2} when the diffuser is operating, given that statistically significant differences are observed in J_{O2} ($p = 2.55\times10^{-6}$, $\alpha = 0.05$) but not in δ_{DBL} ($p = 0.77$, $\alpha = 0.05$) using a student's t-test. If δ_{DBL} is not significantly different during diffuser operation (even though it was observed to be slightly smaller with the diffuser on), k_t must be relatively constant. Thus, an increase in the DO gradient at the SWI due to increased bulk water DO must be the primary driver for the observed increases in J_{O2}.

The longitudinal transect in LH with the microprofiler showed J_{O2} to be quite spatially variable. The mean and range of observed J_{O2} at each of the four locations is displayed in Figure 2.7. J_{O2} increased with increasing distance from the center of the diffuser ring, ranging from an average of 3.9 mmol m^{-2} d^{-1} at the site 30 m inside the diffuser ring to 12.4 mmol m^{-2} d^{-1} at the site 3700 m from the oxygen diffusers. The DO concentration near the sediment is likely a primary driver for this, given that the DO concentration also steadily increased with distance from the center of the diffuser ring. DO concentrations near the SWI were < 3 mg L^{-1} 30 m inside the diffuser ring, ~4 mg L^{-1} 30 m outside the diffuser ring, ~5.5 mg L^{-1} 300 m from the diffuser ring, and ~6.5 mg L^{-1} 3700 m from the diffusers. As the DO concentration in the overlaying water increases, the concentration gradient across the SWI becomes greater, resulting in enhanced oxygen flux across the SWI. Differences in temperature among the sampling sites may also explain a portion of this variability, since increases in temperature may enhance J_{O2}. Temperature was observed to increase with distance from the center of the diffuser ring, however this likely explains only a relatively small portion of the variability observed in J_{O2}, as the differences in temperatures were only around 1°C. Additional factors, beyond the scope of this study, could also be contributing to the observed spatial pattern in J_{O2}. For example, settling organic matter and detritus may be oxidized to a variable extent in the water column before it is incorporated into the sediment. Organic matter in the deeper regions of LH may be more completely oxidized due to the increased exposure to DO (a result of both increased settling depth and oxygenation system operation) before reaching the sediment. Organic matter in shallower portions of the lake are less affected by the oxygenation system operation and have less time to react with DO in the

water column before reaching the sediment; therefore sediments in these regions may have more labile carbon which can exert additional demand for DO, increasing J_{O2}.

Field Data and Interfacial Flux Models Comparison

Figure 2.8 and Figure 2.9 compare daily averages of J_{O2} measured in CCR and LH to values estimated using the interfacial flux models described in this study. J_{O2} calculated using the small-eddy film renewal model is consistently much higher than the J_{O2} measured in situ, overestimating the observed J_{O2} by a factor of 5 or more in all cases. The large-eddy film renewal model, u_* model, and Lorke and Peters model agree reasonably well with observed J_{O2} in both CCR and LH, yet all three are based on different characteristics of turbulent flow. The large-eddy film renewal model and Lorke and Peeters models are based on very different scales and yet yield similar results. The integral timescale in the CCR and LH studies is on the order of 10^1 m, while the Batchelor length scale is on the order of $10^{-3} – 10^{-4}$ m. The u_* model is based on shear stress at the SWI and yet also yields reasonable estimates of J_{O2}. The RMSE shown in Table 2.2 suggest that the large-eddy film renewal model may provide a slightly improved fit over the Lorke and Peeters model and u_* model in LH, while the u_* model provides the best fit in CCR, performing slightly better than the large-eddy film renewal model. The differences between the RMSE from these models are relatively small and may be a result of the limited sample size (n = 6 for CCR; n = 11 for LH). All of these three models seem to provide reasonable estimates of k_t and J_{O2} in both CCR and LH.

Similar studies comparing J_{O2} to interfacial flux models are somewhat lacking in the literature. *O'Connor et al.* [2009] compared experimental measurements of J_{O2} from a recirculating flume [*O'Connor and Hondzo* 2008a,b] to the Lewis-Whitman, film-renewal, and u_* models, finding the film-renewal model to provide the best estimates of k_t. For their study, *O'Connor and Hondzo* [2008a] used particle image velocimetry (PIV) to characterize the renewal frequency used for the film-renewal model, basing r on the period between sweep and eject motions measured with their PIV and ADV experimental setup. To our knowledge, the current study is the first study to compare various models of k_t to simultaneous *in situ* field measurements of J_{O2}, velocity, and turbulence.

In their paper, *Lorke and Peeters* [2006] call for a "new generation of experiments" which couple turbulence measurements with estimates of k_t, as done in the current study, to test the proposed scaling relationship given in equation 2.9. Figure 2.10 presents the transfer velocities calculated using J_{O2} measurements, normalized by the Schmidt number, as a function of the observed turbulence dissipation rate. The line representing the *Lorke and Peeters* model agrees quite well with the observed transfer velocities in CCR, but shows somewhat less agreement with the observed k_t in LH, especially at low dissipation rates. While this supports the idea that this model could represent a universal model for calculating k_t, the J_{O2} calculated using this model does not appear to be a marked improvement over J_{O2} as calculated by the large-eddy or u_* models (Figure 2.8 and Figure 2.9).

Conclusions

Hypolimnetic oxygenation is a lake management strategy that is becoming increasingly common, particularly bubble-plume oxygenation systems. Despite their capability to increase hypolimnetic DO concentrations in deep lakes and reservoirs, oxygenation systems typically stimulate an increase in DO consumption, the magnitude of which is difficult to predict accurately while designing the system.

Field studies in CCR and LH both showed the capability of bubble-plume oxygenation systems to influence J_{O2} through both physical and chemical mechanisms. When the oxygenation systems are operating and supplying additional DO to the hypolimnion, the DO concentration in the bulk hypolimnetic water increases and creates a stronger concentration gradient across the SWI. This drives additional DO to the SWI, enhancing J_{O2}, as observed in both field studies. Additionally, when the oxygenation systems are operated at relatively high flow rates, the additional turbulence caused by the bubble plumes can decrease δ_{DBL}, which also reduces the diffusive resistance to oxygen transport and increases J_{O2}. This phenomena was observed in CCR at flow rates greater than ~35 NCMH. The combination of an elevated concentration gradient at the SWI and a thinning of the DBL leads to the increase in oxygen demand that is normally observed when oxygenation systems are operating.

The small-eddy film renewal model consistently over predicted J_{O2}, while the large-eddy film renewal model, u_* model, and Lorke and Peeters models scale well with measured values of J_{O2}, despite being based on very different characteristics of turbulent flows. These models could be appropriate to include in hydrodynamic models to link lake hydrodynamics to J_{O2}. Incorporating these interfacial flux models into a hydrodynamic model could lead to improvements in design and operation of hypolimnetic oxygenation systems by refining our ability to predict the spatial and temporal variability in J_{O2} in response to oxygenation system operations.

References

Batchelor, G. K. (1959), Small-scale variation of convected quantities like temperature in turbulent fluid, *Journal of Fluid Mechanics,* 5 (1), 113-133.

Beutel, M. W. (2003), Hypolimnetic anoxia and sediment oxygen demand in California drinking water reservoirs, *Lake and Reservoir Management,* 19(3), 208-221.

Beutel, M. (2006), Inhibition of ammonia release from anoxic profundal sediments in lakes using hypolimnetic oxygenation, *Ecological Engineering,* 28(3), 271-279.

Beutel, M. W. and A. J. Horne (1999), A review of the effects of hypolimnetic oxygenation on lake and reservoir water quality, *Lake and Reservoir Management,* 15(4), 285-297.

Beutel, M. W., T. M. Leaonard, S. R. Dent, and B. C. Moore (2008), Effects of aerobic and anaerobic conditions on P, N, Fe, Mn, and Hg accumulation in waters overlaying profundal sediments of an oligo-mesotrophic lake, *Water Research,* 42(8-9), 1953-1962.

Bryant, L. D., C. Lorrai, D. F. McGinnis, A. Brand, A. Wüest, and J. C. Little (2010), Variable sediment oxygen uptake in response to dynamic forcing, *Limnology and Oceangraphy,* 55(2), 950-964.

Bryant, L. D., D. F. McGinnis, C. Lorrai, A. Brand, J. C. Little, and A. Wüest (2010), Evaluating oxygen fluxes using microprofiles from both sides of the sediment-water interface, *Limnology and Oceanography: Methods,* 8, 610-627.

Bryant, L. D., P. A. Gantzer, and J. C. Little (2011), Increased sediment oxygen uptake caused by oxygenation-induced hypolimnetic mixing, *Water Research,* 45(12), 3692-3703.

Danckwerts, P. V. (1951), Significance of liquid-film coefficients in gas absorption, *Industrial and Engineering Chemistry,* 43(6), 1460-1467.

Davison, W. (1993), Iron and manganese in lakes, *Earth-Science Reviews,* 34, 119-163.

Debroux, J. F., M. W. Beutel, C. M. Thompson, and S. Mulligan (2012), Design and testing of a novel hypolimnetic oxygenation system to improve water quality in Lake Bard, California, *Lake and Reservoir Management,* 28(3), 245-254.

Funkey, C. P., D. J. Conley, N. S. Reuss, C. Humborg, T. Jilbert, and C. P. Slomp (2014), Hypoxia sustains cyanobacteria blooms in the Baltic Sea, *Environmental Science and Technology,* 48(5), 2598-2602.

Gantzer, P. A., L. D. Bryant, and J. C. Little (2009a), Controlling soluble iron and manganese in a water-supply reservoir using hypolimnetic oxygenation, *Water Research,* 43(5), 1285-1294.

Gantzer, P. A., L. D. Bryant, and J. C. Little (2009b), Effect of hypolimnetic oxygenation on oxygen depletion rates in two water-supply reservoirs, *Water Research,* 43(6), 1700-1710.

Higbie, R. (1935), The rate of absorption of a pure gas into a still liquid during short periods of exposure, *Transactions of the American Institute of Chemical Engineers,* 31, 365-389.

Holzner, C. P., Y. Tomonaga, A. Stöckli, N. Denecke, and R. Kipfer (2012), Using noble gases to analyze the efficiency of artificial aeration in Lake Hallwil, Switzerland, *Water Resources Research,* 48, W09531, doi:10.1029/2012WR012030.

Jørgensen B. B. and N. P. Revsbech (1985), Diffusive boundary layers and the oxygen uptake of sediments and detritus, *Limnology and Oceanography,* 30(1), 111-122.

King, C. J. (1966), Turbulent liquid phase mass transfer at a free gas-liquid interface, *Industrial and Engineering Chemistry Fundamentals,* 5(1), 1-8.

Lewis, W. K., and W. G. Whitman (1924), Principles of Gas Absorption, *Industrial and Engineering Chemistry,* 16(12), 1215-1220.

Liboriussen, L, M. Søndergaard, E. Jeppesen, I. Thorsgaard, S. Grünfeld, T. S. Jakobsen, and K. Hansen (2009), Effects of hypolimnetic oxygenation on water quality: results from five Danish lakes, *Hydrobiologia*, 625(1), 157-172.

Lorke, A., B. Müeller, M. Maerki, and A. Wüest (2003), Breathing sediments: The control of diffusive transport across the sediment-water interface by periodic boundary-layer turbulence, *Limnology and Oceanography,* 48(6), 2077-2085.

Lorke, A. and F. Peeters (2006), Toward a unified scaling relation for interfacial fluxes, *Journal of Physical Oceanography,* 36(5), 955-961.

Lorke, A., L. Umlauf, T. Jonas, and Wüest, A. (2002), Dynamics of turbulence in low-speed oscillating bottom-boundary layers of stratified basins, *Environmental Fluid Mechanics,* 2(4), 291-313.

McGinnis, D. F., A. Lorke, A. Wüest, A. Stöckli, and J. C. Little (2004), Interaction between a bubble plume and the near field in a stratified lake, *Water Resources Research,* 40, W10206, doi:10.1029/2004WR003038.

Moore, B. C., P. Chen, W. H. Funk, and D. Yonge (1996), A model for predicting lake sediment oxygen demand following hypolimnetic aeration, *Water Resources Bulletin,* 32(4), 723-731.

O'Connor, B. L., M. Hondzo, and J. W. Harvey (2009), Incorporating both physical and kinetic limitations in quantifying dissolved oxygen flux to aquatic sediments, *Journal of Environmental Engineering,* 135(12), 1304-1314.

O'Connor, B. L., and M. Hondzo (2008a), Dissolved oxygen transfer to sediments by sweep and eject motions in aquatic environments, *Limnology and Oceanography,* 53(2), 566-578.

O'Connor, B. L., and M. Hondzo (2008b), Enhancement and inhibition of denitrification by fluid-flow and dissolved oxygen flux to stream sediments, *Environmental Science and Technology,* 42(1), 119-125.

Rezvani, M., K. A. Bierlein, S. A. Socolofsky, and J. C. Little (2015), TITLE, Manuscript in preparation.

Singleton, V. L. and J. C. Little (2006), Designing hypolimnetic aeration and oxygenation systems - a review, *Environmental Science and Technology,* 40(24), 7512-7520.

Singleton, V. L., F. J. Rueda, and J. C. Little (2010), A coupled bubble plume-reservoir model for hypolimnetic oxygenation, *Water Resources Research,* 46, W12538, doi:10.1029/2009WR009012.

Testa, J. M., and W. M. Kemp (2012), Hypoxia-induced shifts in nitrogen and phosphorus cycling in Chesapeake Bay, *Limnology and Oceanography,* 57(3), 835-850.

Toor, H. L., and J. M. Marchello (1958), Film-penetration model for mass and heat transfer, *A.I.Ch.E. Journal,* 4(1), 97-101.

Table 2.1. Physical characteristics of Carvin's Cove Reservoir and Lake Hallwil

	Carvin's Cove Reservoir	Lake Hallwil
Max. Depth (m)	22	48
Surface Area (km^2)	2.5	9.95
Volume (m^3)	24×10^6	285×10^6
Elevation (m amsl)	357	449

Table 2.2. Root mean squared error (RMSE) from comparing 24-hour averages of observed J_{O2} to calculated J_{O2} from interfacial flux models (n = number of data points). RMSE is given in mmol m^{-2} d^{-1}.

	Small Eddy	Large Eddy	u* model	Lorke and Peeters	n
CCR 2013	47.1	1.6	1.4	2.4	6
LH1	92.1	3.9	6.6	9.4	3
LH2	101.6	6.1	5.1	3.3	2
LH3	68.4	7.8	6.5	5.2	2
LH4	29.9	3.9	4.7	3.1	4
LH (All)	73.3	5.2	5.7	5.9	11

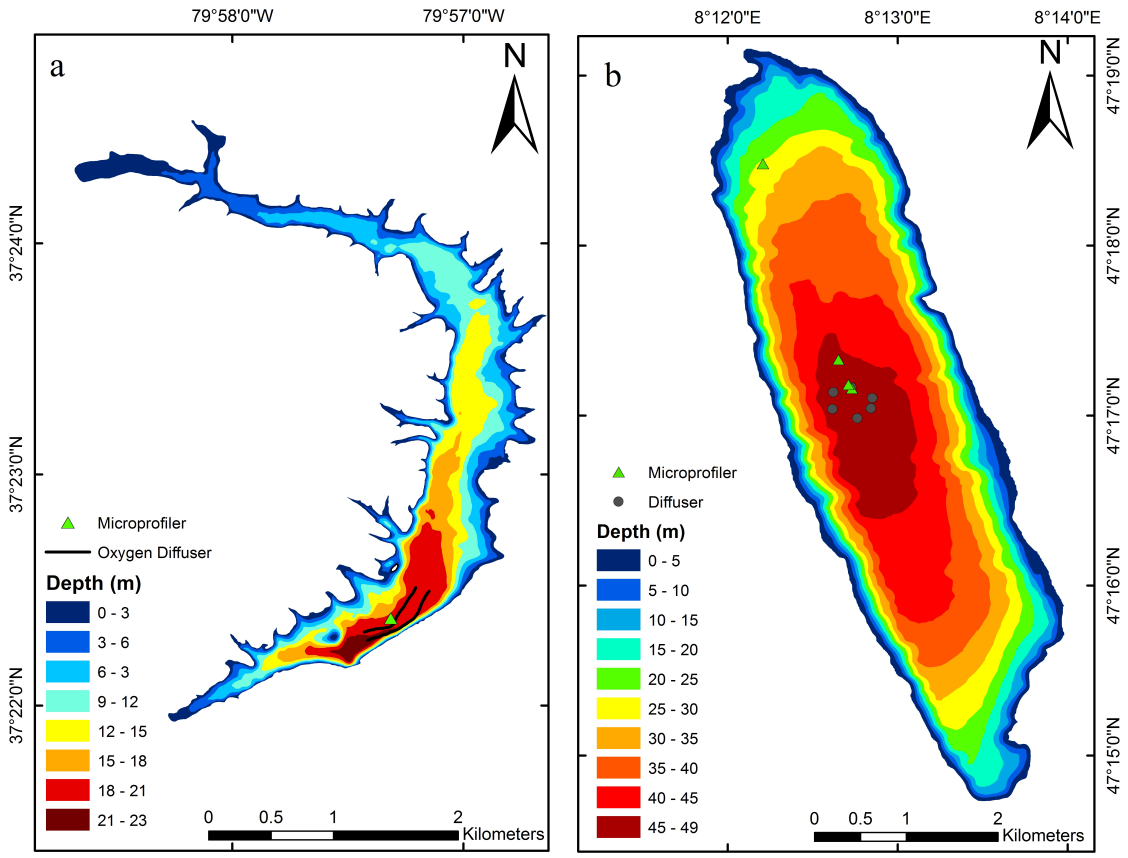

Figure 2.1. Bathymetric maps of (a) Carvin's Cove Reservoir and (b) Lake Hallwil

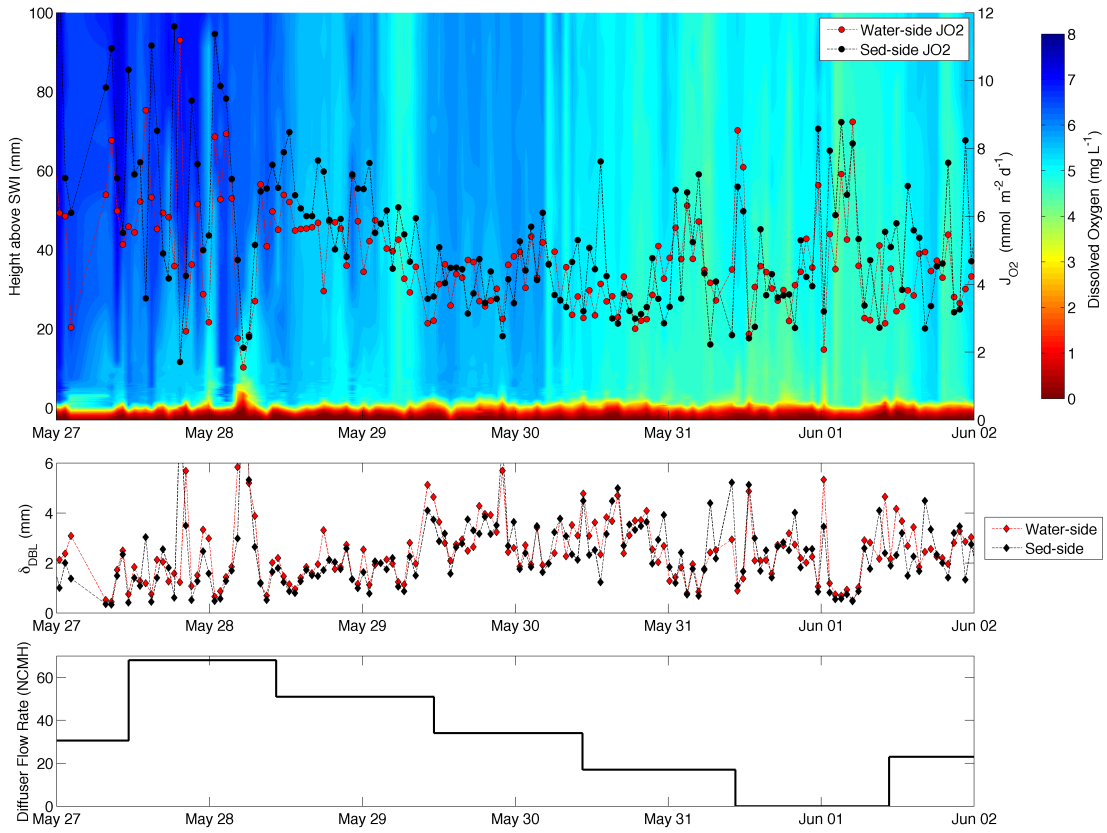

Figure 2.2. Timeseries of dissolved oxygen concentration, J_{O2}, and δ_{DBL}, measured with the microprofiler, and the stepped oxygenation system flow rate regime during the Carvin's Cove 2013 field campaign

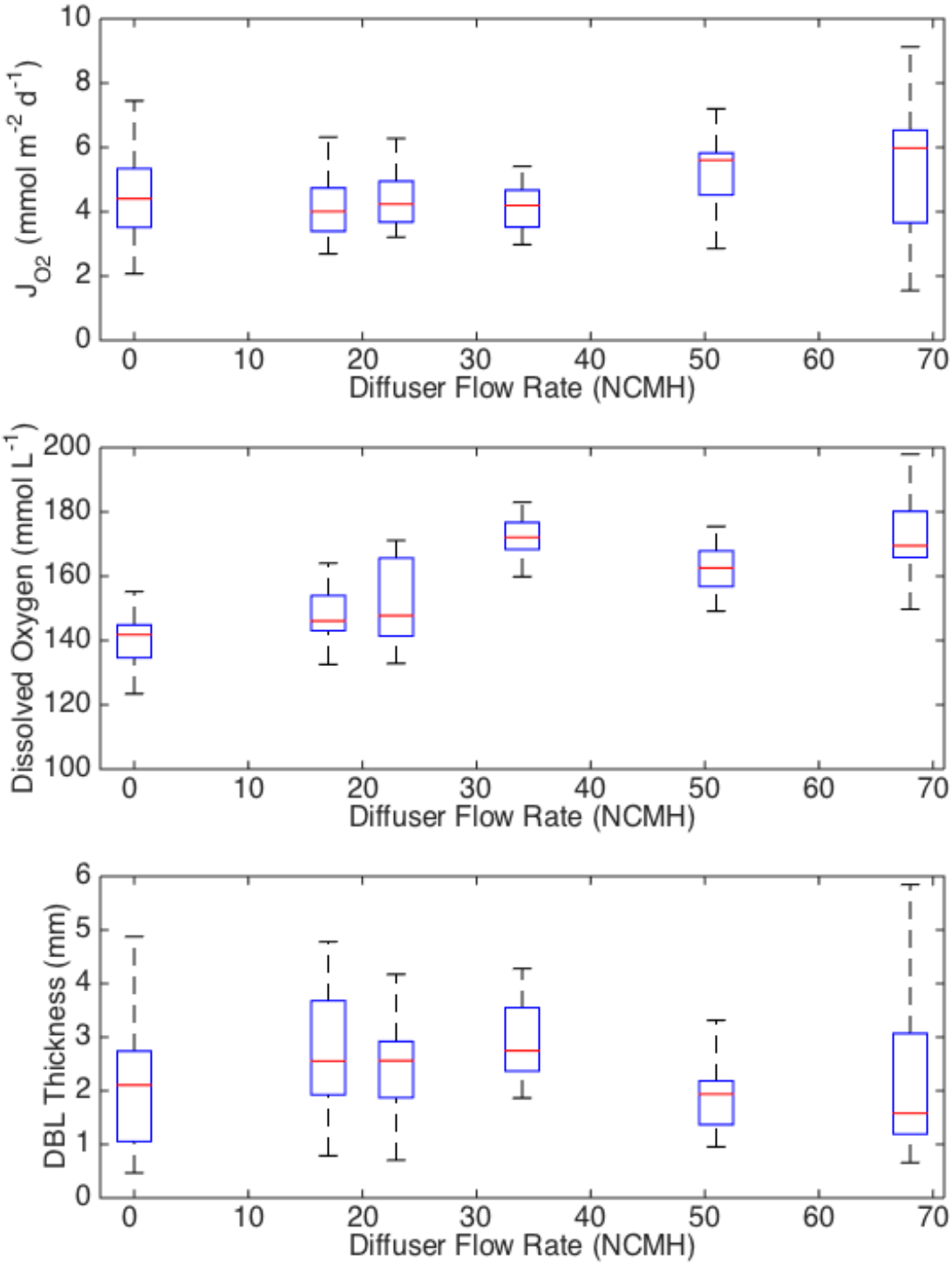

Figure 2.3. Measured sediment oxygen flux (upper panel), bulk dissolved oxygen concentrations above the sediment (middle panel), and diffusive boundary layer thickness (bottom panel) plotted against the oxygen diffuser flow rate. Red lines represent the mean, the blue boxes encompass the 25th to 75th percentile, and the whiskers represent the maximum and minimum.

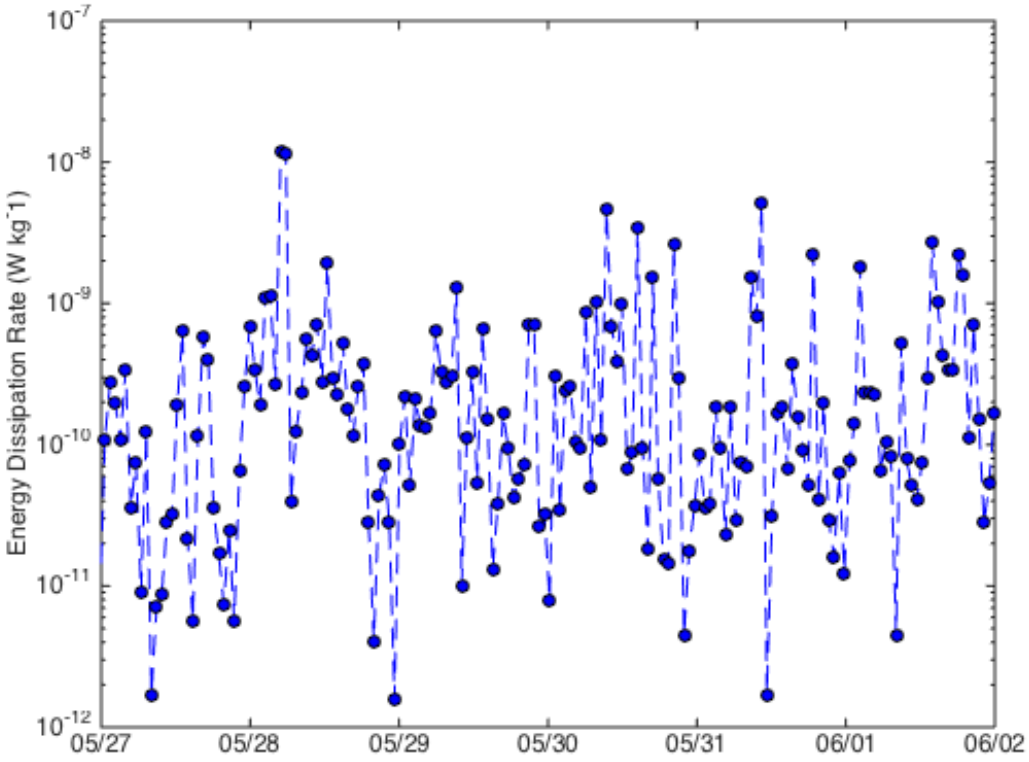

Figure 2.4. Timeseries of turbulence dissipation rates, calculated from ADV velocity measurements, during the Carvin's Cove 2013 field campaign.

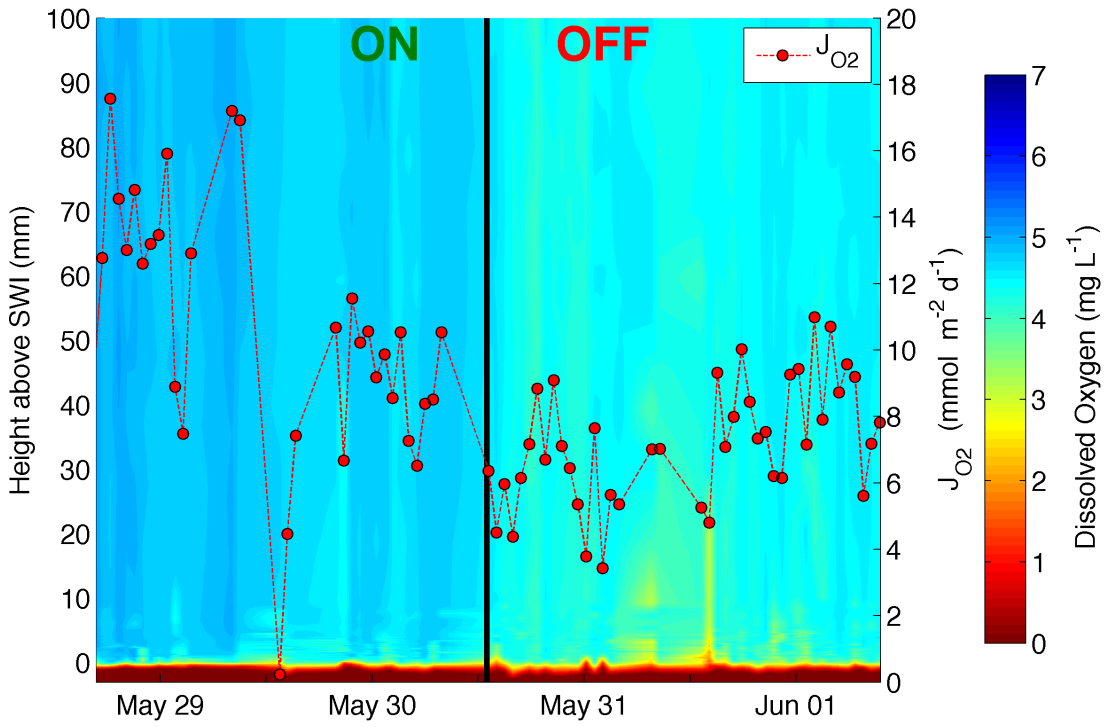

Figure 2.5. Timeseries of dissolved oxygen concentration and J_{O2}, measured with the microprofiler, during the Lake Hallwil 2012 field campaign

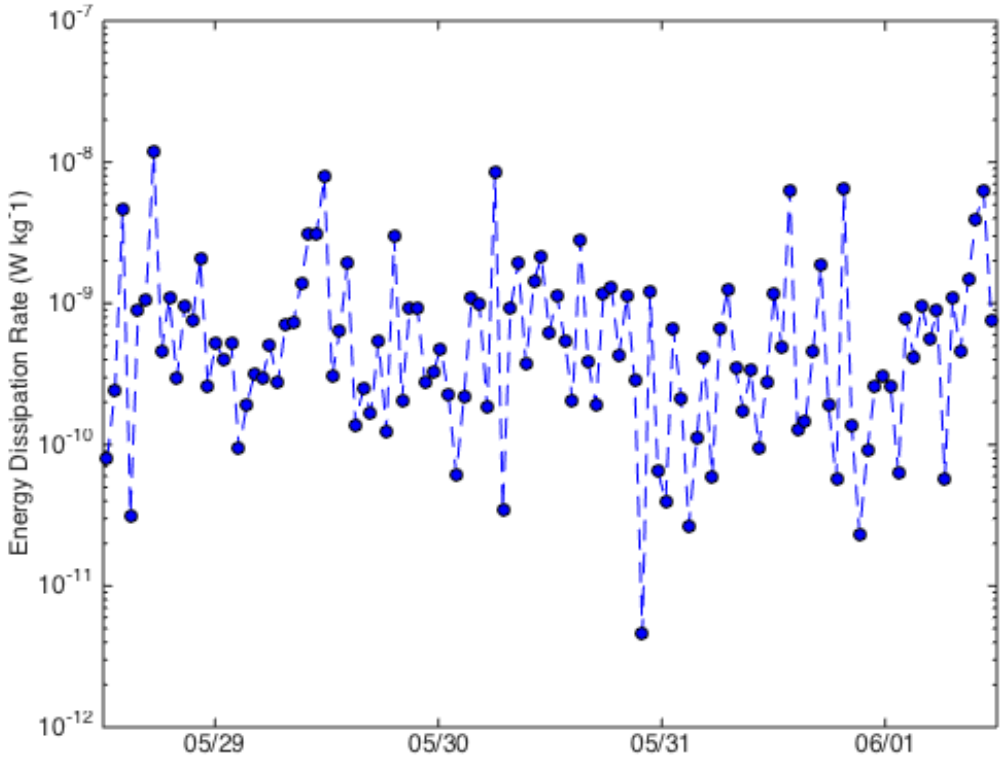

Figure 2.6. Timeseries of turbulence dissipation rates, calculated from ADV velocity measurements, during the Lake Hallwil 2012 field campaign

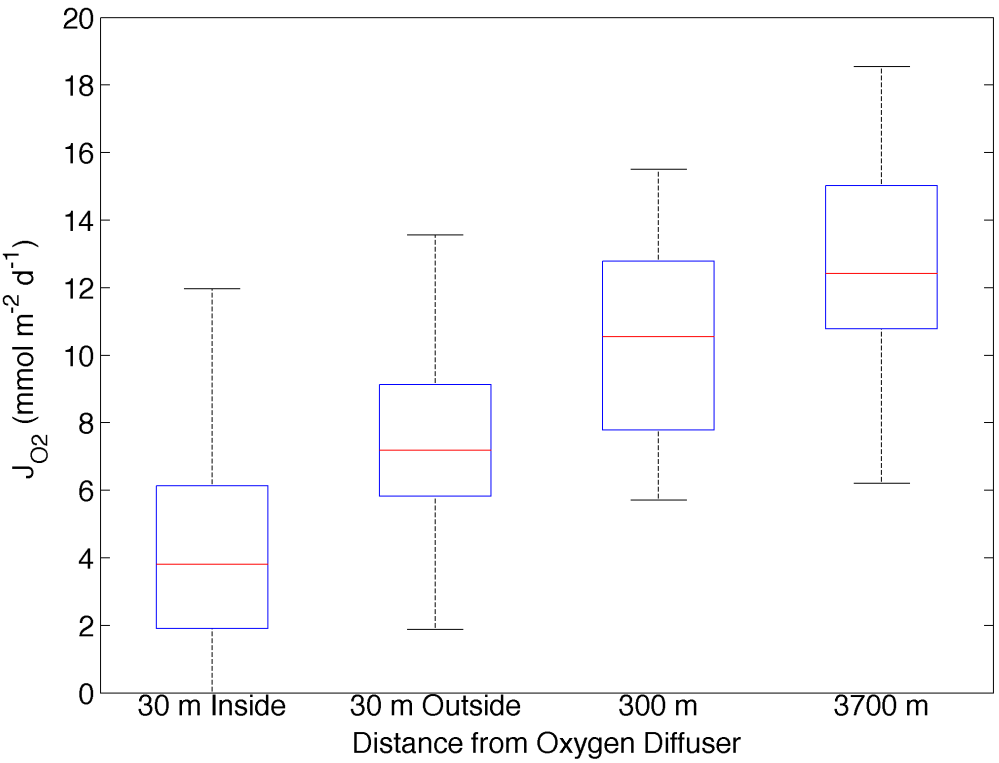

Figure 2.7. Distribution of measured J_{O2} during each deployment of the microprofiler during the spatial transect of Lake Hallwil in 2012. The red lines represent mean J_{O2}, the blue boxes encompass the 25th to 75th percentile, and the whiskers represent the maximum and minimum J_{O2}

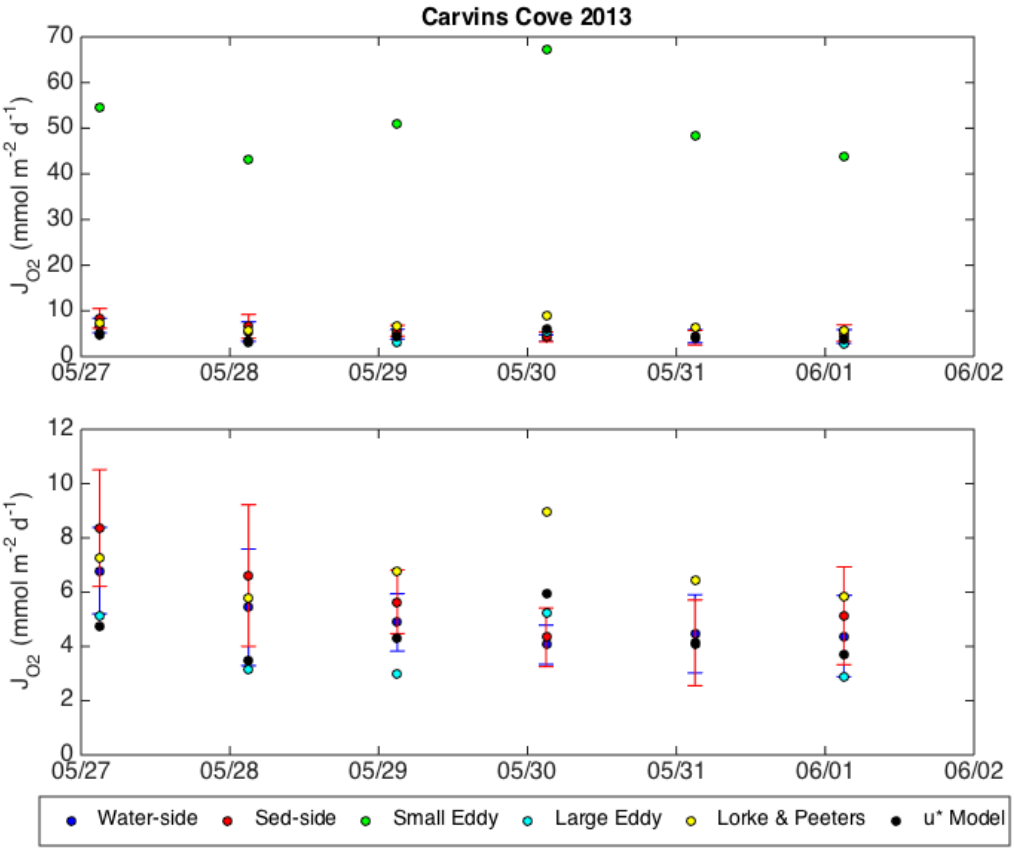

Figure 2.8. Measured J_{O2} from the microprofiler compared to J_{O2} calculated from interfacial flux models for the Carvin's Cove 2013 field campaign. Data in the upper and lower panels are identical, however the vertical axis is in the lower panel is scaled to exclude the small eddy model and better show the differences between the remaining interfacial flux models and the measured J_{O2}.

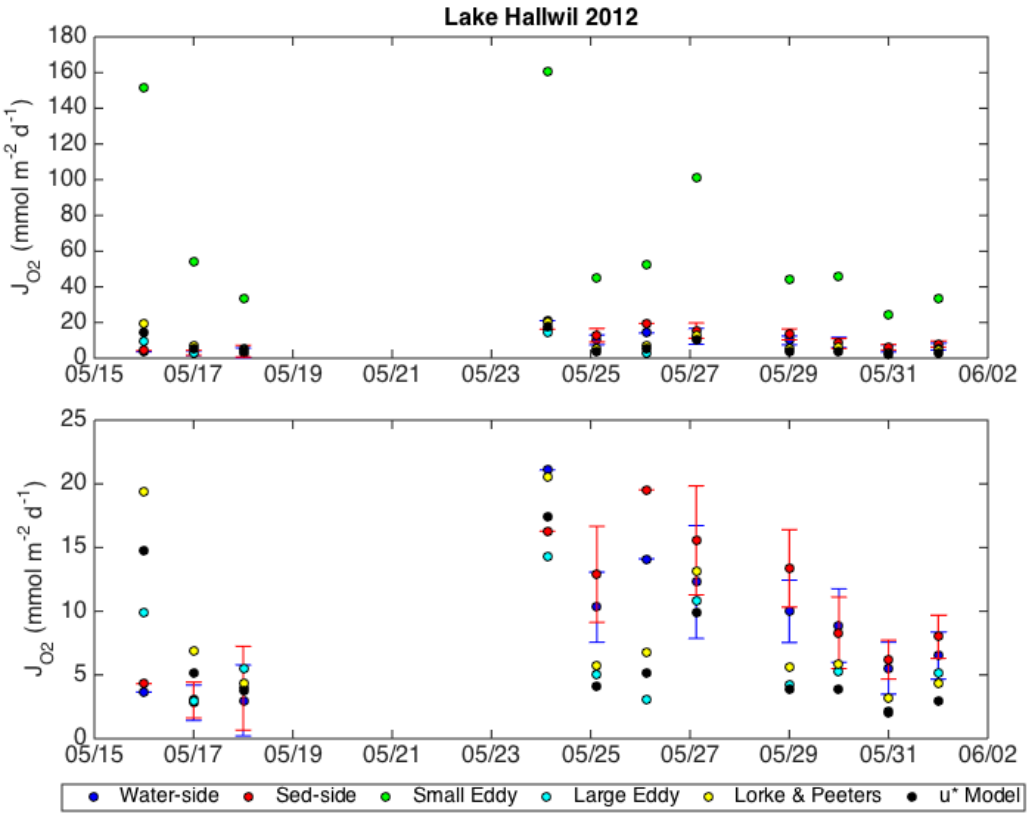

Figure 2.9. Measured J_{O2} from the microprofiler compared to J_{O2} calculated from interfacial flux models for the Lake Hallwil 2012 field campaign. Data in the upper and lower panels are identical, however the vertical axis in the lower panel is scaled to exclude the small eddy model and better show the differences between the remaining interfacial flux models and the measured J_{O2}.

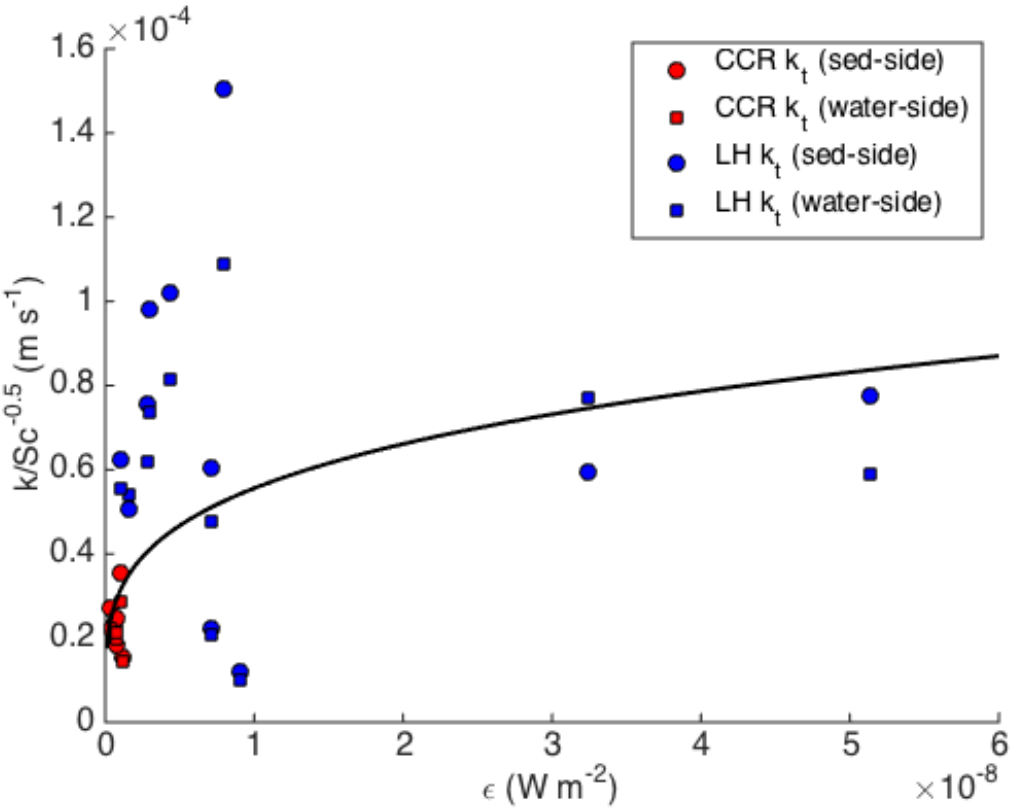

Figure 2.10. Observed transfer velocity (k_t, calculated from oxygen microprofiles) normalized by the Schmidt number versus the observed turbulence dissipation rate. The black line represents the universal scaling relationship proposed by *Lorke and Peeters* [2006].

Chapter 3. A Transient Model of Dissolved Oxygen Kinetics in Lake Sediment

Kevin A. Bierlein[a], Lee D. Bryant[b], and John C. Little[a]

[a]Via Department of Civil and Environmental Engineering, Virginia Tech, 418 Durham Hall, Blacksburg, Virginia, USA

[b]Department of Architecture and Civil Engineering, University of Bath, Bath, United Kingdom

Abstract

A transient model of dissolved oxygen in freshwater sediment was developed, accounting for diffusion and consumption of oxygen in the sediment pore water. Using oxygen microprofiles measured *in situ* in two oxygenated lakes, the model was fit to the microprofiles using zero-order and first-order kinetics to determine which kinetic model most appropriately describes the rate of oxygen consumption within the sediment. Based on goodness-of-fit measures and visual inspection, zero-order kinetics was found to more accurately describe oxygen consumption than first-order kinetics in one lake, while it was less clear in the other lake as to which model is better. Fitted zero-order rate constants ranged from 78 – 591 mg L^{-1} d^{-1}, with variability observed between the two lakes, and within the lakes as well, largely attributed to differences in sediment composition. These rate constants, the first to be obtained from *in situ* microprofiles, agree reasonably well with prior laboratory studies. Oxygen fluxes at the sediment-water interface calculated from the simulated profiles are higher than the observed fluxes for the *in situ* microprofiles. The fluxes calculated from simulated zero-order profiles showed better agreement with the observed fluxes than the simulated first-order profiles, lending additional support for using zero-order rather than first-order kinetics to describe oxygen consumption within the sediment.

Keywords: first-order, in situ, microprofile, sediment oxygen flux, zero-order

Introduction

Seasonal hypoxia and anoxia are common phenomena in the hypolimnion of lakes and reservoirs that experience thermal stratification. Hypoxia and anoxia can lead to increased fluxes of reduced metals (e.g. iron, manganese, mercury), methane, and nutrients (e.g. phosphorus), which may complicate water treatment processes or exacerbate blooms of nuisance and harmful algae and cyanobacteria (Funkey et al. 2014; Gao et al. 2014; Kleeberg et al. 2013; Testa & Kemp 2012; Gantzer et al. 2009; Beutel et al. 2008; Huttunen et al. 2006; Davison 1993).

Sediment oxygen flux (J_{O2}) is typically considered the dominant sink for dissolved oxygen (DO) in the hypolimnion. It often comprises the majority of the total hypolimnetic oxygen demand, which also includes oxygen consumption in the water column resulting from various chemical reactions and biological processes.

Processes on both sides of the sediment-water interface (SWI) influence J_{O2}. On the water side, J_{O2} is controlled by the presence of a diffusive boundary layer (DBL) immediately above the SWI. Molecular diffusion is the primary transport mechanism for DO through this thin, millimeter-scale film and limits the rate of oxygen transport to the SWI. Turbulence in the bottom boundary layer controls the thickness of the DBL (δ_{DBL}), and therefore is an important factor controlling J_{O2} from the water side of the SWI. The concentration gradient of oxygen across the DBL also plays an important role, as it provides the driving force for diffusive transport. On the sediment side, oxygen may be transported deeper into the sediment pore water via diffusion or interstitial flow, and is consumed within the sediments by microbial respiration and chemical oxidation of reduced species (i.e., Fe^{2+}, Mn^{2+}). Under relatively quiescent conditions, water-side processes typically limit J_{O2}. Alternatively, sediment-side processes can limit J_{O2} under very turbulent conditions, when the supply of oxygen to the SWI exceeds the rate at which it can be consumed or transported deeper into the sediment (O'Connor et al. 2009). In the hypolimnion of most lakes, turbulence near the SWI is typically low, meaning J_{O2} is primarily controlled by water-side processes, and oxygen within the sediments is readily consumed.

As previously mentioned, oxygen is consumed within the sediments by myriad processes, both chemical and biological. When simulating oxygen consumption within the sediment, these processes are typically lumped together into an overall reaction rate, following zero-order, first-order, or Monod kinetics. Prior studies (Table 3.1) have investigated the kinetic behavior of oxygen in the sediment by fitting these kinetic models to oxygen microprofiles in the sediment, or by measuring oxygen depletion in the water column above the sediment to calculate J_{O2} and a rate constant. Brewer et al. (1977) tracked DO concentrations above a dredged sediment sample in laboratory incubations, but assumed oxygen consumption in the sediments followed first-order kinetics and did not report a rate constant. Likewise, Beutel et al. (2007) monitored DO depletion in sediment core incubations to calculate J_{O2}, also assuming first-order kinetics and neglecting to report the estimated rate constant. Hall et al. (1989) measured oxygen depletion rates using *in situ* flux chambers deployed in a Swedish fjord. The study assumed zero-order kinetics were appropriate, reporting a rate constant of 1747 mg L^{-1} d^{-1} at an *in situ* temperature of 10°C. Rasmussen and Jørgensen (1992) incubated sediment cores collected from Aarhus Bay, Denmark, and measured oxygen microprofiles across the SWI using microsensors. They considered zero-order and first-order kinetic models, finding zero-order kinetics to fit the microprofiles better than first-order. At an incubated temperature of 4°C, they report a fitted rate constant of 83 mg L^{-1} d^{-1}. House (2003) used dredged riverine sediments in a laboratory flume to measure factors affecting oxygen penetration into the sediment, such as flow velocity above the sediment, sediment grain size, and organic matter content. Oxygen was measured in the water and sediment using microsensors, similar to the Rasmussen and Jørgensen (1992) study. House considered several possible kinetic models, including zero-order, first-order, and Monod. The study found that the zero-order model, despite being one of the simplest models, fit the data equally well or better than the more complex models, such as the Monod model. Depending on the flow conditions above the SWI and the characteristics of the sediment, House reported fitted zero-order rate constants ranging from 9.7 – 44 mg L^{-1} d^{-1} at an average temperature of 18.4°C.

These studies, while informative, are all somewhat limited by their methods or assumptions. Three of the studies only monitor oxygen in the water above the SWI. Therefore they do not capture the behavior of oxygen in the sediments and are forced to assume a kinetic model. Four of the studies are performed on sediment in laboratory incubations, which may disturb the

sediment and SWI during the dredging or coring process. Further, the conditions in the laboratory may not always be representative of *in situ* conditions. The two studies using microsensor measurements assumed the oxygen profiles were at steady state when fitting kinetic models to the data. This is appropriate for a laboratory study under controlled conditions that allow the incubated sediment to reach steady state, however ambient conditions in the field are typically quite variable and oxygen profiles in the sediment may never actually reach steady state. A study by Bryant et al. (2010) measured *in situ* oxygen microprofiles in a seiching lake and highlighted this fact, observing large changes in the vertical oxygen distribution above the SWI and within the sediment on an hourly timescale. To our knowledge, the current study is the first to fit kinetic models using oxygen microprofiles measured *in situ*, rather than using laboratory incubations, as well as the first to use a transient oxygen transport model for a series of microprofiles, rather than using individual oxygen profiles and assuming steady state.

Methods

Microprofile Data Collection

Oxygen microprofiles were measured *in situ* in two oxygenated lakes: Lake Hallwil and Carvin's Cove Reservoir (Figure 3.1 and Table 3.2). Lake Hallwil (LH) is located north of Lucerne, Switzerland, on the Swiss Plateau, and is primarily used for recreational purposes. The microprofiler (Unisense MP-4) was deployed for periods of approximately 2 to 5 days at three locations along the main axis of the lake from 24 May to 1 June 2012. Carvin's Cove Reservoir (CCR) is a water-supply reservoir for the City of Roanoke in southwest Virginia, USA. The microprofiler was deployed at one location in CCR from 26 May to 2 June 2013. While deployed in each lake, the microprofiler was equipped with a Clark-type oxygen microsensor (Unisense OX-100), as well as a thermocouple temperature sensor (Unisense TP-200). Measurements were made in triplicate at a sampling rate of 1 Hz at the following vertical resolution: 10 mm resolution from 100 mm to 10 mm above the SWI, 1 mm resolution from 10 mm to 5 mm above the SWI, and 0.1 mm resolution from 5 mm above the SWI to 5 mm below the SWI. This measurement protocol results in complete microprofiles of DO and temperature roughly every 55 minutes.

The SWI location was visually determined by examining each microprofile to identify the linear region in the DBL and the slope change associated with the porosity difference between the sediment and water column. The standard deviation of the triplicate measurements at each point in the microprofiles was also used to assist and confirm the correct positioning of the SWI, as the standard deviation should decrease as the microsensors approach the SWI.

Sediment Kinetics Fitting

Sediment oxygen kinetics is typically described using zero-order, first-order, or Monod (sometimes referred to as Michaelis-Menten) kinetic models (equations 3.1 – 3.3; House 2003). Rather than trying to account for the myriad chemical and biological processes that consume oxygen in the sediment, oxygen consumption is assumed to be adequately represented using an all-encompassing rate constant, or in the case of the Monod model, a maximum oxidation rate constant (μ) and half-saturation constant (K_{O2}). Monod kinetics have the interesting effect of becoming pseudo zero-order when reactant concentrations are much higher than K_{O2} and becoming pseudo first-order when reactant concentrations are much less than K_{O2}. These model formulations all account for molecular diffusion of oxygen through the sediment pore water and consumption of oxygen within the sediment.

The study by House (2003) showed zero-order and Monod models both described oxygen kinetics within the sediment equally well, though zero-order often agreed slightly better. Olinde (2007) also showed that despite the additional fitting parameter offered by Monod kinetics, it does not result in a substantially improved fit to oxygen microprofiles measured from sediment core incubations. Given these observations, the Monod kinetic model was not considered further in this study. By applying a finite shift to the zero-order and first-order kinetic models (equations 3.1 and 3.2), the transient numerical solutions can be obtained (equations 3.4 and 3.5):

$$\frac{\partial C}{\partial t} = D_s \frac{\partial^2 C}{\partial z^2} - k_0 \tag{3.1}$$

$$\frac{\partial C}{\partial t} = D_s \frac{\partial^2 C}{\partial z^2} - k_1 C \tag{3.2}$$

$$\frac{\partial C}{\partial t} = D_s \frac{\partial^2 C}{\partial z^2} - \mu \frac{C}{K_{O2} + C} \tag{3.3}$$

$$\frac{C_n^i - C_n^{i-1}}{\Delta t} = \frac{D_s}{\Delta z^2}\left(C_{n+1}^{i-1} - 2C_n^{i-1} + C_{n-1}^{i-1}\right) - k_0 \tag{3.4}$$

$$\frac{C_n^i - C_n^{i-1}}{\Delta t} = \frac{D_s}{\Delta z^2}\left(C_{n+1}^{i-1} - 2C_n^{i-1} + C_{n-1}^{i-1}\right) - k_1 C_n^{i-1} \tag{3.5}$$

where C represents DO concentration, t is time, D_s is the effective diffusion coefficient of DO in the sediment ($D_s = \varphi D_m$), φ is sediment porosity, D_m is the molecular diffusion coefficient of DO in water, z is depth below the SWI, k_0 is a zero-order rate constant, and k_1 is a first-order rate constant. The superscript i denotes the profile number in the time series of profiles, and the subscript n represents the depth along the pore water DO profile.

The transient model is coded using Matlab. It is initialized with the first microprofile measured at each deployment of the microprofiler, using only the portion of the microprofile below the SWI. Measured oxygen concentrations below 3 μmol L^{-1} were forced to zero, since concentrations below this level become difficult to discern from zero, and the depth at which DO is < 3 μmol L^{-1} has been defined as the depth of maximum oxygen penetration in previous studies (e.g. Bryant et al. 2011). The model assumes constant temperature over the series of profiles, as well as constant sediment porosity with depth. This results in a constant value of D_s for a given series of profiles. Measurements of φ were made from sediment cores collected from both lakes during field studies conducted prior to this current study following Dalsgaard et al. (2000). The values used for φ in CCR and LH were 0.96 and 0.94, respectively. The upper boundary condition is the measured DO concentration at the SWI, while the lower boundary condition is a zero-flux boundary condition. To ensure a stable solution that does not oscillate, the time step (Δt) was made sufficiently small so that the diffusion number (λ, equation 3.6) is less than 0.25 (Chapra 1997).

$$\lambda = \frac{D_m \Delta t}{\Delta z^2} \tag{3.6}$$

Since the time step necessary to achieve $\lambda < 0.25$ is much smaller than the time between microprofiles measured in the field (Δt = 2 s versus Δt = 55 min), the DO concentration at the SWI used as the upper boundary condition for the modeled profiles was determined by linearly interpolating between measured DO concentrations at the SWI, when needed.

Relative least squares (RLS; Saez and Rittman 1992) was used to determine the best-fit kinetic rate constants (equation 3.7) for each series of microprofiles. Only the portion of the simulated profile corresponding to where the measured DO was greater than 3 μmol L^{-1} was used in calculating the RLS for that profile. After calculating the RLS for each profile in a series, the sum of the RLS from each individual profile was divided by the total number of profiles in the series, giving an RLS that is normalized to the number of profiles (p) in the series. The best-fit value for the kinetic rate constant is the value that minimizes the normalized RLS. It is worth noting that the RLS is a non-traditional statistic, and may reward under-fits while penalizing over-fits. The use of RLS was chosen to weight each data point equally, as other error measures, such as root mean square error, may emphasize the portion of the microprofiles with higher measured concentrations at the expense of those data points with relatively low concentrations. The applicability of data transforms, such as a log transformation, to this type of dataset will be considered in future work.

$$RLS = \frac{\sum\left(\frac{C_{Obs} - C_{Model}}{C_{Obs}}\right)^2}{p} \tag{3.7}$$

Model Versus Field Data Comparisons

Using the fitted zero- and first-order rate constants from each series of profiles, sediment-side oxygen flux was calculated from the simulated profiles and compared to sediment-side oxygen flux measured with the microprofiler. Oxygen flux can be calculated from the sediment-side of the microprofiles as:

$$J_{O2} = D_s \frac{\Delta C}{\Delta z} \tag{3.8}$$

where $\Delta C/\Delta z$ is the DO concentration gradient immediately below the SWI. To compare how well the modeled data agree with the field data, the root mean square error (RMSE) was calculated using equation 3.9.

$$RMSE = \sqrt{\frac{1}{n}\sum_{i=1}^{n}\left(J_{O_2,Sim_i} - J_{O_2,Obs_i}\right)^2} \tag{3.9}$$

Higashino and Stefan (2004; 2011) derived an equation for calculating J_{O2} that integrates hydrodynamic effects above the sediment, and oxygen transport and kinetics below the SWI. Assuming zero-order kinetics and using equations 3.1 and 3.10, Higashino and Stefan arrive at equation 3.11:

$$J_{O2} = k_t\left(C_B - C_{SWI}\right) \tag{3.10}$$

$$J_{O2} = \frac{D_s k_0 - \sqrt{\left(D_s k_0\right)^2 + 2D_s k_0 C_B k_t^2}}{k_t} \tag{3.11}$$

where k_t is the mass transfer coefficient, C_B is the DO concentration in the bulk water, and C_{SWI} is the DO concentration at the SWI. An equation analogous to equation 3.11 can be derived if first-order kinetics is assumed, rather than zero-order kinetics. Using equations 3.2 and 3.10 and following a similar derivation to that presented by Higashino and Stefan (2004), equation 3.12 can be derived, where C_{Zmax} is the DO concentration at the maximum oxygen penetration depth. If the assumption is made that $C_{Zmax} << C_B$, then equation 3.12 can be simplified to equation 3.13.

$$J_{O2} = \frac{-k_t\left(C_B - C_{Z\max}\right)}{\left(1 + \frac{k_t}{\left(k_1 D_s\right)^{0.5}}\right)} \tag{3.12}$$

$$J_{O2} = \frac{-k_t C_B}{\left(1 + \frac{k_t}{\left(k_1 D_s\right)^{0.5}}\right)} \tag{3.13}$$

Equations 3.11 and 3.13 were used to calculate J_{O2} using the best-fit kinetic rate constants and C_B as measured with the microprofiler. These fluxes were compared to J_{O2} calculated from the microprofiles using equation 3.10. The mass transfer coefficient (k_t) was estimated from the DO microprofiles as D_m/δ_{DBL}, where δ_{DBL} is the effective thickness of the diffusive boundary layer, as defined by Jørgensen and Revsbech (1985). As with the sediment-side J_{O2} comparisons, the normalized residual sum of squares (equation 3.9) was used to compare the simulated and observed oxygen fluxes.

Results and Discussion

Fitted Rate Constants

The fitted value of the zero- and first-order kinetic rate constants, as well as the corresponding RLS value for each series of microprofiles is displayed in Table 3.3. Fitted values for the zero-order and first-order rate constants ranged from 312 – 591 mg L^{-1} d^{-1} and 395 – 821 d^{-1} in LH, while fitted values for CCR were noticeably lower at 78 mg L^{-1} d^{-1} and 142 d^{-1}. Differences in the fitted rate constants between the two study sites are likely attributable to differences in the sediment composition between the two lakes, such as the amount of labile organic matter and mineral composition. Labile carbon, reduced metals, and other chemical species exert a demand for oxygen within the sediment, and larger quantities of any of these oxygen-consuming species would result in an increase in the observed rate constant. The large range in fitted rate constants within LH is likewise attributable to spatial variability in sediment composition within LH itself. The first and third deployments were both in the central, deepest portion of LH (~ 42 m depth and approximately 300 m apart) and yielded similar best-fit rate constants. The second deployment, though still in the hypolimnion, was in a much shallower location (~ 25 m depth) and has higher fitted rate constants. Sediment in the shallower portions of LH is likely to have more labile carbon in the sediment than deeper portions of the lake, since settling organic matter has less time to be oxidized in the water column before reaching the sediment. LH also has a bubble-plume oxygenation system located in the deepest portion of the lake, within 300 m of the

first and third microprofiler deployments. This oxygenation system, which has been in operation for over 40 years, would further enhance oxidation of settling organic matter in the water column by increasing the availability of oxygen in the water column, as well as satisfying oxygen demand exerted by the nearby sediment. Thus, it seems reasonable that the fitted rate constant should be higher in the shallower regions of the lake, which are also farther from the oxygenation system. Temperature may also play some role in the increased best-fit rate constants in the shallower site, as temperatures measured near the SWI were warmer at this location than at the other two locations. The effect is likely small, however, since the measured temperature difference was only about 1°C

In the CCR data set, first-order kinetics appears to fit better than zero-order kinetics, evidenced by the lower RLS (Table 3.3). Visual inspection (Figure 3.2) of the fitted microprofiles shows a slightly less clear picture, however, as some field profiles agree quite well with zero-order kinetics, such as the profile from 28 May, while others agree much better with first-order kinetics, such as the profile from 1 June. Repeating the fitting procedure using a two parameter fit in future studies may help to clarify which is the better model for CCR. The kinetic models in equations 3.1 and 3.2 can be generalized to equation 3.14, where α is an exponent that takes a value of 0 in the zero-order model, and a value of 1 in the first-order model. By fitting both the rate constant and α, it would be possible to determine whether 0 or 1 lie within the confidence interval around α, thus clarifying which kinetic model is more appropriate. In LH, zero-order and first-order kinetics appear to fit the data similarly well, as evidenced by the minor differences in RLS values between zero- and first-order fits (Table 3.3). When visually comparing the modeled data to the observed data, as in Figure 3.3 and Figure 3.4, the simulated zero-order profiles appear to fit the shape of the measured profiles much better than the simulated first-order profiles. Taking into account this visual comparison and the similar RLS values, zero-order kinetics seems to be the more appropriate model for describing oxygen kinetics in the sediment of LH.

$$\frac{\partial C}{\partial t} = D_s \frac{\partial^2 C}{\partial z^2} - kC^{\alpha} \tag{3.14}$$

Despite slight differences in the methods used for determining the best-fit rate constants, the fitted values compare quite well with a preliminary study (Olinde 2007) performed in CCR. Olinde found the best-fit zero-order rate constant to be 36 ± 10 mg L^{-1} d^{-1} at 4°C and 130 ± 66 mg L^{-1} d^{-1} at 20°C, while the best-fit first order rate constant was 34 ± 12 d^{-1} at 4°C and 170 ±68 d^{-1} at 20°C. The fitted CCR values in the current study (Table 3.3), measured at an *in situ* temperature of ~7.5°C fit nicely within the range from this preliminary study by Olinde.

Given the differences in methods and sediment composition, the magnitude of the optimized zero-order rate constant for CCR agrees with the zero-order constants reported by Rasmussen and Jørgensen (1992) and House (2003). The fitted zero-order constants for LH are higher than those reported by Rasmussen and Jørgensen (1992) or House (2003), but not unreasonably high, considering that Hall et al. (1989) reported a zero-order rate constant that is an order of magnitude higher than those from LH (1747 mg L^{-1} d^{-1} versus 312 – 591 mg L^{-1} d^{-1}).

Variations in the fitted rate constants among the sampling sites and between the two lakes studies are also reflected in the oxygen penetration depth (z_{max}). CCR has the lowest fitted rate constant and also has the deepest z_{max}, around 2 – 2.5 mm (Figure 3.2). The second deployment in LH, which had the highest fitted rate constant, has the shallowest z_{max}, only ~0.75 – 1.2 mm (Figure 3.4). As would be expected, the other two sites in LH, which had fitted rate constants between these two extremes also have observed z_{max} that fall in the middle range of z_{max} observed during this study (e.g. ~1.2 – 1.5 mm for the first LH deployment; Figure 3.3).

Differences between the simulated and observed profiles are likely a result of the interpolation necessary to force the model. Since the field data only has direct DO measurements at the SWI roughly every 55 minutes, any fluctuations in oxygen concentrations at the SWI occurring on a shorter time scale are not represented in the model forcing. As mentioned in the methods section, to ensure a stable solution, the model time step needed to be 2 seconds, which is much shorter than the time between actual measurements. If higher frequency data were available to force the model, the agreement between the simulated and observed profiles would likely improve.

Oxygen Flux Comparisons

Sediment-side oxygen flux calculated from the simulated oxygen profiles typically resulted in an overestimate of J_{O2} when compared to field measurements (Table 3.4, Figure 3.5, and Figure 3.6). The mean oxygen flux was overestimated by 45% – 146% for each profile series when using first-order kinetics. The zero-order kinetic model agreed somewhat better with the field data, deviating from the field observations by 2% – 62%. This, along with the lower normalized RMSE, lends support to using zero-order kinetics over first-order kinetics when modeling oxygen in LH and CCR sediment.

Observations made from comparing water-side oxygen fluxes mirrored those made from the sediment-side oxygen flux comparisons. In each series of profiles, simulated J_{O2} was higher than the measured J_{O2} (Table 3.4, Figure 3.7, and Figure 3.8). Mean oxygen flux calculated from the first-order simulated profiles overestimated the observed mean flux by 28% – 75%. The simulated zero-order profiles again show better agreement with the field data than the simulated first-order profiles, over predicting J_{O2} by only 11% – 51%, and providing additional support for using the zero-order kinetic model.

When considering the observed versus predicted plots in Figures 3.5 – 3.8, a line fit to the plotted points should have a slope of 1 and an intercept of zero, which would suggest the model successfully reproduces the observed data. Only the oxygen fluxes calculated from the water-side and using first-order sediment kinetics in CCR have a slope of ~1 and an intercept of zero (Table 3.5). Most of the remaining plots have intercepts higher than zero and slopes near zero, which indicates the oxygen fluxes calculated from the simulated microprofiles do not adequately reproduce the observed oxygen fluxes. This poor performance is also likely to be a result of the interpolation necessary to force the model, which was mentioned earlier. With a higher-frequency data set to force the model, the agreement between observed and simulated microprofiles should improve, which should, in turn, improve the fluxes calculated from the simulated profiles.

Conclusions

A transient model of oxygen transport and consumption in lake sediment was fit to oxygen microprofiles measured *in situ* in CCR and LH, using both zero-order and first-order kinetic models to determine the appropriate kinetic formulation. In CCR, first-order kinetics showed better agreement with the simulated microprofiles, based on RLS values. However, visual inspection of the microprofiles, as well as oxygen flux calculations from the microprofiles suggest that zero-order kinetics may be a better model. In LH, zero-order kinetics was more appropriate than first-order kinetics based on RLS measures and visual inspection. The best-fit zero-order and first-order rate constants in CCR were 78 mg L^{-1} d^{-1} and 142 d^{-1} at 7.5°C, which agrees quite well with a preliminary study performed in CCR and is on the same order of magnitude as those reported in previous studies. The best-fit zero-order rate constants for the three microprofiler deployments in LH ranged from 312 – 591 mg L^{-1} d^{-1}, much higher than in CCR and likely attributable to differences in sediment composition between the two lakes, though still within the range of reported values from the literature. The variability in fitted rate constants among the three sampling sites in LH is likely due to spatial heterogeneity in sediment composition within LH. The two sites in the deep, central portion of the lake, near the oxygenation system, had similar best-fit rate constants (312 and 357 mg L^{-1} d^{-1}), while the site in the shallower reaches of LH had a much higher best-fit rate constant (591 mg L^{-1} d^{-1}). Differences in the fitted rate constants also contribute to differences in observed z_{max}. The two are inversely related, with lower k_0 resulting in higher z_{max} and vice versa.

Oxygen flux calculated from each series of simulated profiles typically overestimated J_{O2} calculated from oxygen microprofiles measured *in situ* by up to 146%. Simulated profiles based on first-order kinetics overestimated J_{O2} much more than the simulated profiles based on zero-order kinetics, providing additional support for using zero-order kinetics to describe oxygen transport and consumption within the sediment.

While this study shows the potential capabilities of using a transient model to fit kinetic rate constants to *in situ* microprofiles, further work is necessary to improve the performance of the model. Most notably, a data set with higher frequency measurements of oxygen microprofiles in the sediment and oxygen concentrations at the SWI, would likely improve the agreement

between simulated and observed microprofiles and oxygen fluxes. A two-parameter fitting procedure could also be adopted, in which both the kinetic rate constant and α (see equation 3.14) are simultaneously fit to the oxygen microprofiles. By fitting both parameters, it should become clearer, particularly in the CCR case, as to which kinetic model is most appropriate.

References

Beutel, M., Hannoun, I., Pasek, J., and Kavanagh, K. B., 2007. Evaluation of hypolimnetic oxygen demand in a large eutrophic raw water reservoir, San Vicente Reservoir, Calif.. Journal of Environmental Engineering 133 (2), 130-138.

Beutel, M. W., Leonard, T. M., Dent, S. R., and Moore, B. C., 2008. Effects of aerobic and anaerobic conditions on P, N, Fe, Mn, and Hg accumulation in waters overlaying profundal sediments of an oligo-mesotrophic lake. Water Research 42 (8-9), 1953-1962.

Brewer, W., Abernathy, A. R., and Paynter, M. J. B., 1977. Oxygen consumption by freshwater sediments. Water Research 11 (5), 471-473.

Bryant, L. D., Lorrai, C., McGinnis, D. F., Brand, A., Wüest, A., and Little, J. C., 2010. Variable sediment oxygen uptake in response to dynamic forcing. Limnology and Oeanography 55 (2), 950-964.

Chapra, S. C., 1997. Surface water-quality modeling. McGraw-Hill, Boston, Mass, USA, pg 214.

Dalsgaard, T., Nielsen, L. P., Brotas, V., Viaroli, P., Underwood, G., Nedwell, D. B., Sundbäck, K., Rysgaard, S., Miles, A., Bartoli, M., Dong, L., Thornton, D. C. O., Ottosen, L. D. M., Castaldelli, G., and Risgaard-Petersen, N., 2000. Protocol Handbook for NICE – Nitrogen Cycling in Estuaries: A Project under the EU Research Programme: Marine Science and Technology (MAST). National Environmental Research Institute, Silkeborg, Denmark. http://www2.dmu.dk/LakeandEstuarineEcology/nice/NICE_handbook.pdf

Davison, W., 1993. Iron and manganese in lakes. Earth-Science Reviews 34, 119-163.

Funkey, C. P., Conley, D. J., Reuss, N. S., Humborg, C., Jilbert, T., and Slomp, C. P., 2014. Hypoxia sustains cyanobacteria blooms in the Baltic Sea. Environmental Science and Technology 48 (5), 2598-2602.

Gantzer, P. A., Bryant, L. D., and Little, J. C., 2009. Controlling soluble iron and manganese in a water-supply reservoir using hypolimnetic oxygenation. Water Research 43 (5), 1285-1294.

Gao, Y., Cornwell, J. C., Stoecker, D. K., and Owens, M. S., 2014. Influence of cyanobacteria blooms on sediment biogeochemistry and nutrient fluxes. Limnology and Oceanography 59 (3), 959-971.

Hall, P. O. J., Anderson, L. G., van der Loeff, M. M. R., Sundby, B., and Westerlund, S. F. G., 1989. Oxygen uptake kinetics in the benthic boundary layer. Limnology and Oceanography 34 (4), 734-746.

Higashino, M., Gantzer, C., and Stefan, H., 2004. Unsteady diffusional mass transfer at the sediment/water interface: Theory and significance for SOD measurement. Water Research 38 (1), 1-12.

Higashino, M., and Stefan, H., 2005. Oxygen demand by a sediment bed of finite length, Journal of Environmental Engineering 131 (3), 350-358.

Higashino, M., and Stefan, H., 2011. Dissolved oxygen demand at the sediment-water interface of a stream: near-bed turbulence and pore water flow effects. Journal of Environmental Engineering 137 (7), 531-540.

House, W., 2003. Factors influencing the extent and development of the oxic zone in sediments. Biogeochemistry 63 (3), 317-334.

Huttunen, J. T., Väisänen, T. S., Hellsten, S. K., and Martikainen, P. J., 2006. Methane fluxes at the sediment-water interface in some boreal lakes and reservoirs. Boreal Environment Research 11 (1) 27-34.

Jørgensen, B. B., and Revsbech, N. P., 1985. Diffusive boundary layers and the oxygen uptake of sediments and detritus. Limnology and Oceanography 30 (1), 111-122.

Kleeberg, A., Herzog, C., and Hupfer, M., 2013. Redox sensitivity of iron in phosphorus binding does not impede lake restoration. Water Research 47 (3), 1491-1502.

O'Connor, B., Hondzo, M., and Harvey, J., 2009. Incorporating both physical and kinetic limitations in quantifying dissolved oxygen flux to aquatic sediments. Journal of Environmental Engineering 135 (12), 1304-1314.

Olinde, L. J., 2007. Sediment oxygen demand kinetics, Master's Thesis, Virginia Polytechnic Institute and State University.

Rasmussen, H, and Jørgensen, B. B., 1992. Microelectrode studies of seasonal oxygen uptake in a coastal sediment: role of molecular diffusion. Marine Ecology Progress Series 81 (3), 289-303.

Testa, J. M., and Kemp, W. M., 2012. Hypoxia-induced shifts in nitrogen and phosphorus cycling in Chesapeake Bay. Limnology and Oceanography 57 (3), 835-850.

Saez, P. B., and Rittman, B. E., 1992. Model-parameter estimation using least squares. Water Research 26 (6), 789-796.

Table 3.1. Summary of previous studies investigating oxygen kinetics in sediment pore water

Study	Experiment Type	Sediment Type	Temperature	Reaction Order	Rate Constant
Brewer et al. 1977	Laboratory incubation, dredged sediment	freshwater lake	18°C	1*	Not explicitly stated
Hall et al. 1989	*In-situ* flux chambers	marine	10°C	0*	1747 mg L^{-1} d^{-1}
Rasmussen & Jørgensen 1992	Laboratory incubation, sediment cores	marine	4°C	0	83 mg L^{-1} d^{-1}
House 2003	Laboratory flume, dredged sediment	riverine	18.4°C	0	9.7 - 44 mg L^{-1} d^{-1}
Beutel et al. 2007	Laboratory incubation, sediment cores	freshwater reservoir	12°C	1*	Not explicitly stated

* Reaction order assumed

Table 3.2. Physical characteristics of Carvin's Cove Reservoir and Lake Hallwil

	Carvin's Cove Reservoir	Lake Hallwil
Max. Depth (m)	22	48
Surface Area (km^2)	2.5	9.95
Volume (m^3)	24×10^6	285×10^6
Elevation (m amsl)	357	449

Table 3.3. Summary of fitted kinetic rate constants and relative least squares (RLS)

		Zero Order k_0 (mg L^{-1} d^{-1})	First Order k_1 (d^{-1})
CCR 2013	Rate Constant	78	142
	RLS	6.00	3.28
LH-1	Rate Constant	357	395
	RLS	1.12	1.70
LH-2	Rate Constant	591	821
	RLS	1.78	1.44
LH-3	Rate Constant	312	488
	RLS	1.61	1.91

Table 3.4. Comparison between mean observed oxygen flux (field) and mean predicted oxygen flux using zero- and first-order kinetics. RMSE is the root mean square error with units of mmol m^{-2} d^{-1} (equation 3.9).

		Carvin's Cove		Lake Hallwil - 1		Lake Hallwil - 2		Lake Hallwil - 3	
		Mean Flux (mmol m^{-2} d^{-1})	RMSE	Mean Flux (mmol m^{-2} d^{-1})	RMSE	Mean Flux (mmol m^{-2} d^{-1})	RMSE	Mean Flux (mmol m^{-2} d^{-1})	RMSE
Sediment Side	Field	6.0	-	12.6	-	18.3	-	8.6	-
	Zero-order	6.1	3.2	16.9	6.3	19.1	10.4	14.0	6.7
	First-order	8.7	4.8	24.6	13.0	26.6	15.1	21.2	13.9
Water Side	Field	5.0	-	9.7	-	12.7	-	7.5	-
	Zero-order	5.5	1.1	14.4	5.8	15.3	5.2	11.3	4.7
	First-order	6.4	2.1	16.9	8.6	16.7	7.4	13.2	6.8

Table 3.5 Intercepts and slopes of lines fitted to observed versus predicted oxygen fluxes. Values are reported with 95% confidence intervals. Intercepts of zero and slopes of one would be indicative of a good fit.

			CCR	LH-1	LH-2	LH-3
Sediment-side	Zero Order	Intercept	6.1 ± 0.4	16.2 ± 1.6	20.2 ± 1.6	14.4 ±1.2
		Slope	0.0 ± 0.1	0.1 ± 0.1	-0.1 ± 0.1	-0.1 ± 0.1
	First Order	Intercept	8.7 ± 0.9	21.9 ± 3.1	29.4 ± 4.0	22.0 ± 3.0
		Slope	0.0 ± 0.1	0.2 ± 0.2	-0.1 ± 0.2	-0.1 ± 0.3
Water-side	Zero Order	Intercept	2.1 ± 0.3	11.9 ± 1.8	12.6 ± 3.5	8.8 ± 1.4
		Slope	0.7 ± 0.1	0.3 ± 0.2	0.2 ± 0.3	0.3 ± 0.2
	First Order	Intercept	0.5 ± 0.7	12.4 ± 3.6	13.8 ± 5.6	8.9 ± 2.4
		Slope	1.2 ± 0.1	0.5 ± 0.3	0.2 ± 0.4	0.6 ± 0.3

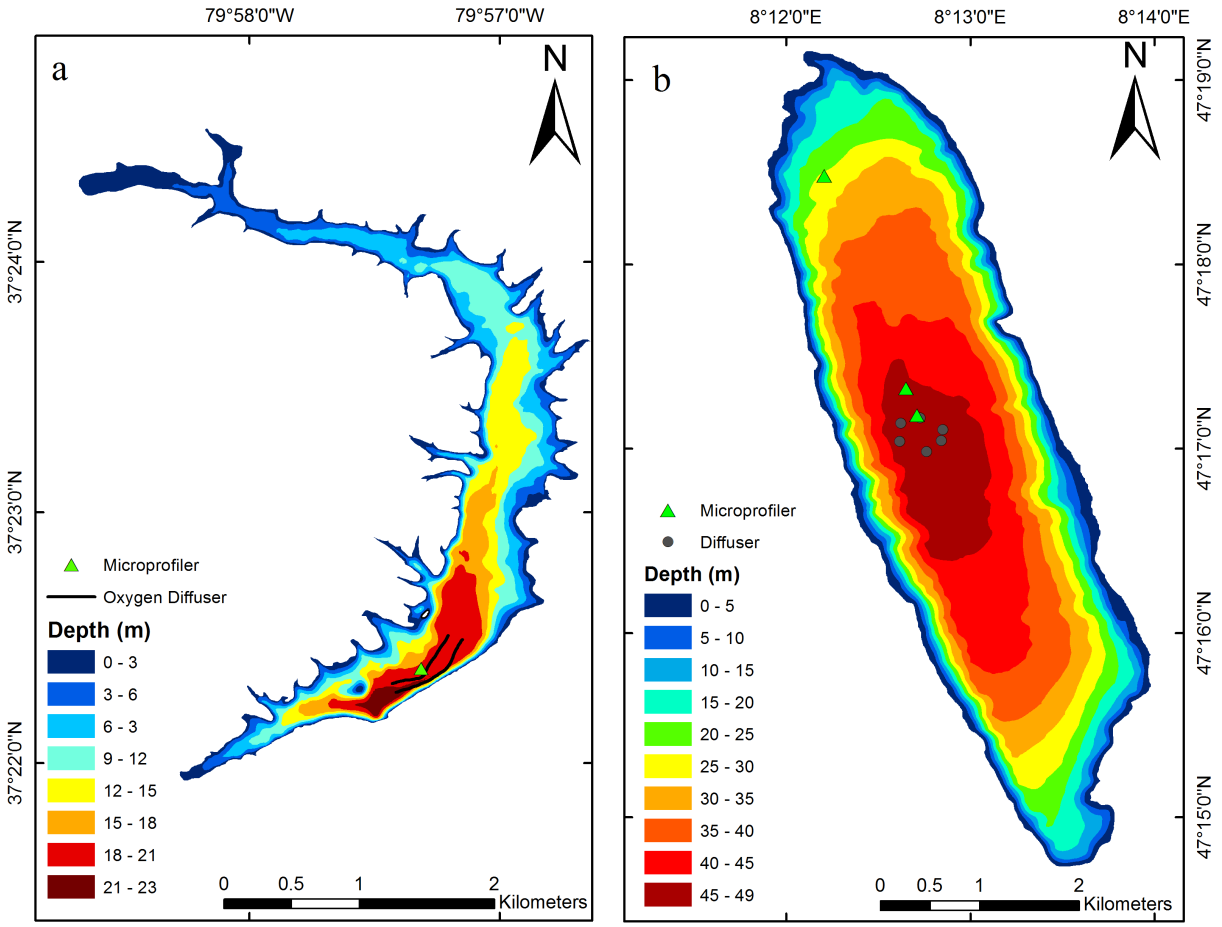

Figure 3.1. Bathymetric maps of (a) Carvin's Cove Reservoir and (b) Lake Hallwil.

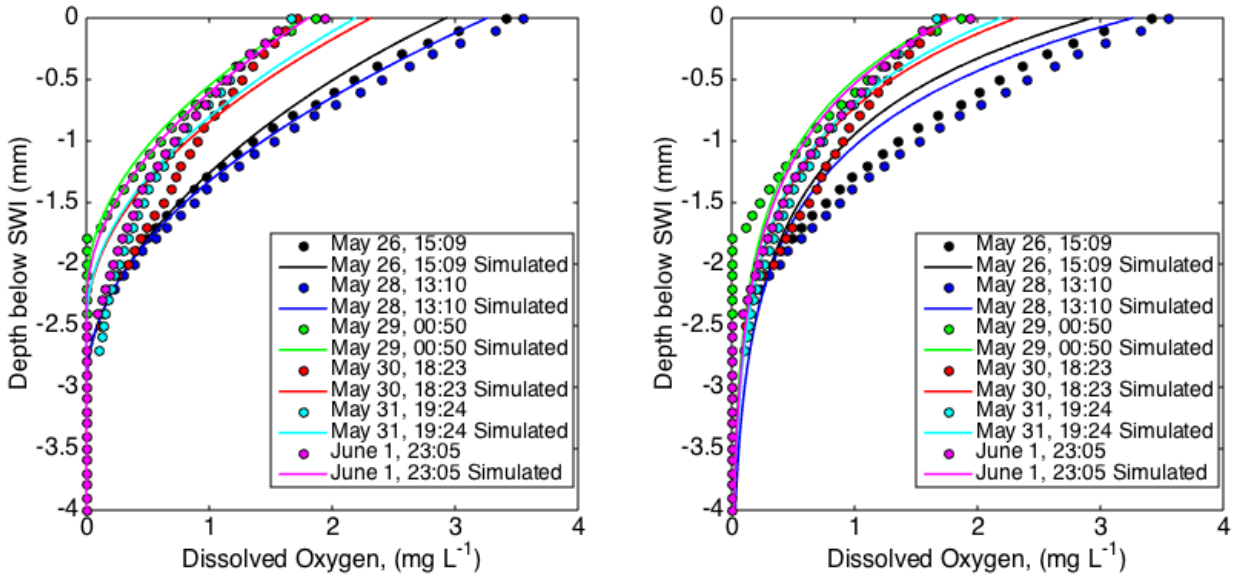

Figure 3.2. Comparison between simulated and observed oxygen microprofiles in Carvin's Cove Reservoir. Simulated profiles in the left panel are based on zero-order kinetics (k_0 = 78 mg L^{-1} d^{-1}) and simulated profiles in the right panel are based on first-order kinetics (k_1 = 142 d^{-1}).

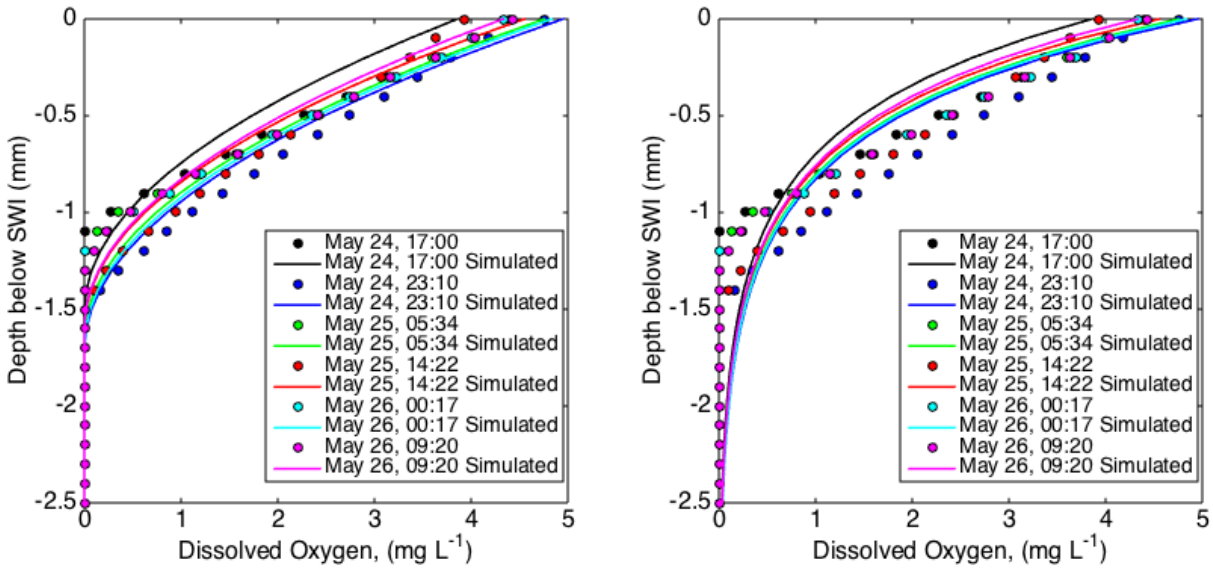

Figure 3.3. Comparison between simulated and observed oxygen microprofiles in Lake Hallwil during the first microprofiler deployment. Simulated profiles in the left panel are based on zero-order kinetics (k_0 = 357 mg L^{-1} d^{-1}) and simulated profiles in the right panel are based on first-order kinetics (k_1 = 395 d^{-1}).

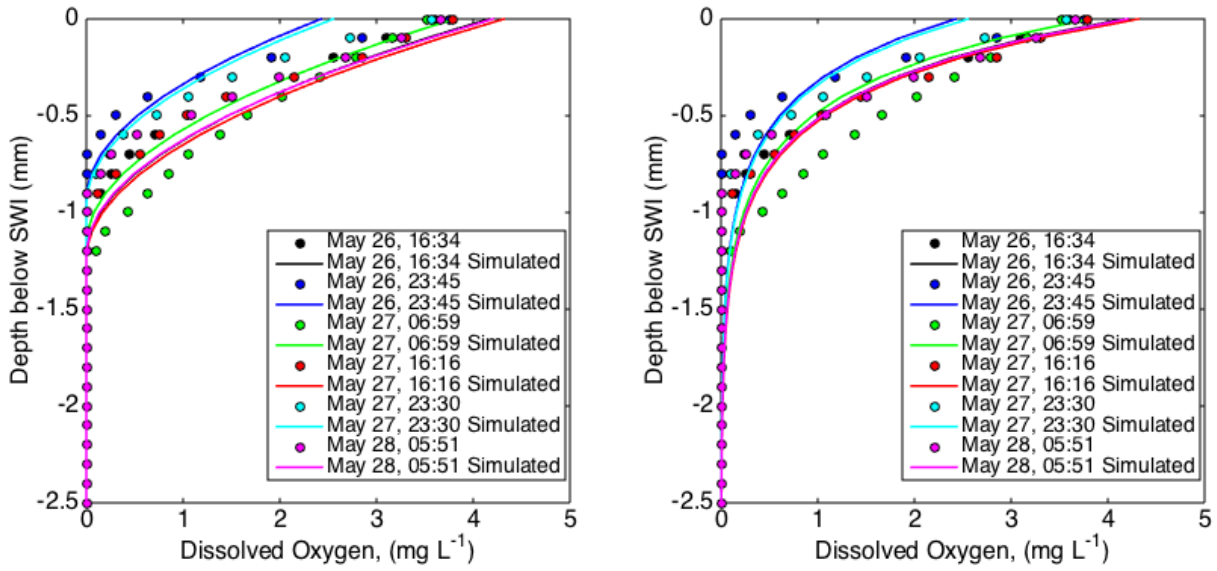

Figure 3.4. Comparison between simulated and observed oxygen microprofiles in Lake Hallwil during the second microprofiler deployment. Simulated profiles in the left panel are based on zero-order kinetics (k_0 = 591 mg L^{-1} d^{-1}) and simulated profiles in the right panel are based on first-order kinetics (k_1 = 821 d^{-1}).

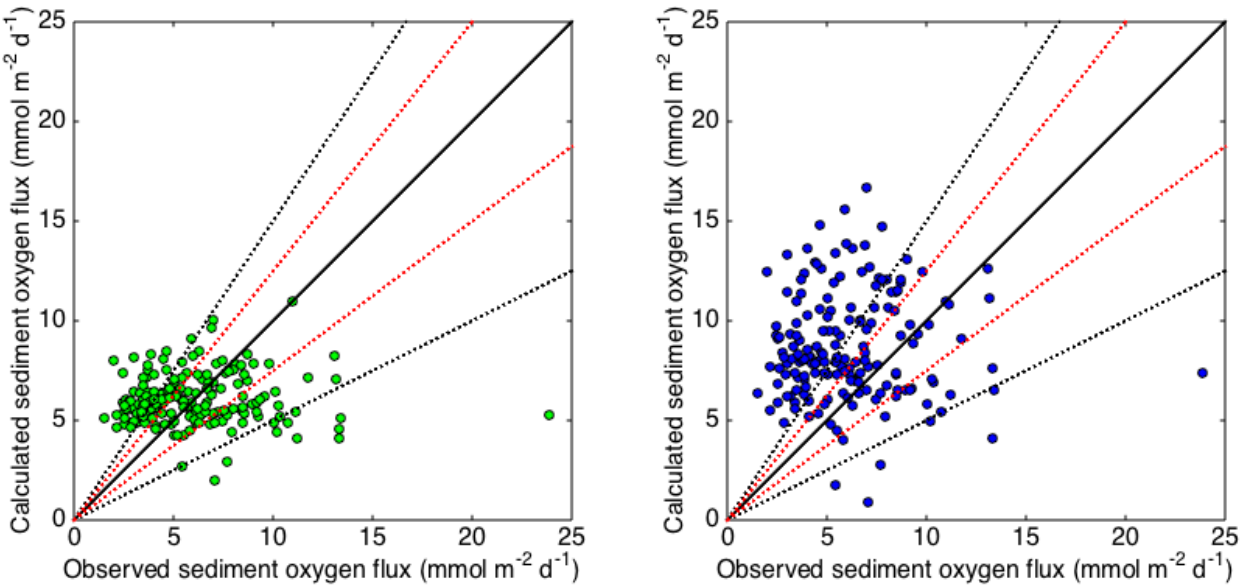

Figure 3.5. Observed versus calculated sediment oxygen flux in Carvin's Cove Reservoir using zero-order (left) and first-order (right) kinetics. Calculated fluxes are calculated from the simulated sediment microprofiles. Solid black lines represent 1:1 line, dashed red lines represent ±25%, and dashed black lines represent ±50%.

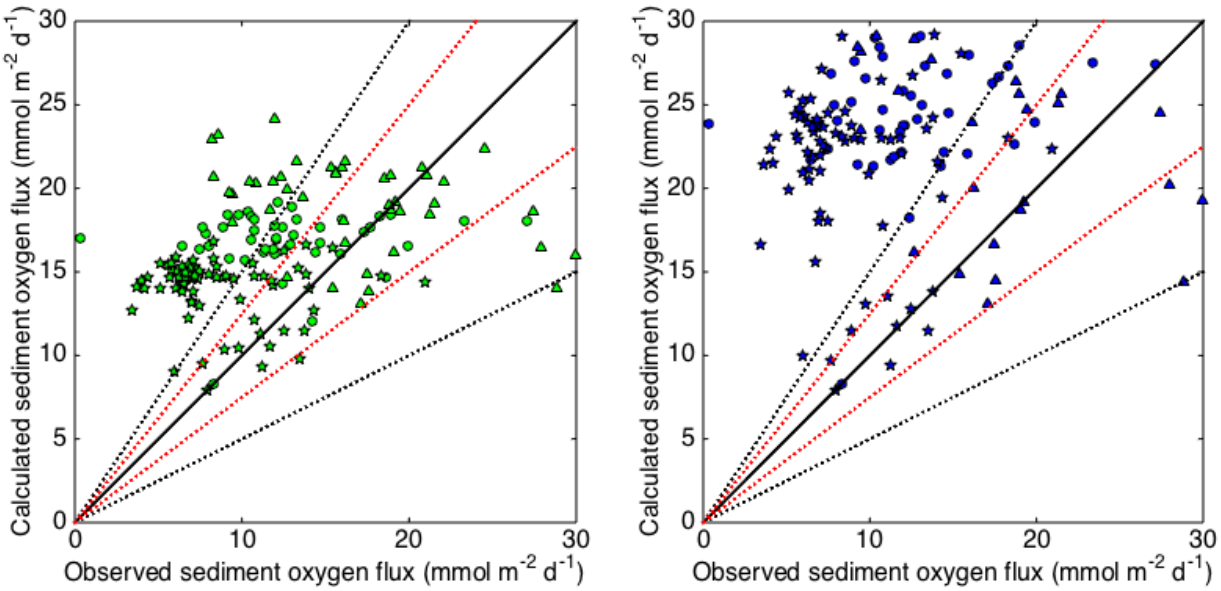

Figure 3.6. Observed versus calculated sediment oxygen flux in Lake Hallwil using zero-order (left) and first-order (right) kinetics. Calculated fluxes are calculated from the simulated sediment microprofiles. Circles, triangles, and stars represent the first, second, and third microprofiler deployments, respectively. Solid black lines represent 1:1 line, dashed red lines represent ±25%, and dashed black lines represent ±50%.

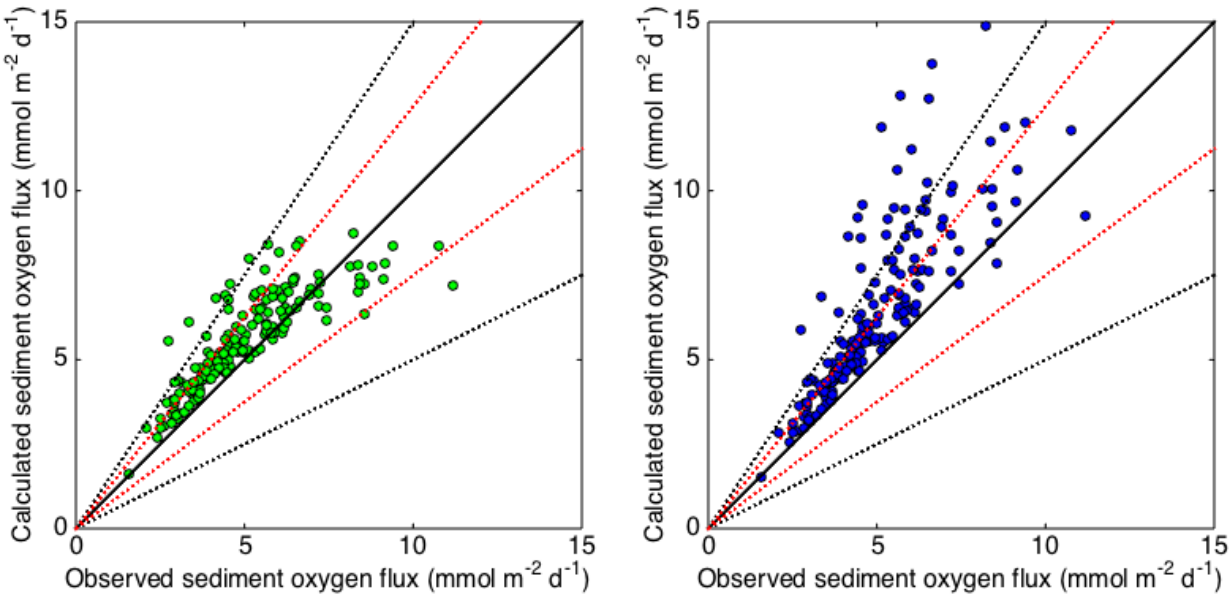

Figure 3.7. Observed versus calculated sediment oxygen flux in Carvin's Cove Reservoir using zero-order (left) and first-order (right) kinetics. Calculated fluxes are calculated using fitted rate constants and equations 3.11 and 3.13. Solid black lines represent 1:1 line, dashed red lines represent ±25%, and dashed black lines represent ±50%.

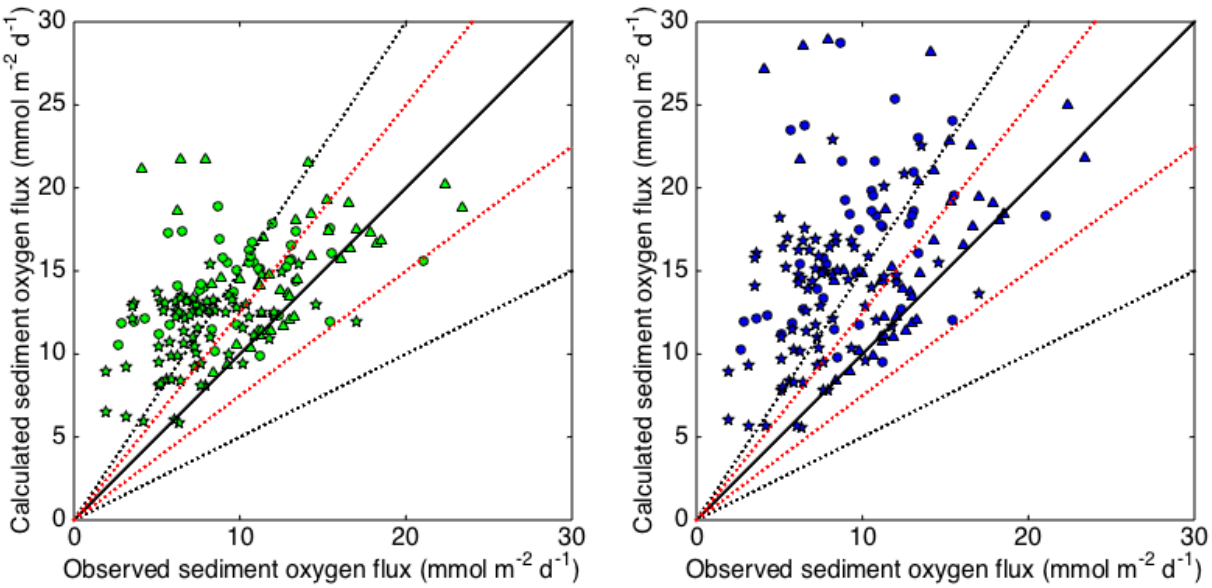

Figure 3.8. Observed versus calculated sediment oxygen flux in Lake Hallwil using zero-order (left) and first-order (right) kinetics. Calculated fluxes are calculated using fitted rate constants and equations 3.11 and 3.13. Circles, triangles, and stars represent the first, second, and third microprofiler deployments, respectively. Solid black lines represent 1:1 line, dashed red lines represent ±25%, and dashed black lines represent ±50%.

Chapter 4. Toward a comprehensive lake model for predicting mixing-induced sediment oxygen uptake

Kevin A. Bierlein[1], Francisco J. Rueda[2], and John C. Little[1]

[1]Via Department of Civil and Environmental Engineering, Virginia Tech, Blacksburg, Virginia, USA

[2]Instituto del Agua and Departamento Ingenieria Civil, Universidad de Granada, Granada, Spain

Abstract

Hypolimnetic oxygenation via bubble plumes is an increasingly common lake management strategy for maintaining and improving water quality, yet there remains a need to be able to predict the impact of these systems on the oxygen budget and, in particular, sediment oxygen flux (J_{O2}). An expression for J_{O2} is incorporated into a coupled bubble plume and hydrodynamic lake model, allowing J_{O2} to vary according to lake hydrodynamics and oxygen kinetics in the sediment. This comprehensive bubble-plume oxygenation model is calibrated and validated using data sets from two separate field campaigns on a water supply reservoir, using the zero-order oxygen consumption rate in the water column as the sole fitting parameter. The simulated temperature profiles agree quite well with observed temperature profiles. Dissolved oxygen profiles show reasonable agreement in the bulk hypolimnion, but deviate from measured concentrations in the bottom 1 – 3 m of the water column and overestimate oxygen concentrations near the sediment, resulting in high values of J_{O2}. The discrepancy in oxygen concentrations is attributed to additional chemical sinks of oxygen that are not accounted for in the hydrodynamic model. If additions to the hydrodynamic model which account for these chemical sinks are included and the discrepancy between simulations and observations is resolved, the comprehensive model could provide a mechanistic method for simulating the effect of bubble plume oxygenation on J_{O2} and lead to improvements in oxygenation system design methods.

Keywords: Bubble plume, hypolimnetic oxygenation, oxygen, sediment oxygen flux

Introduction

Seasonal depletion of dissolved oxygen in the hypolimnion is a common occurrence in thermally stratified lakes and can have negative implications for water quality. Anoxia can increase internal loading of nutrients from the sediment, stimulating algal and cyanobacterial growth [*Funkey et al.* 2014]. It can also lead to increased fluxes of reduced metals, including soluble iron and manganese, and methyl-mercury [*Gantzer et al.* 2009a*; Beutel et al.* 2008]. Reduced metals can cause taste, odor, and color issues if not removed during water treatment processes. Increases in these soluble metals require water utilities to purchase additional oxidants, adding to the cost of water treatment. Methyl-mercury is an extremely toxic form of mercury, due to its bioavailability, and is capable of bioaccumulating in higher trophic levels.

To mitigate seasonal anoxia and its deleterious effects on water quality, many lake managers are turning to hypolimnetic oxygenation, which replenishes oxygen in the hypolimnion. Several types of systems have been designed to add oxygen, including the Speece Cone, airlift aerator, side-stream super-saturation systems, and bubble plume diffusers [*Gerling et al.* 2014; *Singleton and Little* 2006]. Bubble plumes are one of the more common systems, particularly in relatively deep lakes. These plumes may be linear or circular and can inject either air or oxygen gas into the bottom of the hypolimnion. The gas bubbles dissolve in the ambient water as they rise through the water column, and, at the low gas flow rates typically used with bubble plumes, thermal stratification is preserved. When correctly designed and operated, these systems successfully mitigate seasonal anoxia and its harmful effects.

Despite effectively adding oxygen, bubble plumes can also induce large-scale hypolimnetic mixing and slight hypolimnetic warming, both of which can result in increased sediment oxygen flux (J_{O2}) [*Bryant et al.* 2011a; *Singleton et al.* 2010]. Hypolimnetic warming increases the rate of temperature-sensitive oxygen consuming processes in the hypolimnion and also decreases the solubility of oxygen in water. Mixing of the hypolimnetic water by the bubble plume enhances turbulence, eroding the millimeter-scale diffusive boundary layer (DBL) above the sediment and increasing diffusive transport of oxygen to the sediment-water interface, increasing sediment oxygen flux. This increase in oxygen flux can be significant, increasing by over a factor of 5 – 7 in many cases [*Gantzer et al.* 2009b; *Prepas and Burke* 1997]. Successfully predicting the

extent of bubble-plume induced oxygen flux is therefore a critical design parameter and is largely responsible for the success or failure of the oxygenation system.

Even as hypolimnetic oxygenation has become a common and accepted method for improving water quality in lakes, the design practices for these systems are still somewhat lacking, particularly when it comes to predicting the effects of oxygenation on lake hydrodynamics, thermal structure, and the oxygen budget. Accurately predicting the induced sediment oxygen flux is critically important to ensuring successful oxygenation system design and operation, yet there remains no method to reliably predict the magnitude of the induced oxygen flux. Current best practice is to use the measured oxygen demand before oxygenation and a factor of safety. Studies by *Moore et al.* [1996], *Beutel* [2003], and others provide guidelines for estimating an appropriate factor of safety. These approaches are not ideal, however, as they are based on empirical equations derived from laboratory experiments. Ideally, estimates of oxygenation-induced sediment oxygen flux should be derived from appropriate physical and chemical models. As hypolimnetic oxygenation becomes more widely used, there is a great need to move from an empirical approach to a mechanistic approach and improve the ability to predict induced sediment oxygen flux.

Relatively few studies have focused on simulating the complex interaction between bubble plumes and the surrounding water bodies, despite the development of many models for predicting bubble plume dynamics and/or oxygen transfer from bubble-plumes. Those studies that do combine bubble plume models with a lake model typically do not account for oxygen transfer from the bubbles to the ambient water, since they simulate circulation or destratification systems, in which gas transfer to the ambient water is not a primary concern [*Johnson et al.* 2000; *Schladow* 1993; *Zic et al.* 1992]. *Lindenschmidt and Hamblin* [1997] coupled a 1-D model (DYRESM) to stirring and bubbler modules to simulate vertical mixing resulting from lake aeration. *Imteaz and Asaeda* [2000] coupled DYRESM to a bubble-plume model and an ecological model to track phytoplankton growth, investigating the potential for bubble-plume destratification to reduce or control algal blooms. Neither of these models account for mass transfer between the bubbles and water, which is a crucial process for accurately predicting the performance of hypolimnetic oxygenation systems. Further, 1-D models such as DYRESM

assume homogeneous conditions in both horizontal directions and are unable to resolve the substantial differences between the near-field and far-field conditions. Resolving these differences is critical, since the near-field conditions strongly influence and determine the behavior of the bubble plumes [*McGinnis et al.* 2004].

Singleton et al. [2010] successfully coupled a validated linear bubble plume model [*Singleton et al.* 2007] with a 3-D hydrodynamic model to simulate the interaction between bubble-plumes and the natural hydrodynamics. *Singleton et al.* [2010] demonstrated the ability of such a coupled model to simulate the complex interaction between bubble plumes and large-scale oxygen transport and mixing processes. The coupled model accurately simulated the development and evolution of oxygen and temperature fields that were measured during two full-scale tests in Spring Hollow Reservoir, Virginia. The model correctly predicted the overall rate of oxygen addition from bubble plume operation to the hypolimnion. A sensitivity analysis showed the model was most sensitive to bathymetry, which was responsible for ~90% of the total uncertainty. The sensitivity analysis also suggested that accurate values of sediment oxygen flux are not critical to obtaining reasonable results for predicted oxygen concentrations, but that the relative scale of the oxygen flux should be well defined, since reported values can vary across two orders of magnitude [*Chapra* 1997].

The coupled model from *Singleton et al.* [2010] estimated sediment oxygen flux using an empirical correlation from *Gantzer et al.* [2009b] based on diffuser gas flow rate. While this approach may have provided reasonable end results, a comprehensive bubble-plume and 3-D hydrodynamic lake model should ideally include expressions for sediment oxygen flux based on simulated chemical and physical processes within the lake, rather than an empirical expression. Additionally, the scenario modeled by *Singleton et al.* [2010] represents a relatively simple scenario, in which there is a relatively small sediment surface area in the hypolimnion, and minimal natural currents, thus the empirical equation for J_{O2} proved acceptable. Larger and more energetic systems, such as those studied by *Bryant et al.* [2011a], are subject to increased spatial variability in turbulence, oxygen concentration, and thus J_{O2}, which reduces the likelihood of a simple correlation between J_{O2} and diffuser gas flow rate providing acceptable results for an overall oxygen budget in the hypolimnion.

In the current study, we build upon the work by *Singleton et al.* [2010] by incorporating an expression for J_{O2} based on local hydrodynamics and oxygen concentrations, thus improving upon the empirical expression previously used. By incorporating this mechanistically based expression, J_{O2} is allowed to vary throughout the lake according to changes in the local hydrodynamics, diffuser operation, and oxygen distribution, in an attempt at improving the simulation of the overall oxygen budget in the hypolimnion. This more comprehensive model could vastly improve our ability to predict diffuser-induced sediment oxygen flux, leading to improvements in oxygenation system design methods.

Methods

This study builds upon the coupled bubble-plume 3-D hydrodynamic model from *Singleton et al.* [2010]. The linear bubble plume model, 3-D hydrodynamic model, and coupling procedures are thoroughly detailed in the published with a brief overview of the models provided here.

Linear Bubble Plume Model

The linear bubble plume model is based on the circular plume model of *Wüest et al.* [1992] and modified for linear geometry [*Singleton et al.* 2007]. It is based on horizontally integrated equations for conservation of mass, momentum, and heat, and accounts for vertical density gradients resulting from differences in temperature and salinity. Eight equations are solved simultaneously, calculating water flow rate, temperature, salinity, oxygen and nitrogen transfer between the bubbles and water, aqueous oxygen and nitrogen concentrations, and plume rise height for a given diffuser geometry, gas flow rate, and initial bubble size. Entrainment of water into the plume is proportional to the local plume water velocity. The bubble size changes due to expansion and dissolution as the bubbles rise through the water column. Bubble slip velocity and gas transfer coefficients are a function of bubble radius, and Henry's constants for oxygen and nitrogen are a function of temperature [*Wüest et al.* 1992]. A correlation from *McGinnis and Little* [2002] is used to calculate the initial bubble size and a Froude number (Fr) is used to calculate the initial water velocity [*Wüest et al.* 1992], initially set to a value of 2.0 [*Singleton et al.* 2007, 2010]. A top-hat profile is assumed for water velocity, temperature, salinity, dissolved and aqueous oxygen and nitrogen, and bubble velocity. The plume entrainment coefficient (α)

and spreading coefficient (λ) are set to 0.11 and 0.93, respectively, based on work by *Fanneløp and Sjøen* [1980] and *Fanneløp et al.* [1991]. Vertical profiles of temperature and oxygen from the grid cell in which the plume is located are used as boundary conditions for the plume model. Further details regarding the linear plume model may be found in *Singleton et al.* [2007]. Details of the procedures for coupling the bubble plume model to the 3-D hydrodynamic model (described in the following section) may be found in *Singleton et al.* [2010].

3-D Hydrodynamic Model

The three-dimensional hydrodynamic model (Si3D) is used to simulate large-scale transport and mixing processes in the lake. It is based on the continuity equation for incompressible fluids, the Reynolds-averaged form of the Navier-Stokes equations for momentum, the transport equation for temperature, and an equation of state for density as a function of temperature. The turbulence closure model is a 2.5 order Mellor – Yamada type model [*Mellor and Yamada* 1982] with modifications proposed by *Galperin et al.* [1988] and *Kantha and Clayson* [1994] to calculate eddy diffusivity and eddy viscosity for simulating sub-grid size turbulent transport [*Rueda and Schladow* 2002, 2003]. A semi-implicit, three-level, iterative leapfrog-trapezoidal finite difference scheme on a structured Cartesian grid is used to solve the layer-averaged form of the governing equations. Further detailed description of the hydrodynamic model may be found in *Smith* [2006]. Si3D has been validated against analytical solutions and field observations from several lakes and is extensively described in the literature [*Acosta et al.* 2015; *Singleton et al.* 2010; *Smith* 2006; *Rueda et al.* 2005; *Smith et al.* 2005; *Rueda and Schladow,* 2002, 2003].

The version of Si3D used by *Singleton et al.* [2010] treated dissolved oxygen as a conservative tracer. Oxygen addition calculated from the bubble plume model is the sole source of oxygen, and flux of oxygen into the sediment is the only sink of oxygen, based on a zero-order value derived from an empirical relationship with diffuser gas flow rate. To improve the hydrodynamic model's capacity for simulating oxygen dynamics, additions were made to the code to account for oxygen flux at the lake surface, consumption of oxygen in the water column, and linking J_{O2} to the hydrodynamics.

Gaseous flux of oxygen at the surface (J) is calculated using equation 4.1, following the method of *Read et al.* [2012] to calculate the transfer velocity (k_t), where C is the dissolved oxygen concentration at the surface and C_{sat} is the saturated dissolved oxygen concentration. This method is based on the surface renewal model (equation 4.2), where η and n are empirical constants (taken to be 0.29 and 0.5, respectively), ε is the turbulence dissipation rate, ν is the kinematic viscosity of water, Sc is the Schmidt number (ν/D), and D is the molecular diffusivity of oxygen in water. The turbulence dissipation rate is calculated as the sum of turbulent inputs from wind shear (ε_u) and convection (ε_w). Turbulence from convection is given by $\varepsilon_w = -\beta$, where β is the buoyancy flux, while turbulence from wind shear is given by equation 4.3, where τ_t is the tangential shear stress, κ is the Von Karman constant, and δ_v is the stirring-dependent thickness of the diffusive sublayer [*Soloviev et al.* 2007].

$$J = k_t\left(C - C_{sat}\right) \tag{4.1}$$

$$k_t = \eta\left(\varepsilon\nu\right)^{1/4} Sc^n \tag{4.2}$$

$$\varepsilon_u = \frac{\left(\tau_t / \rho_w\right)^{3/2}}{\kappa\delta_v} \tag{4.3}$$

Oxygen demand in the water column, known as water oxygen demand (WOD), is often simulated based on organic carbon concentrations or biochemical oxygen demand (BOD), which typically follows first-order kinetics with respect to BOD [*Chapra* 1997]. In the absence of sufficient BOD data, a zero-order oxygen depletion rate was incorporated as a surrogate to account for WOD, as oxygen depletion rates in the bulk hypolimnion follow a zero-order pattern over the course of a stratified season [*Gantzer et al.* 2009b]. The zero-order rate constant at 20°C ($k_{\mathrm{WOD},20}$) was adjusted for temperature in each grid cell using an Arrhenius equation (equation 4.4), where T is temperature in Celsius and θ is the temperature adjustment factor. A value of 1.047 was assumed for θ_{WOD}, as this is a commonly used value for simulating WOD from BOD and within the range of values reported in the literature (1.02 – 1.075) [*Bowie et al.* 1985].

$$k_T = k_{20^\circ C}\theta^{(T-20)} \tag{4.4}$$

Oxygen flux across the SWI can be represented by equation 4.5, where C_B is the bulk oxygen concentration above the SWI and C_{SWI} is the concentration of oxygen directly at the SWI. *Bierlein et al.* [2015a] studied the impact of diffuser operation and hydrodynamics on J_{O2} in two oxygenated lakes, identifying two distinct mechanisms through which bubble plumes influence J_{O2}. First, the additional mixing and turbulence caused by the bubble plumes at high gas flow rates erodes the DBL, decreasing diffusive resistance to oxygen transport to the SWI and increasing J_{O2}. Second, the additional supply of oxygen from the bubble plume increases bulk oxygen concentrations, which increase the oxygen concentration gradient across the DBL and drives additional oxygen to the SWI. The study compares J_{O2} measured *in situ* with a microprofiler to estimates of J_{O2} calculated from various models of interfacial flux using turbulence data collected during the field study. *Bierlein et al.* [2015a] identified three interfacial flux models from the literature that scaled well with the measured J_{O2}.

For the current study, a model for calculating k_t proposed by *Lorke and Peeters* [2006] based on the Batchelor scale is incorporated into the hydrodynamic model (equation 4.6). *Bierlein et al.* [2015a] showed this model scales well with field measurements of J_{O2} in two oxygenated lakes. The *Lorke and Peeters* model, unlike other models considered in *Bierlein et al.*, does not rely on law-of-the-wall scaling arguments and is therefore most appropriate for boundary layers which may deviate from law-of-the-wall scaling due to periodic forcing, as is often the case in the hypolimnion of lakes [*Lorke et al.* 2002]. Equation 4.6 is used in each grid cell which directly overlays the sediment to calculate k_t from ε and ν in each cell. Viscosity is calculated from temperature using an equation of state, and the dissipation rate is calculated using equation 4.7, where q^2 is the turbulent kinetic energy production, B_1 is an empirical constant set to a value of 16.6, and l is the master turbulence length scale, calculated from the turbulence closure model.

$$J_{O2} = k_t \left(C_B - C_{SWI} \right) \tag{4.5}$$

$$k_t = \frac{1}{2\pi} Sc^{-1/2} \left(\varepsilon \nu \right)^{1/4} \tag{4.6}$$

$$\varepsilon = \frac{q^3}{B_1 l} \tag{4.7}$$

The hydrodynamic model cannot resolve oxygen concentration gradients at scales smaller than the discretized cells, and therefore it cannot predict C_{SWI}, the oxygen concentration at the SWI. To address this issue, an expression for J_{O2} that does not depend on C_{SWI} is incorporated into the model (equation 4.8) [*Higashino et al.* 2004; *Bierlein et al.* 2015b], where D_s is the diffusivity of oxygen in the sediment pore water (where $D_s = \varphi D$), φ is the sediment porosity, D is the diffusivity of oxygen in water, and k_0 is a zero-order kinetic rate constant describing oxygen consumption below the SWI. This expression links oxygen supply from the water side of the SWI, represented by C_B and k_t, with oxygen demand below the SWI, represented by D_s and k_0. The zero-order rate constant (k_0) is specified as 157 mg L^{-1} d^{-1} (see *Bierlein et al.* 2015b) at a temperature of 20°C and adjusted for temperature using equation 4.4 with a value of $\theta = 1.065$, a value often used for adjusting sediment-oxygen flux for temperature [*Joehnk and Umlauf* 2001; *Antonopoulous and Gianniev* 2003; *Demetracopoulus and Stefan* 1983]. The sediment oxygen flux is thus allowed to vary with time according to simulated changes in temperature, dissolved oxygen concentration, and turbulence in the bottom cells overlaying the sediment. Further, variability in J_{O2} is able to be included without incorporating an additional sediment model or sub grid size transport model. The effect of diffuser operations on C_B, k_t, and J_{O2} can therefore be accounted for in a comprehensive model.

$$J_{O2} = \frac{D_s k_0 - \sqrt{\left(D_s k_0\right)^2 + 2 D_s k_0 C_B k_t^2}}{k_t} \tag{4.8}$$

Field Data Collection

Carvin's Cove Reservoir (CCR, Figure 4.1) is a eutrophic water supply reservoir near Roanoke, Virginia, that serves as one of the primary sources of drinking water for the City of Roanoke. It has a surface area of approximately 2.5 km^2, maximum depth of 23 m, and a volume of approximately 24×10^6 m^3. A hypolimnetic oxygenation system composed of two linear bubble-plume diffusers, bubbling oxygen gas into the hypolimnion, was installed in the deepest portion of the hypolimnion near the water-treatment plant intake in 2005 to mitigate episodes of elevated soluble iron and manganese stemming from seasonal hypoxia. The oxygenation system has been quite successful at maintaining adequate DO in the hypolimnion and preventing hypoxic release of reduced iron and manganese [*Gantzer et al.* 2009a].

Two field-sampling campaigns were performed on CCR to collect data for initializing, calibrating, and validating the hydrodynamic model. The first campaign was from 25 July to 16 August 2011. During this campaign, vertical profiles of temperature and DO were collected 1 – 2 times per day at seven sampling locations (Figure 4.1) covering the extent of the hypolimnion, in both the plume near- and far-field, using a CTD (SeaBird Electronics SBE 19plus) that samples at 4 Hz. The diffuser system was operated at the maximum design flow rate of 68 NCMH for the entirety of the field campaign, except for a 48-hour period when it was switched off completely, from approximately 08:30 on 29 July to 09:15 on 31 July. The second field campaign was performed from 26 May to 2 June 2013. Vertical profiles of temperature and DO were collected once per day with the CTD at the same seven locations from the 2011 campaign. Additionally, a microprofiler (Unisense MP-4) was deployed near the oxygen diffuser to collect *in situ* measurements of J_{O2}. Complete details of the microprofiler setup, sampling scheme, and J_{O2} calculations may be found in *Bierlein et al.* [2015a]. Diffuser flow rate was adjusted roughly every 24-hours, covering the entire operational range of flow rates.

During both field campaigns, a weather station (Campbell Scientific) was installed on the reservoir dam, collecting time-averaged measurements of wind speed and direction, total solar radiation, air temperature, relative humidity, and rainfall intensity every 10 minutes. Water inflows to the reservoir during the campaigns were negligible, and daily records of water withdrawal volumes to the Carvin's Cove water treatment plant were obtained from the Western Virginia Water Authority, which manages CCR and the water treatment plant. Updated bathymetric data for CCR was collected prior to the 2011 field campaign using an ADCP (RD Instruments Workhorse RioGrande, 1200kHz) connected to a GPS unit (Trimble DSM232) and towed alongside a boat.

Model Setup

The hydrodynamic model was set up in a similar fashion to *Singleton et al.* [2010]. Using the updated bathymetric data, the bathymetry was discretized into 15×15×0.5 m grid cells. The model is initialized using a single temperature and DO profile measured at the midpoint of the diffuser, since the bubble plume model is sensitive to the boundary conditions [*McGinnis et al.*

2004]. A constant time step of 10 s was used, and approximately five days of simulated time was included before the simulated field campaigns to allow for model spin-up. The model is forced using meteorological data collected with the weather station during the field campaigns, water withdrawal volumes from the drinking water treatment plant intakes, and bubble plume applied gas flow rate. The bubble plume is modeled in discrete segments at the bottom of each grid cell, which allows the elevation of the diffuser to vary with the reservoir bathymetry. In each cell, the plume rises to the depth of maximum plume rise (DMPR) and detrains perpendicular to the diffuser into the adjacent cells at the DMPR. The total flow rate to each diffuser line is distributed equally among the grid cells in which that diffuser line in located. The plume model is updated every 90 time steps (15 minutes).

Model calibration and validation procedures

Data from the field campaign on CCR in 2011 is used to calibrate the model to the observed dissolved oxygen profiles, using k_{WOD} as the sole fitting parameter. To compare runs, several measures of error were considered: mean error (*ME*), relative error (*RE*), root mean square error (*RMSE*), and modeling efficiency (*EF*), represented by equations 4.9 – 4.12 [*Mayer and Butler* 1993; *Power* 1993]. *ME* provides a measure of model bias, and *RE* and *RMSE* provide a measurement of accuracy. *EF* provides a measure of how well the model reproduces the observed data, similar to the more commonly used regression coefficient (R^2) in that a value equal to 1 represents a perfect agreement between the observed and simulated data, but *EF* may also have a value less than zero, which indicates that a simple mean of the observed data performs better than the model [*Mayer and Butler* 1993]. The value of k_{WOD} that maximizes *EF* was selected as the best-fit water oxygen demand constant. This best-fit value is assumed for the validation run, which uses field data from CCR in 2013, and the results are compared to observed oxygen and temperature profiles, as well as measurements of J_{O2} and k_t made with the microprofiler in the diffuser near field. Because the intended use of this model is to be able to simulate and predict the effects of bubble plume oxygenation on oxygen concentrations and J_{O2} in the hypolimnion, the results and discussion presented in the following section are focused on the hypolimnion, rather than the entire water column.

$$ME = \frac{\sum (y_{obs} - y_{sim})}{n} \quad (4.9)$$

$$RE = \frac{\sum (y_{obs} - y_{sim})}{\sum y_{obs}} \quad (4.10)$$

$$RMSE = \left[\frac{\sum (y_{obs} - y_{sim})^2}{n} \right]^{0.5} \quad (4.11)$$

$$EF = 1 - \frac{\sum (y_{obs} - y_{sim})^2}{\sum (y_{obs} - \overline{y}_{obs})^2} \quad (4.12)$$

Results and Discussion

Model Calibration

Following the calibration procedures outlined previously, a value of k_{WOD} = 0.34 mg L^{-1} d^{-1} at a temperature of 20°C was found to maximize *EF* for the simulated 2011 field campaign in CCR. The calibrated simulation, on average, slightly overestimates the observed temperature and dissolved oxygen when compared to the field CTD profiles, as evidenced by the negative values for *ME* and *RE* (Table 4.1). The simulated temperatures agree quite well with the observed temperatures, as evidenced by the high *EF* (0.973), while simulated dissolved oxygen concentrations show less agreement (Table 4.1 and Figure 4.2). Plots of modeled versus observed oxygen concentration (Figure 4.2a) show two main areas of deviation from the 1:1 line. The region where observed DO is higher than the modeled DO corresponds to an underestimate of DO near the metalimnion. The region with high simulated DO relative to the observed DO corresponds to overestimated oxygen concentrations near the SWI. The points in Figure 4.2b that deviate from the 1:1 line are a result of modeled temperatures being overestimated in the upper reaches of the hypolimnion.

Model Validation

The validation simulation, which assumes the best-fit value of k_{WOD} from the calibrated simulation, agreed much better with the observed temperature and oxygen profiles than the calibration run, as evidenced by the higher values of *EF* for both oxygen and temperature (Table

4.1). The model still has a tendency to overestimate both temperature and dissolved oxygen to a similar extent as in the calibrated simulation, but overall performs much better, as *EF* for temperature is nearly 1 and *EF* for dissolved oxygen is nearly 0.9. Plots of modeled versus observed oxygen and temperature in Figure 4.3 also show the paired data points following the 1:1 line more closely than in the calibration simulation, indicating a better reproduction of observed temperature and oxygen profiles. The underestimation of dissolved oxygen near the thermocline is no longer present in the validation simulation, and the overestimation of oxygen near the SWI is less prevalent and less severe, though it does still exist (Figure 4.3a).

Temperature profiles, shown in Figure 4.4b, show reasonable agreement between observed and simulated temperature in the hypolimnion at sampling point CV, which is in the plume near field. In the upper reaches of the hypolimnion, near the thermocline, the temperature profiles are in good agreement, but deviate by ~0.3°C near the SWI. This temperature discrepancy is likely due to the fact that the observed profile on 27 May was used to initialize the model, which starts on May 22, but then is also compared to the simulated profile on 27 May. Thus, in order to have perfect agreement between the observed and simulated profiles, the simulated temperature profile would need to remain constant during the 5-day spin up period. Despite the small discrepancy in temperature, the rate of temperature increase shows good agreement, with observed temperature profiles increasing by ~0.15 – 0.2°C from 27 May to 2 June, and simulated temperature profiles showing similar increases over the same period. The slight temperature gradients in the bottom 1 – 2 meters in the observed profiles are not preserved by the model, however, as the bottom 1 – 2 meters in the simulated profiles have a constant temperature.

Dissolved oxygen profiles (Figure 4.4a) show somewhat less agreement between the field observations and simulations, as suggested by the lower *EF* for oxygen than for temperature. Simulated oxygen concentrations in the upper and mid-hypolimnion, which would be receiving dissolved oxygen from the bubble plume operation, are generally quite reasonable, though in some instances the concentrations may deviate by up to 1 mg L^{-1}, though the differences are typically less. In the bottom 3 m, and especially the bottom 1 m, the simulated oxygen profiles begin to deviate from field observations more than in the bulk hypolimnion. The simulated profiles do not fully preserve the concentration gradients seen in the field profiles, though they

do show a decline in concentration relative to the middle and upper regions of the hypolimnion. The oxygen concentrations at the very bottom of the profiles deviate the most from field observations, by as much as 3 – 4 mg L^{-1}.

This discrepancy in oxygen concentration could potentially be a result of either excessive vertical mixing in the bottom 1 m or some chemical process exerting an additional local demand for oxygen in the bottom 1 m of water. Simulations performed with a user-specified vertical eddy diffusivity, rather than the vertical eddy diffusivity calculated from the turbulence closure model, show that vertical eddy diffusivity would need to be on the order of 10^{-8} – 10^{-9} m^2 s^{-1} to preserve the concentration gradients seen in the field profiles, however these values are 2 – 3 orders of magnitude smaller than what is typical in the hypolimnion. The turbulence closure model calculates vertical eddy diffusivities on the order of 10^{-6} m^2 s^{-1} in the hypolimnion, which is of similar magnitude to field studies which report measured vertical eddy diffusivities in the hypolimnion [*Quay et al.* 1980]. Thus, calculated vertical eddy diffusivities from the turbulence closure model seem reasonable and are not likely the cause of the differences between simulated and observed oxygen profiles.

Missing oxygen-consuming chemical processes may contribute to the discrepancy between the simulated and observed oxygen profiles, given the lack of a comprehensive water quality model in the coupled bubble plume and Si3D model. One possible source of additional oxygen demand in the bottom 1 m of water could be manganese. *Bryant et al.* [2011b] showed that oxygenation actually enhances soluble manganese flux from below the SWI, as the increased availability of oxygen in the hypolimnion oxidizes soluble manganese, increasing the concentration gradient between the zone below the SWI where manganese is reduced and the bulk hypolimnion. *Gantzer et al.* [2009a] also observed that despite maintaining high oxygen concentrations and low soluble manganese in the bulk hypolimnion during oxygenation, both soluble and particulate manganese were present in high concentrations (upwards of 4 mg L^{-1}) in the bottom 1 m of CCR. While there were no water quality samples collected in the bottom 1 m of water during the 2013 field experiments on CCR, conductivity and turbidity profiles (Figure 4.5) both increase sharply in the bottom 1 m of water, coinciding with the sharp decrease in oxygen concentrations. This provides additional evidence for an oxygen-consuming chemical process occurring in the bottom

1 m that is not accounted for in the hydrodynamic model. Increased conductivity could be the result of high concentrations of soluble metals (such as reduced manganese or iron) diffusing from the sediments, and the turbidity increase may be a result of increased particulates, as the soluble metals are oxidized by oxygen to an insoluble form and settle toward the SWI. The turbidity increase may also be a result of sediment resuspension caused by the bubble plume, which may also enhance oxygen consumption in the bottom 1 m of water if the sediment contains labile carbon.

As a result of the high simulated oxygen concentrations near the SWI, the modeled J_{O2} is also higher than what was observed in the field (Figure 4.6). Simulated J_{O2} is 2x – 3x higher than J_{O2} measured with the microprofiler. This largely stems from the high simulated oxygen concentrations in water overlaying the sediment, as these simulated concentrations are typically 2x – 2.5x higher than concentrations measured with the microprofiler at 10 cm above the SWI (Figure 4.7). The same gradual decreasing trend in oxygen concentration near the sediment is preserved in the simulations (Figure 4.7), however the concentrations are overestimated by ~ 5 – 6 mg L^{-1}. The transfer velocity (k_t) calculated from equation 4.6 scales well with observed k_t, calculated from the microprofiles as $k_t = D/\delta_{DBL}$, though the simulated k_t is not as variable as the observed k_t (Figure 4.8). Thus, high oxygen concentrations near the sediment contribute to the overestimation of J_{O2} in the model, and the decreased variability in k_t calculated from the turbulence closure model dampens the temporal variability in J_{O2} when compared to the field measurements. If simulated oxygen concentrations from the hydrodynamic model were able to accurately reproduce those seen in the field, simulated J_{O2} should also agree much better with measurements of J_{O2} in the field.

Impact of Bubble Plume Operation

Despite the high simulated J_{O2} and oxygen concentrations near the sediment, the effects of diffuser operation on J_{O2} can still be seen in the simulations. As shown in Figure 4.9, when the diffuser is in operation, J_{O2} is higher than when the diffuser is turned off, as shown by the warmer colors in Figure 4.9a relative to Figure 4.9b. Additionally, differences in the total mass of oxygen lost from the hypolimnion to J_{O2} can be determined by running scenarios without the oxygen diffuser. For example, total J_{O2} in the hypolimnion during the validation run, with the

simulated oxygen diffuser operating as it did during the field experiments, totals ~2200 kg of oxygen over the seven day period. Performing the simulation again, but without the diffuser operating at all during the simulated period, results in a total of ~2000 kg of oxygen entering the sediments. This suggests only a 10% increase in J_{O2} as a result of diffuser operation, which is relatively low compared to typically observed increases in the field and factors of safety used by engineers designing hypolimnetic oxygenation systems. Worth noting, however, is that even in the scenario without oxygenation, the model was initialized with an oxygen profile for CCR that was collected while the reservoir was actually being oxygenated. Thus, there was already a large mass of oxygen in the hypolimnion and the differences in oxygen distribution between simulations with and without the bubble plume over the short period of seven days was not great. If, on the other hand, the scenarios were initialized with an oxygen profile collected before turning on the oxygenation system, the effect of diffuser operation on J_{O2} should be much more pronounced.

Toward a Comprehensive Oxygenation Model

The methods and simulations described show the relatively straightforward manner in which J_{O2} can be linked to turbulence and oxygenation system operation in a hydrodynamic model. This provides a mechanistic expression for calculating J_{O2} from oxygen concentrations and turbulence near the SWI, rather than using it as a fitting parameter for the oxygen budget. It also allows the hydrodynamic model to account for the lake-specific consumption of oxygen in the sediments to be incorporated into the model, without the need for a detailed and comprehensive sediment model. Thus, J_{O2} can be represented in a mechanistic fashion, varying in accordance with oxygen concentration and hydrodynamics, without significantly increasing model run times or complexity. By incorporating a more comprehensive water quality model into the coupled bubble plume and hydrodynamic model presented here, a comprehensive lake oxygenation model could be realized, which would account for hydrodynamics, bubble plume operation, and variable J_{O2}. Conversely, the expression for J_{O2} described here and an appropriate oxygenation system model could be incorporated into existing hydrodynamic and water quality models to arrive at a comprehensive model for lake oxygenation. Either way, a comprehensive model for could be achieved and used to improve current oxygenation system design practices.

Conclusions

As hypolimnetic oxygenation becomes a relatively common lake management tool, there is a growing need to better understand the impact that these systems have on lake hydrodynamics and oxygen distribution, which will lead to improved methods for designing and operating hypolimnetic oxygenation systems. Of particular importance is the ability to predict the effects of oxygenation on J_{O2} and move oxygenation system design practices from the current empirical approach to a mechanistically based approach.

The modeling work presented in this study advances the field toward a comprehensive model for predicting oxygenation-induced J_{O2}. An expression for J_{O2} was incorporated into a coupled bubble plume and 3D hydrodynamic lake model, allowing J_{O2} to vary spatially and temporally. Additional oxygen sources and sinks were also added to improve the ability of the hydrodynamic model to simulate oxygen dynamics. Oxygen consuming processes in the bottom 1 meter of the water column that are not accounted for contribute to artificially high oxygen concentrations near the SWI and ultimately result in high simulated J_{O2}. Despite this, the model is able to capture the effect of diffuser operation on J_{O2} and provide an estimate of J_{O2} induced by the diffuser operation. A more comprehensive water quality model needs to be incorporated into the hydrodynamic model presented here, which should improve the simulated oxygen budget, especially near the SWI. Once these improvements are made, the simulated oxygen concentrations above the SWI and J_{O2} should agree much better with field observations, and, following additional calibration and validation, the model could be used to improve oxygenation system design and operation.

References

Acosta, M., M. Anguita, F. J. Fernández-Baldomero, C. L. Ramón, S. G. Schladow, and F. J. Rueda (2015), Evaluation of a nested-grid implementation for 3D finite-difference semi-implicit hydrodynamic models, *Environmental Modelling and Software*, 64(2), 241-262.

Antonopoulous, V. Z., and S. K. Gianniou (2003), Simulation of water temperature and dissolved oxygen distribution in Lake Vegoritis, Greece, *Ecological Modelling,* 160(1), 39-53.

Beutel, M. W. (2003), Hypolimnetic anoxia and sediment oxygen demand in California drinking water reservoirs, *Lake and Reservoir Management,* 19(3), 208-221.

Beutel, M. W., T. M. Leonard, S. R. Dent, and B. C. Moore (2008), Effects of aerobic and anaerobic conditions on P, N, Fe, Mn, and Hg accumulation in waters overlaying profundal sediments of an oligo-mesotrophic lake, *Water Research,* 42(8-9), 1953-1962.

Bierlein, K. A., M. Rezvani, S. A. Socolofsky, L. D. Bryant, and J. C. Little (2015a), Increased sediment oxygen flux in oxygenated lakes: the impact of bubble plumes, Manuscript in preparation.

Bierlein, K. A., L. D. Bryant, and J. C. Little (2015b), A transient model of dissolved oxygen kinetics in lake sediment, Manuscript in preparation.

Bowie, G. (1985), Rates, constants, and kinetics formulations in surface water quality modeling, TetraTech.

Bryant, L. D., P. A. Gantzer, and J. C. Little (2011a), Increased sediment oxygen uptake caused by oxygenation-induced hypolimnetic mixing, *Water Research,* 45(12), 3692-3703.

Bryant, L. D., H. Hsu-Kim, P. A. Gantzer, and J. C. Little (2011b), Solving the problem at the source: Controlling Mn release at the sediment-water interface via hypolimnetic oxygenation, *Water Research,* 45(19), 6381-6392.

Chapra, S. C. (1997), *Surface Water-Quality Modeling,* 844 pp., McGraw-Hill, Boston, Mass.

Demetracopoulus, A. C., and H. G. Stefan (1983), Model of Mississippi river pool: dissolved oxygen, *Journal of Environmental Engineering,* 109(5), 1020-1034.

Fanneløp, T. K., and K. Sjøen (1980), Hydrodynamics of underwater blowouts, *Norwegian Maritime Research,* 4, 17-33.

Fanneløp, T. K., S. Hirschberg, and J. Küffer (1991), Surface current and recirculating cells generated by curtains and jets, *Journal of Fluid Mechanics,* 229, 629-657.

Funkey, C. P., D. J. Conley, N. S. Reuss, C. Humborg, T. Jilbert, and C. P. Slomp (2014), Hypoxia sustains cyanobacteria blooms in the Baltic Sea, *Environmental Science and Technology,* 48(5), 2598-2602.

Galperin, B., L. H. Kantha, S. Hassid, and A. Rosati (1988), A quasi-equilibrium turbulent energy model for geophysical flows, *Journal of the Atmospheric Sciences,* 45(1), 55-62.

Gantzer, P. A., L. D. Bryant, and J. C. Little (2009a), Controlling soluble iron and manganese in a water-supply reservoir using hypolimnetic oxygenation, *Water Research,* 43(5), 1285-1294.

Gantzer, P. A., L. D. Bryant, and J. C. Little (2009b), Effect of hypolimnetic oxygenation on oxygen depletion rates in two water-supply reservoirs, *Water Research,* 43(6), 1700-1710.

Gerling, A. B., R. G. Browne, P. A. Gantzer, M. H. Mobley, J. C. Little, and C. C. Carey (2014), First report of the successful operation of a side stream supersaturation hypolimnetic oxygenation system in a eutrophic shallow reservoir, *Water Research,* 67, 129-143.

Higashino, M., C. Gantzer, and H. Stefan (2004), Unsteady diffusional mass transfer at the sediment/water interface: Theory and significance for SOD measurement, *Water Research,* 38(1), 1-12.

Imteaz, M. A., and T. Asaeda (2000), Artificial mixing of lake water by bubble plumes: effects of bubbling operations on algal blooms, *Water Research,* 34(6), 1919-1929.

Joehnk, K. D., and L. Umlauf (2001), Modelling the metalimnetic oxygen minimum in a medium sized alpine lake, *Ecological Modelling,* 136(1), 67-80.

Johnson, G. P., N. J. Hornewer, D. M. Robertson, D. T. Olson, and J. Gioja (2000), Methodology, data collection and data analysis for determination of water-mixing patterns induced by aerators and mixers, *Water Resources Investigations Report 00-4101,* U.S. Geological Survey.

Kantha, L. H., and C. A. Clayson (1994), An improved mixed layer model for geophysical applications, *Journal of Geophysical Research,* 99(C12), 25235-25266.

Lindenschmidt, K. E. and P. F. Hamblin (1997), Hypolimnetic aeration in Lake Tegel, Berlin, *Water Research,* 31(7), 1619-1628.

Lorke, A., L. Umlauf, J. Tobias, and A., Wüest (2002), Dynamics of turbulence in low-speed oscillating bottom-boundary layers of stratified basins, *Environmental Fluid Mechanics*, 2, 291-313.

Lorke, A., and F. Peeters (2006), Toward a unified scaling relation for interfacial fluxes, *Journal of Physical Oceanography,* 36(5), 955-961.

Mayer, D. G., and D. G. Butler (1993), Statistical validation, *Ecological Modelling,* 68(1), 21-32.

McGinnis, D. F., and J. C. Little (2002), Predicting diffused-bubble oxygen transfer rate using the discrete-bubble model, *Water Research,* 36(18), 4627-4635.

McGinnis, D. F., A. Lorke, A. Wüest, A. Stockli, and J. C. Little (2004), Interaction between a bubble plume and the near field in a stratified lake, *Water Resources Research,* 40(10), W10206.

Mellor, G. L., and T. Yamada (1982), Development of a turbulence closure model for geophysical fluid problems, *Reviews of Geophysics and Space Physics,* 20(4), 851-875.

Moore, B. C., P. Chen, W. H. Funk, and D. Yonge (1996), A model for predicting lake sediment oxygen demand following hypolimnetic aeration, *Water Resources Bulletin,* 32(4), 723-731.

Power, M. (1993), The predictive validation of ecological and environmental models, *Ecological Modelling,* 68(1), 33-50.

Prepas, E. E., and J. M. Burke (1997), Effects of hypolimnetic oxygenation on water quality in Amisk Lake, Alberta, a deep, eutrophic lake with high internal phosphorus loading rates, *Canadian Journal of Fisheries and Aquatic Sciences,* 54(9), 2111-2120.

Quay, P. D., W. S. Broecker, R. H. Hesslein, and D. W. Schindler (1980), Vertical diffusion rates determined by tritium tracer experiments in the thermocline and hypolimnion of two lakes, *Limnology and Oceanography,* 25(2), 201-218.

Read, J. S., D. P. Hamilton, A. R. Desai, K. C. Rose, S. MacIntyre, J. D. Lenters, R. L. Smyth, P. C. Hanson, J. J. Cole, P. A Staehr, J. A. Rusak, D. C. Pierson, J. D. Brookes, A. Laas, and C. H. Wu (2012), Lake-size dependency of wind shear and convection as controls on gas exchange, *Geophysical Research Letters,* 39, L09405.

Rueda, F. J., and S. G. Schladow (2002), Quantitative comparison of models for barotropic response of homogeneous basins, *Journal of Hydraulic Engineering,* 128(2), 201-213.

Rueda, F. J., and S. G. Schladow (2003), Dynamics of a large polymictic lake II: Numerical simulations, *Journal of Hydraulic Engineering,* 129(2), 92-101.

Rueda, F. J., S. G. Schladow, S. G. Monismith, and M. T. Stacey (2005), On the effects of topography on wind and the generation of currents in a large multi-basin lake, *Hydrobiologia,* 532, 139-151.

Schladow, S. G. (1993), Lake destratification by bubble-plume systems – design methodology, *Journal of Hydraulic Engineering – ASCE,* 119(3), 350-368.

Singleton, V. L., and J. C. Little (2006), Designing hypolimnetic aeration and oxygenation systems – A review, *Environmental Science and Technology,* 40(24), 7512-7520.

Singleton, V. L., P. Gantzer, and J. C. Little (2007), Linear bubble plume model for hypolimnetic oxygenation: full-scale validation and sensitivity analysis, *Water Resources Research,* 43(2), W02405.

Smith, P. E. (2006), A semi-implicit, three-dimensional model of esturarine circulation, *U.S. Geological Survey Open File Report, 2006-1004.*

Smith, P., J. Donovan, and H. Wong (2005), Applications of 3D hydrodynamic and particle tracking models in the San Francisco Bay-Delta estuary, *Impacts of Global Climate Change*, pp. 1-8. doi: 10.1061/40792(173)393.

Soloviev, A., M. Donelan, H. Graber, B. Haus, and P. Schlüssel (2007), An approach to estimation of near-surface turbulence and CO_2 transfer velocity from remote sensing data, *Journal of Marine Systems,* 66, 182-194.

Wüest, A., N. H. Brooks, and D. M. Imboden (1992), Bubble plume modeling for lake restoration, *Water Resources Research,* 28(12), 3235-3250.

Zic, K., H. G. Stefan, and C. Ellis (1992), Laboratory study of water destratification by a bubble plume, *Journal of Hydraulic Research,* 30(1), 7-27.

Table 4.1. Summary of goodness-of-fit measures for calibration and validation simulations

	Temperature				Dissolved Oxygen			
	Mean Error	Relative Error	Root Mean Square Error	Modeling Efficiency	Mean Error	Relative Error	Root Mean Square Error	Modeling Efficiency
Calibration	-0.071	-0.010	0.485	0.973	-0.176	-0.025	1.193	0.697
Validation	-0.083	-0.007	0.147	0.994	-0.267	-0.023	0.933	0.890

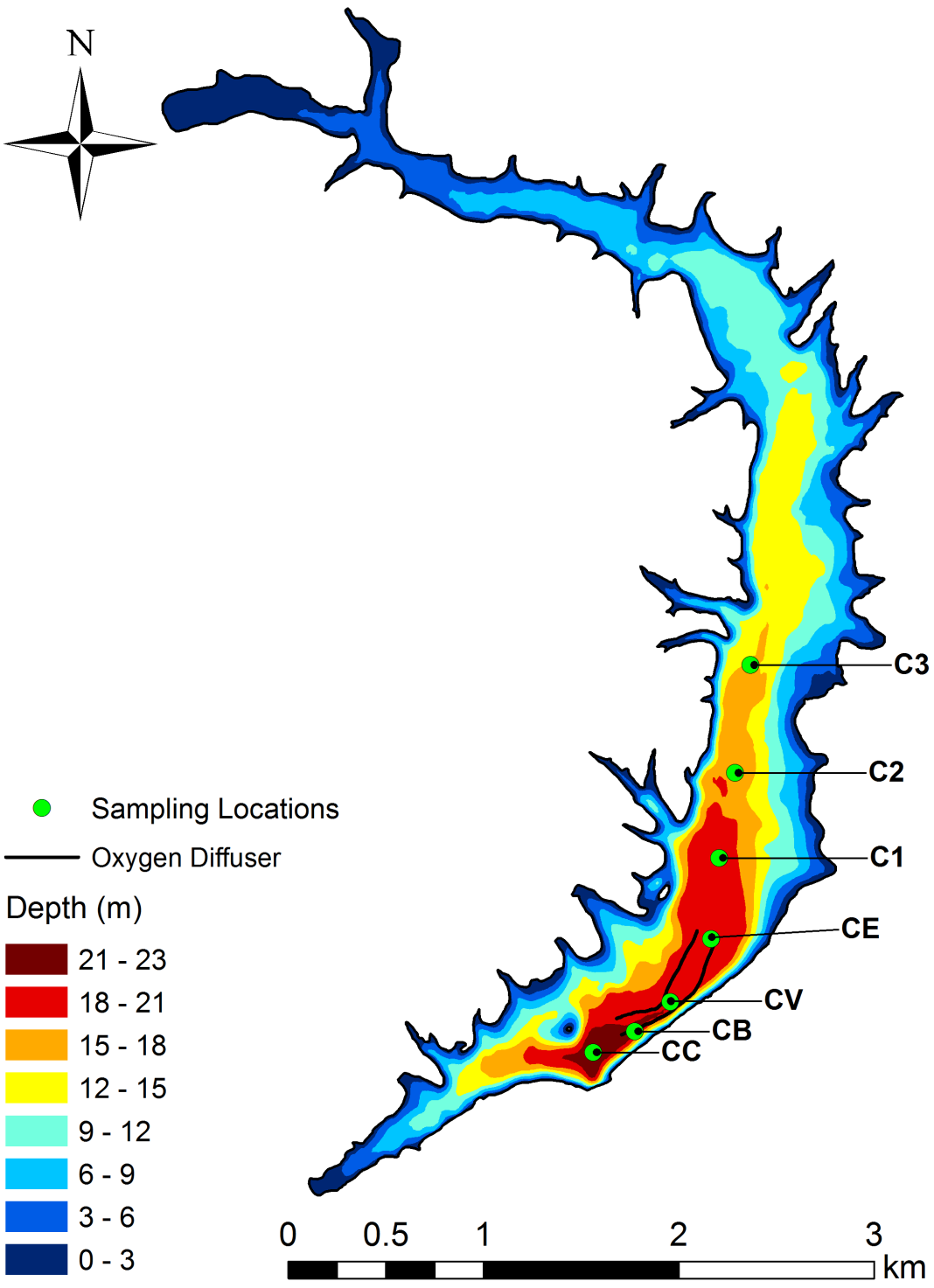

Figure 4.1. Bathymetric map of Carvin's Cove Reservoir, including the location of the two linear oxygen diffuser lines and seven sampling locations.

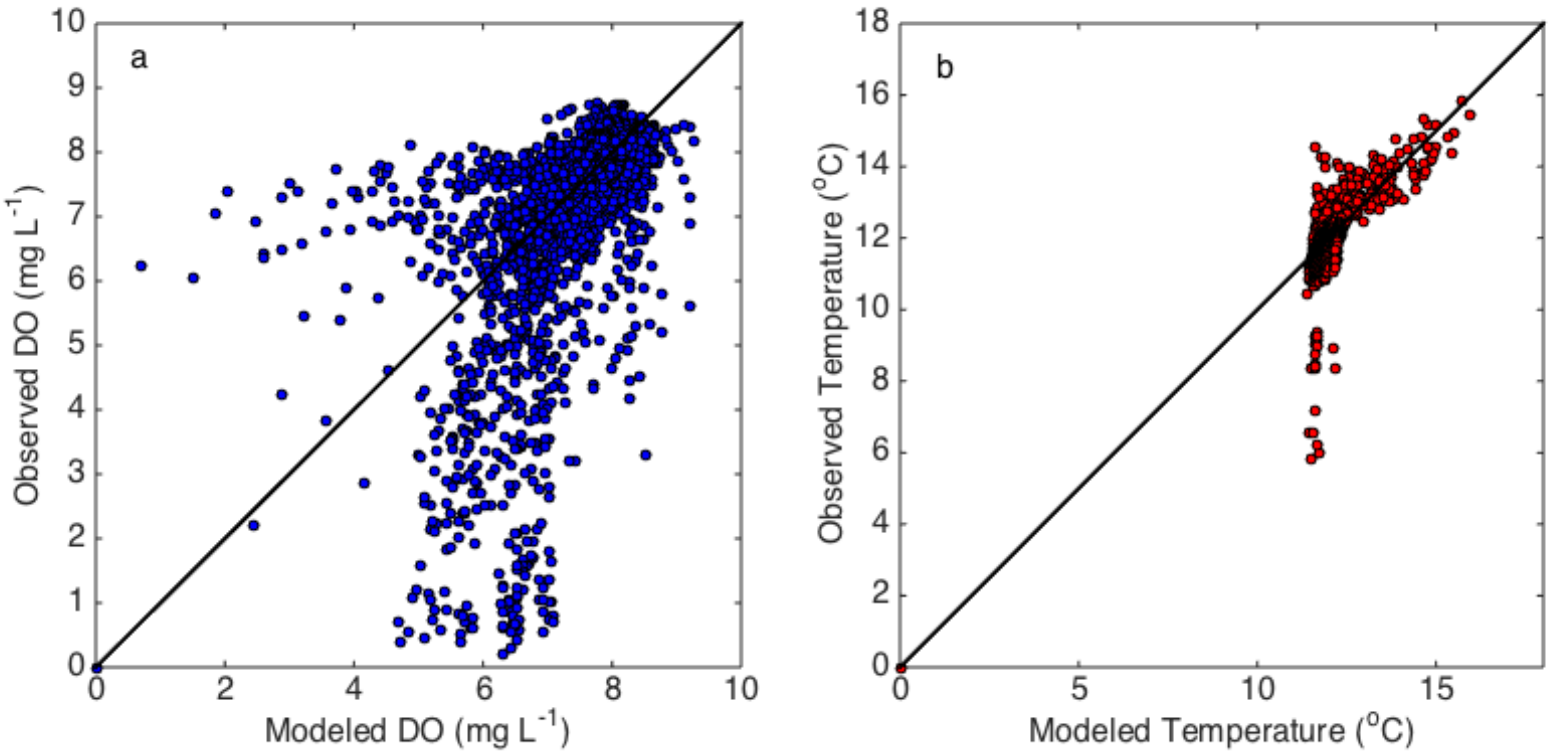

Figure 4.2. Comparisons between modeled and observed dissolved oxygen (a) and temperature (b) in the hypolimnion for the calibrated Carvin's Cove Reservoir 2011 simulation. Black lines represent a 1:1 line.

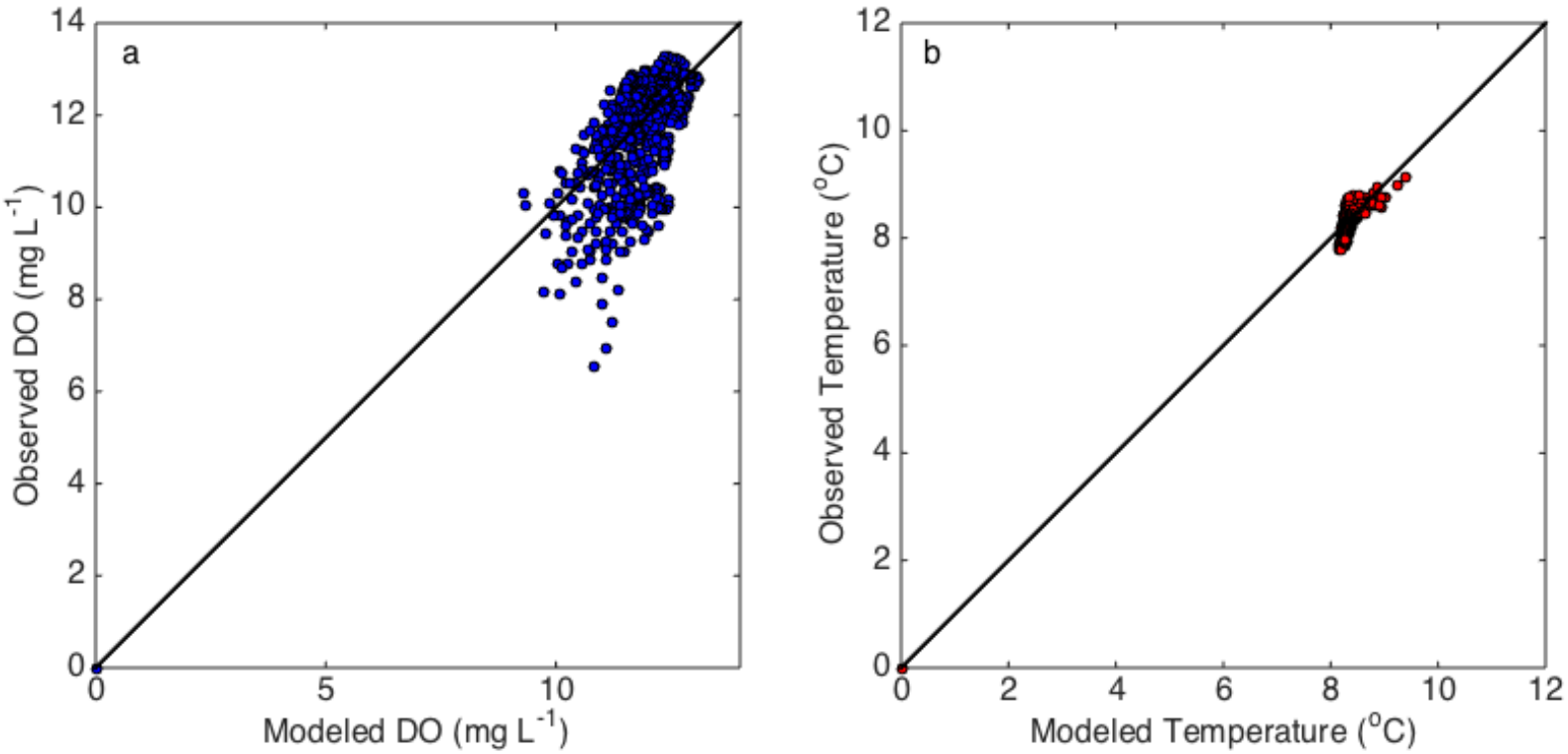

Figure 4.3. Comparisons between modeled and observed dissolved oxygen (a) and temperature (b) in the hypolimnion for the validation Carvin's Cove Reservoir 2013 simulation. Black lines represent a 1:1 line.

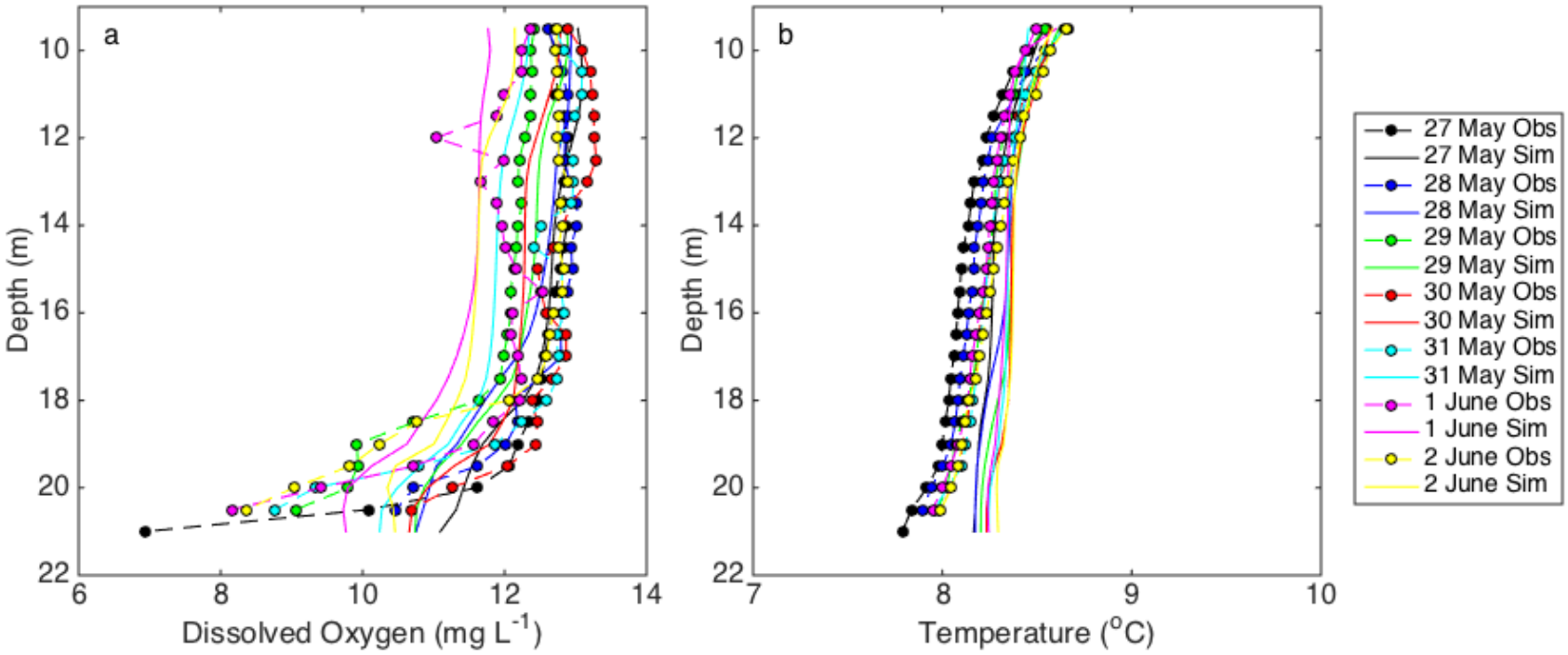

Figure 4.4. Comparison between simulated and observed dissolved oxygen (a) and temperature (b) profiles in the hypolimnion for the Carvin's Cove 2013 simulations at sampling point CV.

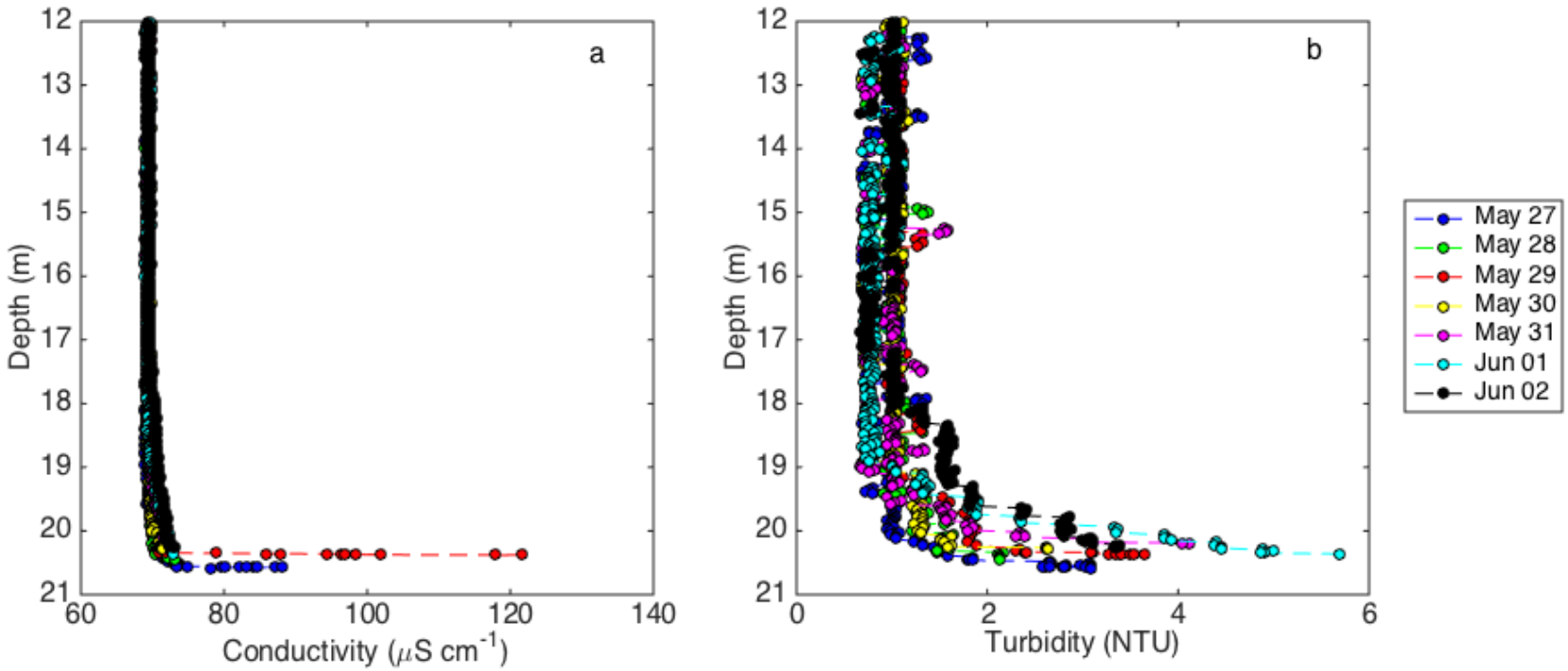

Figure 4.5. Conductivity (a) and turbidity (b) profiles in the hypolimnion collected during the Carvin's Cove Reservoir 2013 field campaign at sampling location CV.

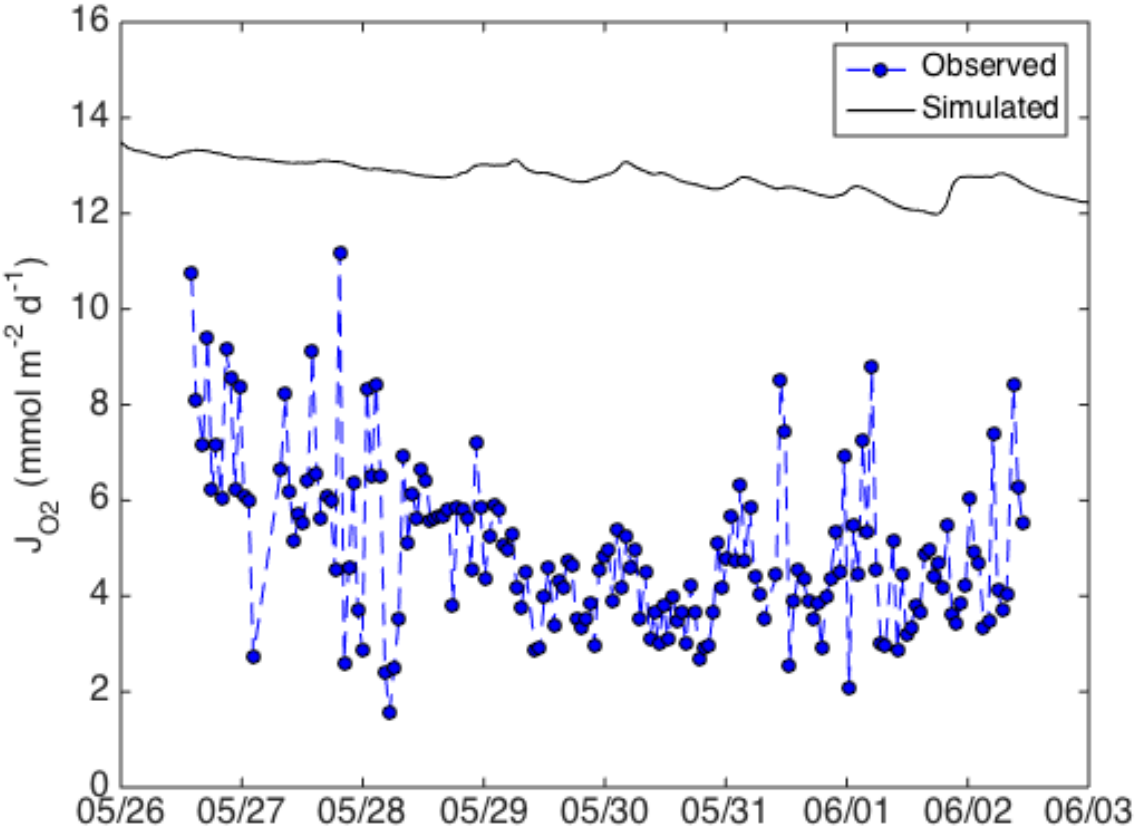

Figure 4.6. Comparison between the observed sediment oxygen flux (J_{O2}) measured with the microprofiler at location CV during the 2013 field campaign and the simulated J_{O2} at CV during the simulated 2013 period.

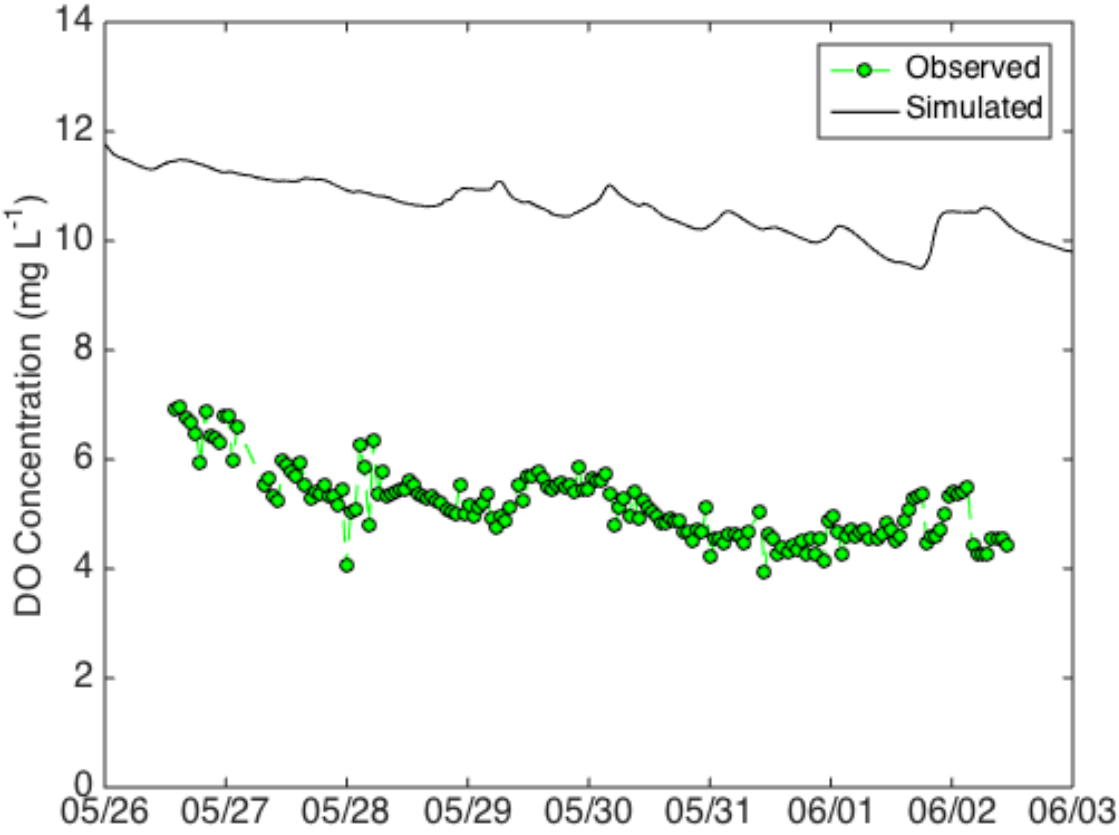

Figure 4.7. Comparison between the observed dissolved oxygen (DO) concentration measured with the microprofiler at 10 cm above the SWI at sampling point CV during the 2013 field campaign and the simulated oxygen concentration at 25 cm above the SWI at CV.

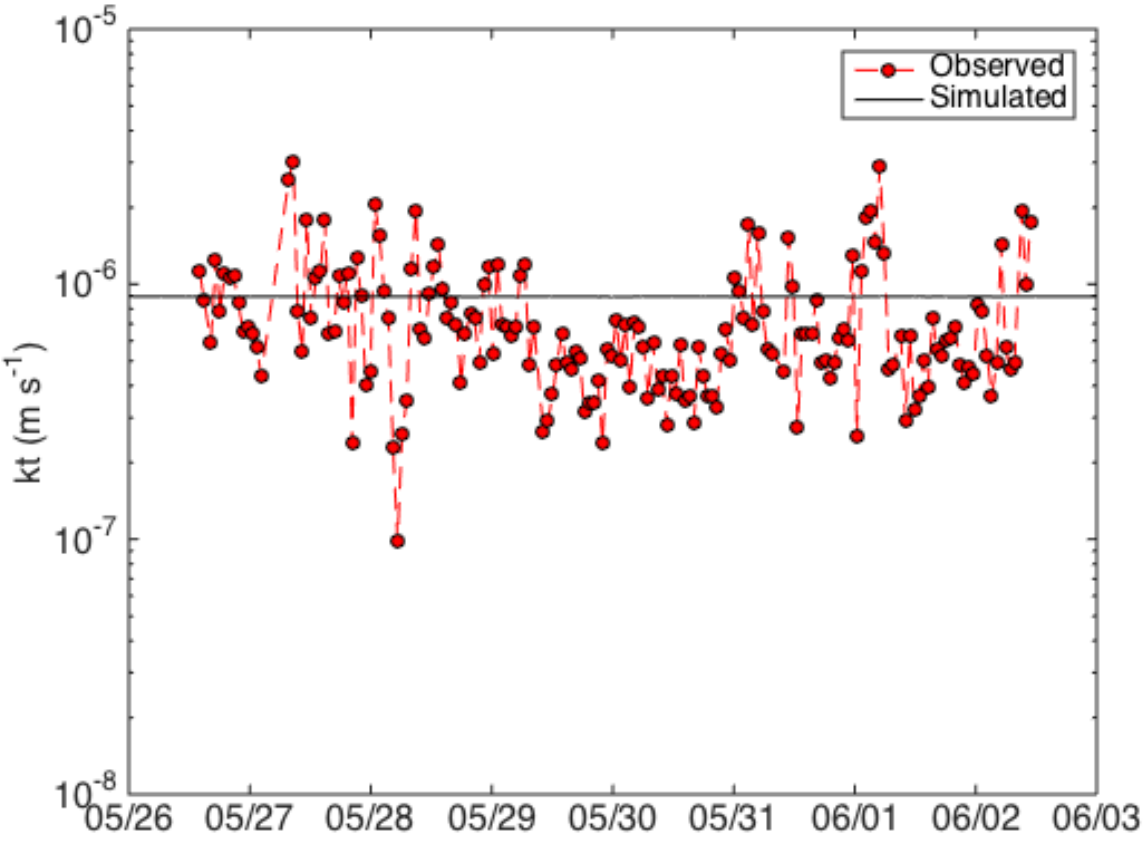

Figure 4.8. Comparison between observed transfer velocity (k_t) measured with the microprofiler at CV during the Carvin's Cove Reservoir 2013 field campaign and calculated as $k_t = D/\delta_{DBL}$ and k_t calculated from the hydrodynamic model using equations 4.6 and 4.7.

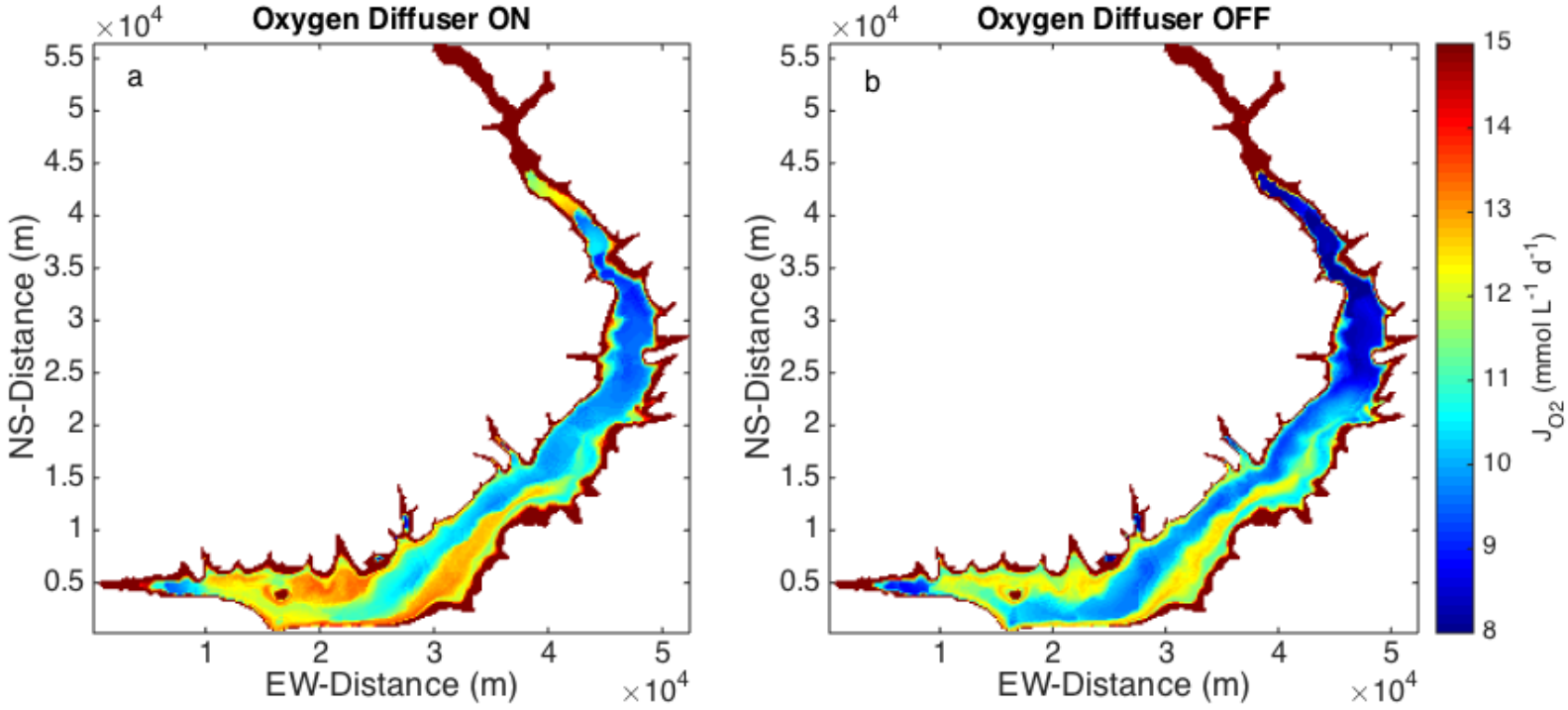

Figure 4.9. Simulated sediment oxygen flux (J_{O2}) during the calibration period. Simulated J_{O2} is higher when the diffuser is on (a) than when it is off (b), as shown by the warmer colors in (a).

Chapter 5. Summary and Conclusions

Hypolimnetic oxygenation is an increasingly common lake management tool for improving and maintaining water quality in freshwater lakes and reservoirs. Successful operation and design of these systems is no trivial task, as the oxygenation system can influence lake hydrodynamics and increase demand for oxygen in the hypolimnion as a result of increased turbulence and higher oxygen concentrations. Studies by Lorke et al. (2003) and Bryant et al. (2010) show the influence of hydrodynamics on sediment oxygen flux, and the impact of oxygenation on hypolimnetic oxygen demand, sediment oxygen flux, and circulation patterns in the hypolimnion has been observed in both field studies and modeling studies (Bryant et al. 2011; Singleton et al. 2010; Gantzer et al. 2009). Despite the current body of knowledge on sediment oxygen flux (J_{O2}) and hypolimnetic oxygenation, methods for designing hypolimnetic oxygenations still rely on empirical methods and factors of safety. There is no mechanistic method or model for predicting the impact of a proposed oxygenation system design on lake hydrodynamics and oxygen budget. Studies such as Bryant et al. (2010), which observed a close relationship between hydrodynamics and J_{O2}, have not, as of yet, proposed a model for directly calculating J_{O2} from local hydrodynamics. To address this knowledge gap, this research focused on identifying and incorporating hydrodynamic and sediment controls on sediment oxygen flux into an existing coupled bubble plume and 3-D hydrodynamic model, with the goal that the model might ultimately be useful for improving oxygenation system design methods.

Field experiments in Carvin's Cove Reservoir and Lake Hallwil were performed to collect simultaneous measurements of turbulence and J_{O2}, the first field experiments of their kind in oxygenated lakes. Using the data from these campaigns, models of interfacial flux from the literature were used to calculate J_{O2} from the hydrodynamics and were then compared to the direct J_{O2} measurements. Models based on film-renewal theory, the Batchelor scale, and law-of-the-wall scaling all scaled well with field observations, and could be used to predict J_{O2} based on characteristics of turbulent flow near the sediment-water interface.

Microprofiler data from the field campaigns was used to investigate the kinetic behavior of oxygen in lake sediment. A transient oxygen model was developed and fit to series of oxygen microprofiles from Carvin's Cove Reservoir and Lake Hallwil. Zero-order kinetics was shown

to be more appropriate for describing oxygen transport in the sediment than first-order kinetics. The fitted zero-order rate constant was variable both across lakes and within lakes, resulting from spatial differences in sediment composition.

The interfacial flux and kinetic models identified in the second and third chapters were then incorporated into an existing coupled bubble-plume 3-D hydrodynamic model (Si3D) developed by Singleton et al. (2010). By combining oxygen supply to the sediment-water interface with oxygen demand below the interface, an overall expression for J_{O2} was identified that can account for the influence of hydrodynamics and oxygen consumption within the sediment, without the need for an additional sediment model. This allows J_{O2} to vary with local hydrodynamics, as it has been shown to do in field experiments. The coupled model was applied to Carvin's Cove Reservoir, using field data from 2011 for model calibration and field data from 2013 for model validation. The coupled model provided good agreement with observed temperature profiles, while simulated oxygen profiles deviated from the observed oxygen profiles. Oxygen concentrations in the bulk portion of the hypolimnion showed reasonable agreement, but the simulations and observations disagreed most near the sediment, as the model failed to reproduce the sharp oxygen concentration gradients observed in the field. As a result, simulated oxygen concentrations in the bottom 1 m of water were higher than field observations, which also lead to simulated J_{O2} being higher than was observed in the field. This highlighted the need for an improved water quality model in the version of Si3D used for this study, particularly with respect to oxygen, as it seems the model is missing some oxygen-consuming chemical processes occurring within the bottom meter of the water column. Despite this discrepancy, the model was still able to capture the effect of diffuser operation on J_{O2}, as J_{O2} was higher when the diffuser was operating than when the diffuser was off. Additionally, the variable J_{O2} expression is simple enough to incorporate into other existing water quality models, allowing J_{O2} to be a predicted variable, rather than a fitting parameter, as is often the case.

While the research presented here has not ultimately produced a comprehensive model for predicting oxygenation-induced J_{O2}, it has identified the final remaining pieces of the puzzle, and a comprehensive model could be realized via two different approaches. First, by improving the water quality model in the current version of Si3D and identifying the missing oxygen sinks, the

coupled model described in this work should be able to be brought into agreement with field measurements of oxygen near the sediment and J_{O2}. Alternatively, the expression for J_{O2} presented here could be incorporated into other hydrodynamic models with more advanced water quality models (such as ELCOM-CAYDEM) along with a model for a proposed oxygenation system (such as a bubble plume) to predict the impact of the proposed oxygenation system on lake hydrodynamics and J_{O2}. Following additional calibration and validation, either approach would likely provide a comprehensive model for oxygenated lakes, which could be used to move oxygenation system design and operation away from the current empirical approach to a mechanistically based approach.

References

Bryant, L. D., Lorrai, C., McGinnis, D. F., Brand, A., Wuest, A., and Little J. C., 2010. "Variable sediment oxygen uptake in response to dynamic forcing." *Limnology and Oceanography*, 55 (2), 950-964.

Bryant, L. D., Gantzer, P. A., and Little, J. C., 2011. "Increased sediment oxygen uptake caused by oxygenation-induced hypolimnetic mixing." *Water Research,* 45 (12), 3692-3703.

Gantzer, P. A., Bryant, L. D., and Little, J. C., 2009b. "Effect of hypolimnetic oxygenation on oxygen depletion rates in two water-supply reservoirs." *Water Research,* 43 (6), 1700-1710.

Lorke, A., Müeller, B., Maerki, M., and Wüest, A., 2003. "Breathing sediments: The control of diffusive transport across the sediment-water interface by periodic boundary-layer turbulence." *Limnology and Oceanography,* 48 (6), 2077-2085.

Singleton, V. L., Rueda, F. J., and Little, J. C., 2010. "A coupled bubble plume-reservoir model for hypolimnetic oxygenation." *Water Resources Research*, 46 (12), W12538.